Tectonophysics 618 (2014) 1–34

Contents lists available at ScienceDirect

Tectonophysics

journal homepage: www.elsevier.com/locate/tecto

Invited Review Article

The global aftershock zone

Tom Parsons [a,*], Margaret Segou [b], Warner Marzocchi [c]

[a] U.S. Geological Survey, Menlo Park, CA, USA
[b] Geosciences Azur, France
[c] Istituto Nazionale di Geofisica e Vulcanologia, Rome, Italy

ARTICLE INFO

Article history:
Received 27 September 2013
Received in revised form 24 January 2014
Accepted 28 January 2014
Available online 5 February 2014

Keywords:
Earthquake triggering
Dynamic triggering
Aftershocks
Seismic hazard

ABSTRACT

The aftershock zone of each large ($M \geq 7$) earthquake extends throughout the shallows of planet Earth. Most aftershocks cluster near the mainshock rupture, but earthquakes send out shivers in the form of seismic waves, and these temporary distortions are large enough to trigger other earthquakes at global range. The aftershocks that happen at great distance from their mainshock are often superposed onto already seismically active regions, making them difficult to detect and understand. From a hazard perspective we are concerned that this dynamic process might encourage other high magnitude earthquakes, and wonder if a global alarm state is warranted after every large mainshock. From an earthquake process perspective we are curious about the physics of earthquake triggering across the magnitude spectrum. In this review we build upon past studies that examined the combined global response to mainshocks. Such compilations demonstrate significant rate increases during, and immediately after (~45 min) $M > 7.0$ mainshocks in all tectonic settings and ranges. However, it is difficult to find strong evidence for $M > 5$ rate increases during the passage of surface waves in combined global catalogs. On the other hand, recently published studies of individual large mainshocks associate $M > 5$ triggering at global range that is delayed by hours to days after surface wave arrivals. The longer the delay between mainshock and global aftershock, the more difficult it is to establish causation. To address these questions, we review the response to 260 $M \geq 7.0$ shallow ($Z \leq 50$ km) mainshocks in 21 global regions with local seismograph networks. In this way we can examine the detailed temporal and spatial response, or lack thereof, during passing seismic waves, and over the 24 h period after their passing. We see an array of responses that can involve immediate and widespread seismicity outbreaks, delayed and localized earthquake clusters, to no response at all. About 50% of the catalogs that we studied showed possible (localized delayed) remote triggering, and ~20% showed probable (instantaneous broadly distributed) remote triggering. However, in any given region, at most only about 2–3% of global mainshocks caused significant local earthquake rate increases. These rate increases are mostly composed of small magnitude events, and we do not find significant evidence of dynamically triggered $M > 5$ earthquakes. If we assume that the few observed $M > 5$ events are triggered, we find that they are not directly associated with surface wave passage, with first incidences being 9–10 h later. We note that mainshock magnitude, relative proximity, amplitude spectra, peak ground motion, and mainshock focal mechanisms are not reliable determining factors as to whether a mainshock will cause remote triggering. By elimination, azimuth, and polarization of surface waves with respect to receiver faults may be more important factors.

Contents

* Corresponding author at: U.S. Geological Survey, MS-999, 345 Middlefield Rd., Menlo Park, CA, 94025,USA
E-mail address: tparsons@usgs.gov (T. Parsons).

http://dx.doi.org/10.1016/j.tecto.2014.01.038

1. Introduction

Aftershocks of large ($M \geq 7$) earthquakes can happen nearly anywhere on Earth because their surface waves distort fault zones and volcanic centers as they travel through the crust, triggering seismic failures (Anderson, 1994; Árnadóttir et al., 2004; Beresnev et al., 1995; Brodsky et al., 2000; Cannata et al., 2010; Chelidze et al., 2011; Daniel et al., 2008; Doser et al., 2009; Felzer and Brodsky, 2006; Glowacka et al., 2002; Gomberg, 1996; Gomberg et al., 1997, 2001, 2004; Gomberg and Bodin, 1994; Gomberg and Davis, 1996; Gomberg and Felzer, 2008; Gomberg and Johnson, 2005; Gonzalez-Huizar and Velasco, 2011; Gonzalez-Huizar et al., 2012; Hill, 2008; Hill et al., 1993; Hirosi et al., 2011; Hough, 2001, 2005, 2007; Hough and Kanamori, 2002; Husen et al., 2004; Husker and Brodsky, 2004; Jiang et al., 2010; Johnston et al., 2004; Jousset and Rohmer, 2012; Kilb et al., 2000; Lei et al., 2011; Lin, 2012; Meltzner and Wald, 2003; Miyazawa, 2011; Miyazawa and Mori, 2006; Mohamad et al., 2000; Moran et al., 2004; Pankow et al., 2004; Papadopoulos, 1998; Peng et al., 2011a, 2010, 2012; Pollitz et al., 2012; Prejean et al., 2004; Savage and Marone, 2008; Shanker et al., 2000; Singh et al., 1998; Spudich et al., 1995; Stark and Davis, 1996; Steeples and Sreeples, 1996; Sturtevant et al., 1996; Surve and Mohan, 2012; Taira et al., 2009; Tape et al., 2013; Tibi et al., 2003; Tzanis and Makropoulos, 2002; Ukawa et al., 2002; Van Der Elst and Brodsky, 2010; Velasco et al., 2008; Wen et al., 1996; West et al., 2005; Wu et al., 2011, Yukutake et al., 2011; Zhao et al., 2010). Example results (Velasco et al., 2008) are reprised in Fig. 1; hundreds of Global Seismograph Network (GSN) stations that recorded surface waves from 15 $M \geq 7.1$ mainshocks were filtered and analyzed for local events. A nearly two-fold rate increase is evident when the observations are stacked (Fig. 1A). We plot results from a catalog search for $M > 5$ events on the same time range scales (Fig. 1B), but no $M > 5$ rate increase is associated with 260 $M \geq 7$ mainshocks (e.g., Huc and Main, 2003; Parsons and Velasco, 2011).

At near radii ($r < 1000$ km) there is a very clear (~50-fold) $M > 5$ earthquake rate increase during the first hour after 260 $M \geq 7$ mainshocks that decays rapidly by Omori's law, and is obvious for at least 10 days (Fig. 2). The same analysis for the rest of the planet outside 1000 km radii from mainshocks shows no detectible rate increase during any period (Fig. 2B). The 1000 km radius was chosen because Parsons and Velasco (2011) found that to be the greatest distance that significant $M > 5$ earthquake rate increases were seen. Elevated rates within a 300 km radius are observed to persist for ~7–10 years (Faenza et al., 2003; Parsons, 2002).

Key questions then are: Why aren't dynamically triggered $M > 5$ earthquakes correlated with passing surface waves across the global aftershock zone the way smaller earthquakes are? Is there no comparable hazard in the global aftershock zone to that in the local zone? Perhaps we haven't yet observed this simply because $M > 5$ earthquakes are orders of magnitude less frequent than smaller shocks by the Gutenberg and Richter law ($\log(N) = a\text{-}b\mathrm{M}$; Ishimoto and Iida, 1939; Gutenberg and Richter, 1954). However, extrapolation of the Velasco et al. (2008)

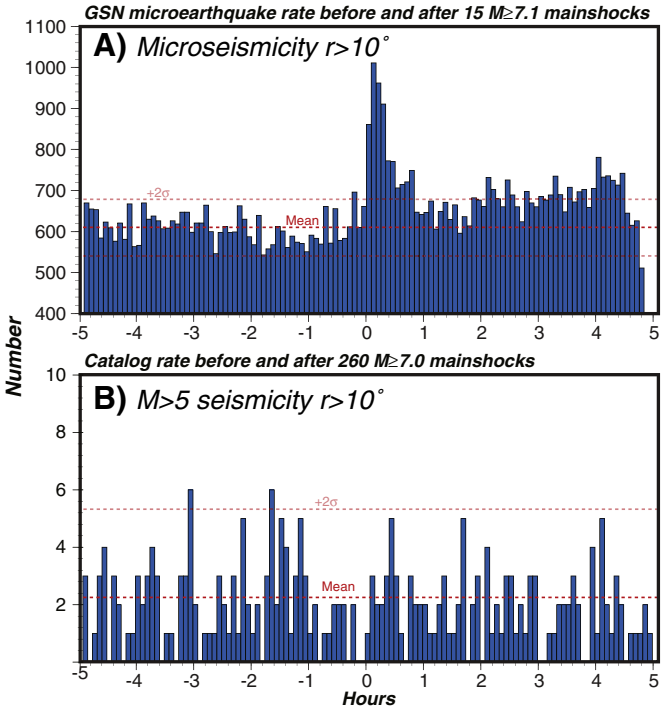

Fig. 1. In (A) remotely triggered earthquakes recorded on GSN stations identified by Velasco et al. (2008) are shown. The significant rate increase persists for slightly less than 1 h. Little is known about these events, which were not located by regional networks. In (B) a search of the 34-year $M > 5$ catalog shows no rate increase associated with 260 $M \geq 7$ mainshocks.

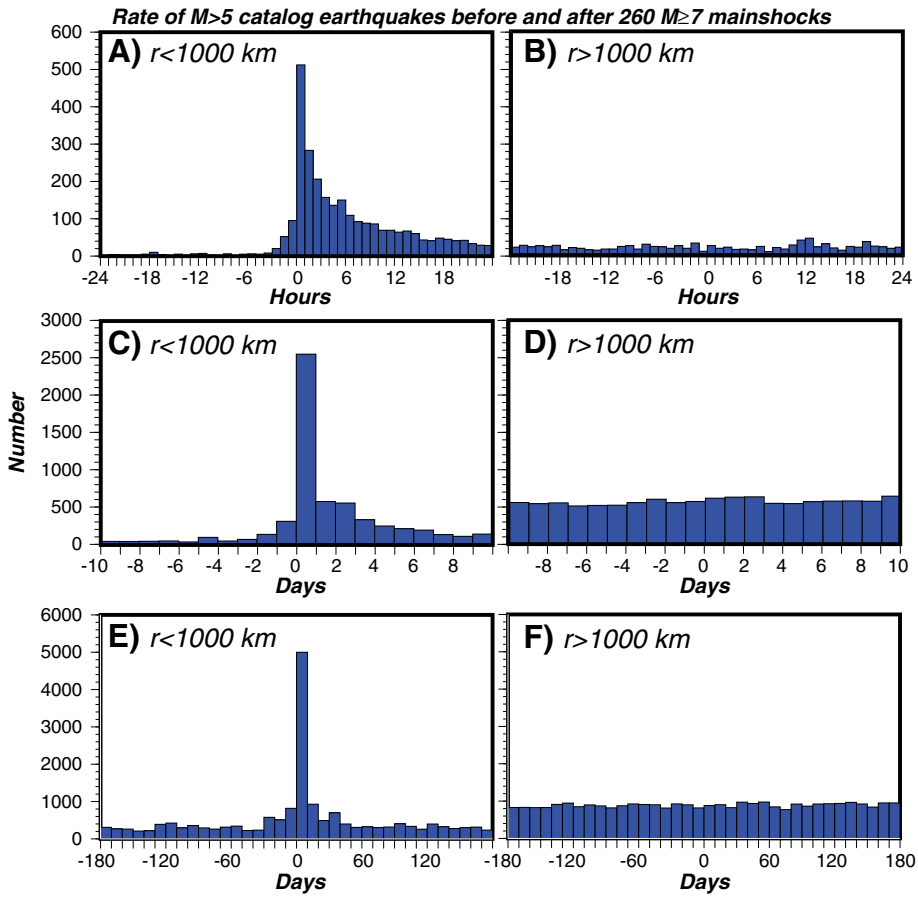

Fig. 2. In (A) all $M > 5$ earthquakes that occurred in 24 h periods before and after 260 $M \geq 7$ mainshocks, and within a 1000 km radius of the mainshocks are stacked. A clear rate increase and Omori-law decay is evident. In (B) the same process is applied except all global $M > 5$ events outside of the 1000 km radius are considered. No rate change is evident. In (C) and (D) the same process is followed except ±10 day intervals are considered. Periods of ±180 days are shown in (E) and (F).

observations, assuming that the maximum magnitudes detected lie between $M = 2$ and $M = 3$, and a b-value = 1, implies that about 70 $M > 5$ events should be observed within 15 min of surface wave passage (Parsons and Velasco, 2011).

We can gain some insight by examining a specific location such as the Basin and Range province, which demonstrated widespread remote earthquake triggering after the 2002 $M = 7.9$ Denali earthquake (Gomberg et al., 2004; Husker and Brodsky, 2004; Pankow et al., 2004; Fig. 3). While the seismicity rate is clearly increased significantly by Denali surface waves, the overall rate of triggered earthquakes is too low to necessarily expect $M > 5$ earthquakes during the first 24-h period following the mainshock. This can be determined by extrapolating the Gutenberg–Richter distribution based on the number of $M > 2$ events at a b-value = 1, which yields an expected rate of $M > 5$ events to be ~0.6/day.

An intriguing (and concerning from a hazard perspective) explanation for the lack of $M > 5$ remote triggering directly associated with passing surface waves is the possibility that larger magnitude earthquake triggering occurs, but is delayed relative to surface wave arrivals. Many such cases of delayed (hours to days) larger earthquake occurrence have been temporally correlated with mainshocks at remote global distances (e.g., Gomberg and Bodin, 1994; Gonzalez-Huizar et al., 2012; Pollitz et al., 2012; Tzanis and Makropoulos, 2002). If the response/nucleation time is longer for a larger earthquake than a smaller magnitude event, then there may be information about the initial phases of the earthquake rupture process being conveyed, and a suggestion that this may be magnitude dependent.

In global analyses to date, systematic regional observations of seismic response to passing surface waves across the magnitude scale are lacking. Since $M \geq 5$ triggering during surface wave arrivals appears to be rare or absent, we want to look at as broad a magnitude range as is possible on regional networks where non-detection of $M \geq 5$ events is nearly impossible. We take the approach that if we can amass as many unequivocal remote-triggering responses (like that in Fig. 3) as possible, then we can more confidently assess large earthquake triggering by greatly reducing the possibility of coincidental associations.

In this review we examine 21 local and regional seismic catalogs from many parts of the world (Fig. 4) for response to 260 $M \geq 7$ global mainshocks. This paper is therefore an earthquake catalog review rather than a literature review. We address the following questions: (1) how often is there a significant increase in seismic activity at a given location in response to an earthquake more than 1000 km away? (2) What is the magnitude distribution of dynamically triggered earthquakes? (3) If large earthquakes are triggered, are they always preceded by a cascade of lower magnitude events? (4) Is there any information from magnitude response that might enable speculation about the earthquake nucleation process? (5) Are there identifying features in common among mainshocks that cause remote triggering?

2. Methods and data

Looking at stacked data from many locations simultaneously increases the number of events and adds statistical power to a triggering analysis, but this also makes it difficult to grasp regional frequency and variability in triggering response to passing surface waves. Further, the events shown in Fig. 2A were recorded at single stations rather than by a regional network, meaning no detailed information about locations and magnitudes is available. The stacked $M > 5$ events shown in Fig. 2B

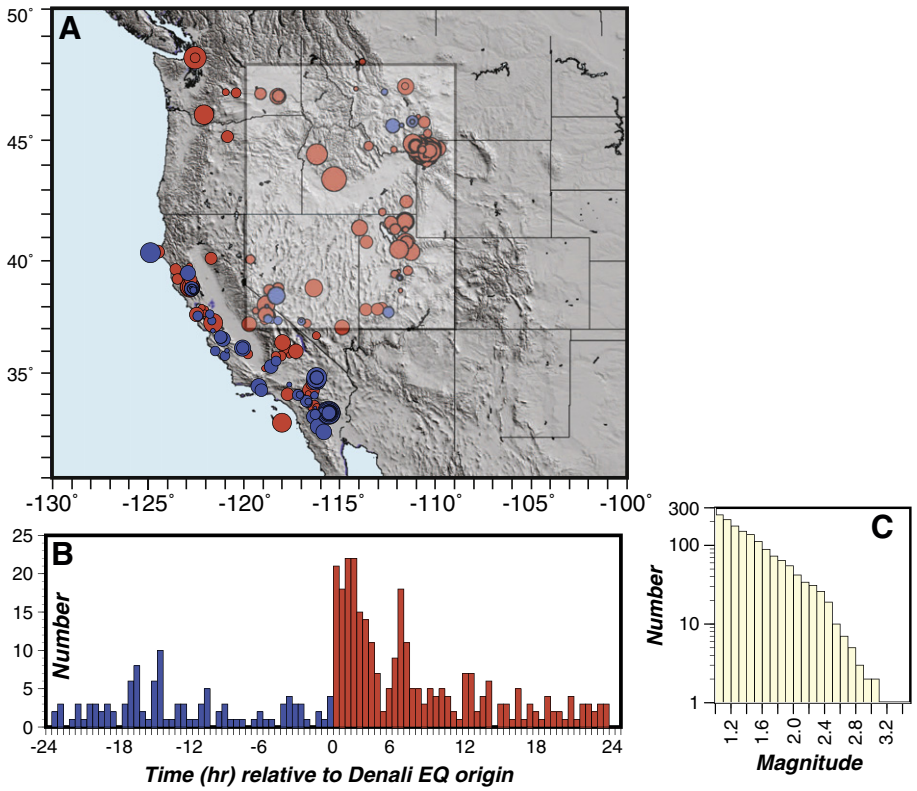

Fig. 3. Remote earthquake triggering in the Basin and Range extensional province of the western United States is shown. In (A) a map of seismicity 24 h prior to (blue) and after (red) the 2002 M = 7.9 Denali earthquake is shown. (B) A histogram of earthquake number per 30 min is shown that demonstrates the earthquake rate increase observed by Gomberg et al. (2004), Husker and Brodsky (2004), and Pankow et al. (2004). The cumulative magnitude frequency of the post-Denali seismicity is shown in (C); extrapolation of this relation to $M > 5$ rates suggests an expected rate of ~0.6 $M > 5$ events/day.

have magnitude and location information, but represent only the sparsest part of the magnitude spectrum, and only tell a partial story.

The backbone of this review is thus a compilation of earthquake catalogs that are complete to lower magnitudes. These are secured from a variety of sources including the Advanced National Seismic System (ANSS), which assembles numerous regional USA and international network catalogs together, the Japan Meteorological Agency, the World Data Center for Seismology Beijing, Geoscience Australia, GNS Science New Zealand, Istituto Nazionale di Geofisica e Vulcanologia in Italy, The Kandili Observatory in Turkey, and The National Observatory of Athens in Greece. The Global Seismograph Network (GSN) catalog is used to fill in where no local network observations are available. Areas are selected either because of catalog availability constraints, or as representative sampling. All data are assembled prior to analysis, and in no cases are catalog bounds or other properties altered after examination. We seek catalogs from active regions with quality networks as well as samples from all continents and different tectonic environments. We end up with 21 individual catalogs with a cumulative 1,524,873 unique events.

A key motivation for using these regional catalogs is that their lower completion magnitudes (typically $M = 2$) means that the question of

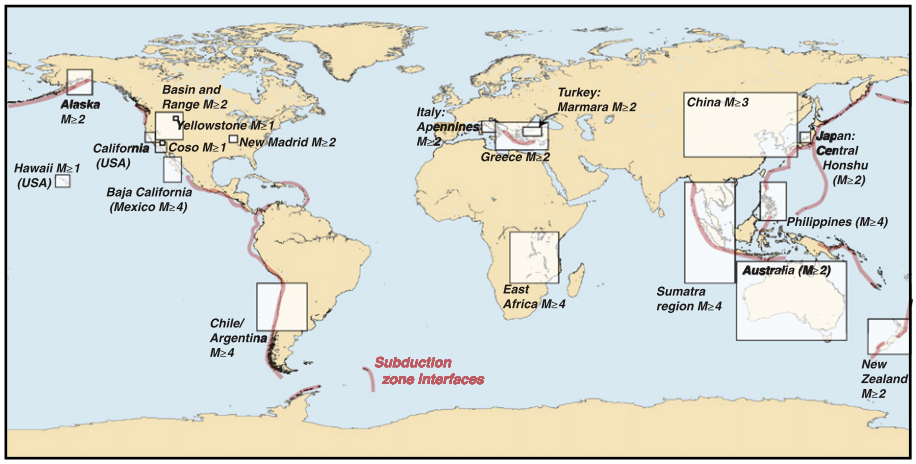

Fig. 4. Map of the regions sampled and discussed in this review of global seismic response to teleseismic surface waves. Many of these regions were selected because they have dense enough seismic station coverage to enable a complete earthquake catalog from $M \geq 2$. In other cases the ANSS/GSN catalog was applied to sample the major continents. Additionally, the global subduction interface catalog of Heuret et al. (2011) was included and illustrated by the red lines.

remote higher-magnitude triggering can be directly addressed. The results presented in Fig. 1B show stacked $M \geq 5$ rates that are unchanged after surface wave passage. Questions from that analysis remain that include the expected $M \geq 5$ rates during these short intervals (hours), and possible masking of events in the global catalog. However, in a regional catalog that is complete to low magnitudes, it is virtually impossible that a $M \geq 5$ earthquake could be missed. Further, we can extrapolate expected numbers of $M \geq 5$ shocks based on the lower magnitude rates, and by assuming Gutenberg–Richter magnitude–frequency relations, determine if there are absent high magnitude events.

A second catalog of 260 global $M \geq 7.0$ mainshocks is also assembled; the $M \geq 7.0$ threshold is arbitrary, but this magnitude was shown to be capable of triggering earthquakes at global distances by Velasco et al. (2008), and we adopted the same threshold for the Parsons and Velasco (2011) study. The duration of the mainshock catalog runs from 1979 through 2012 and includes 41 new potential $M \geq 7$ triggers over the catalog used by Parsons and Velasco (2011), including the February 2010 $M = 8.8$ Maule, March 2011 $M = 9$ Tohoku, and April 2012 $M = 8.6$ Indian Ocean events. All earthquakes used in this study are shallow, spanning 0–50 km in depth.

In this review we want to test the broadest magnitude spectrum possible for remote triggering, particularly in light of the disparity illustrated in Fig. 1. We therefore include the lowest magnitudes available in each region, but we do not imply that this value represents a magnitude of completeness. As described below, we compare ± 24 h, local earthquake rate changes associated with remote sources, and therefore assume that detection thresholds are unchanged over these 48-h periods. The primary occurrence that could affect this assumption would be the period just after a large local earthquake, when data losses are expected (e.g., Iwata, 2008; Kagan, 2003). To obviate this, we track the occurrence of larger earthquakes within regional catalogs very carefully, and any significant daily rate change that is observed is hand checked for local effects.

Another concern might be the data losses for low magnitude events during the passage of surface waves across local networks. From D. Oppenheimer, personal communication (2013) we note with regard to ANSS stations, "For short-period stations, the passband is 0.5–30 Hz, so the surface waves are mostly outside the passband, and the picker does a fair job detecting the local, triggered events. However, the short period stations are typically analog, so the signal clips if the surface waves are big. In this case, we can't easily time the local events. On more modern digital stations (after 2005) we avoid that problem, as the dynamic range of the sensors is high enough." Therefore it is possible that we lack coverage during the actual passage of surface waves, particularly at lower magnitudes; this problem is reduced at about the $M \sim 5$ threshold because GSN stations can observe them remotely at many locations where the mainshock and triggered event arrivals do not interfere.

We apply the following procedure to every catalog. We begin by calculating the observed daily change in the number of earthquakes in each regional catalog, excluding the 260 24-h periods after global mainshocks occurred (Fig. 5). This is intended to establish the expected background daily variability that is not affected by global mainshocks. We establish the mean daily change and the variance on that change by examining 2-year windows at 0.5 year intervals (the preceding 2 years of observed rate changes are evaluated at each 0.5-year interval). We do this because virtually all catalogs grow more complete and record more events with time as new stations are installed, thus the magnitude and significance of the mean daily rate change will change with time. Additionally, earthquake rates fluctuate dramatically when larger events occur within the region that trigger many aftershocks. We calculate the mean rate change and significance independently for increases and decreases because aftershocks can cause instant rate increases to a degree that cannot occur as a daily decrease. We experimented with different durations used to calculate the mean daily rate changes, and settled on 2 years as an optimal balance between having sufficient numbers to calculate a stable mean, while

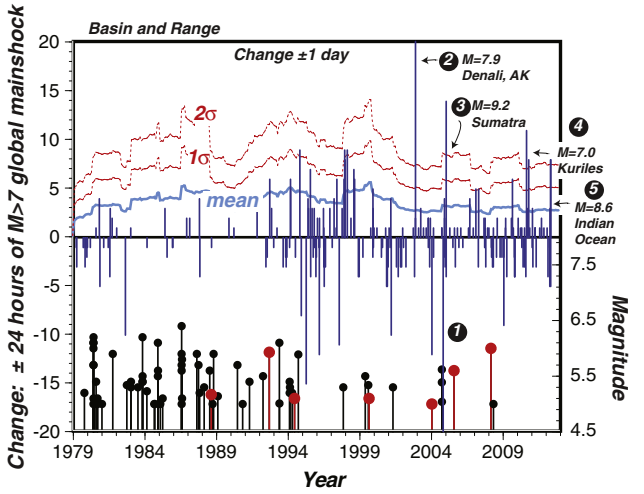

Fig. 5. Daily rate changes in the Basin and Range Province of the western USA (see Fig. 4 for location) following 260 $M \geq 7.0$ global mainshocks. Blue spikes show changes in the number of earthquakes in the catalog for 24 h periods before and after each of 260 global $M \geq 7.0$ mainshocks. The mean daily rate increases across the whole catalog are shown by the light blue line. One and two standard deviations (1σ and 2σ) on daily rate changes are shown by dashed red lines. We take daily rate changes that exceed two standard deviations as significant. Important events are labeled, numbered, and analyzed in Fig. 6. Local earthquakes of $M \geq 4.5$ are indicated by the stick plot along the base of the horizontal axis; those shaded in red occurred within 24 h after the global mainshocks.

still representing catalog time-dependence. We do not decluster the catalogs, because we are looking for clustering behavior caused by remote mainshock triggers.

We calculate time dependent variance and hence standard deviations (σ) on the mean rate changes by fitting daily rate changes over 2-year periods to negative binomial distributions, which are found to better represent clustered phenomena (e.g., Jackson and Kagan, 1999; Vere-Jones, 1970). An indication that a negative binomial distribution is a more appropriate than a Poisson process occurs when the data are dispersive, with the variance greater than the mean. We apply a maximum likelihood regression technique (Cameron and Trivedi, 1998) that starts with fitting a Poisson model, then a null model (intercept only model), and finally the negative binomial model. We iterate until the change in the log likelihood is vanishingly small. We estimate the dispersion (α) inherent to each catalog from the maximum likelihood regressions, calculate variance as $\text{var} = \mu + \alpha\mu^2$, and find the 1σ and 2σ variations on rate changes from the variance. We note significant dispersion in every catalog that we analyzed, with α ranging from 0.19 to 0.55, which means a Poisson process is rejected.

We isolate earthquake rate changes in regional catalogs across ± 24 h periods relative to $M \geq 7.0$ global mainshock events that happen more than 1000 km away from any of the events in the regional catalog. The 1000 km distance was chosen because it was the maximum distance where earthquake rates were detected significantly above background levels by Parsons and Velasco (2011) during the first 24 h following 205 post-1979 mainshocks. It was thus interpreted to be the maximum extent of static stress triggering. Global distance ranges between mainshocks and possibly triggered events are calculated with the inverse method of Vincenty (1975) using the NAD83 ellipsoid. We highlight local rate changes that exceed a 2σ level above the mean. We take the 2σ threshold to be a guideline because an exact confidence interval depends on the degree of smoothing that results from the duration of the catalog used to calculate it (2 years in incremental 0.5-year steps in this review) and on the statistical distribution used (negative binomial). Therefore, if a rate increase approaches the 2σ, or if a specific mainshock was noted to cause remote triggering by other authors, we investigate it as a possible example of remote

triggering. Our results depend on the chosen significance threshold, with an increase or decrease changing the number of triggering cases that we identify. The detailed analyses that we conduct suggest that we admit more cases for consideration than we omit.

The 1000-km exclusion zone removes the possibility of local, static stress change induced processes from being mistaken for remote triggering. Significant local events of $M < 7.0$ that happen within 24 h of a global mainshock tend to be associated with their own aftershocks, which then contribute to a significant earthquake rate increase. Indeed these sequences could be a cascade that is set off by a global mainshock, or could instead be a coincidence. We therefore examine every significant rate increase in detail to establish its character.

We find an array of responses to remote earthquakes in regional catalogs that range from: (1) widespread seismicity rate increases, (2) isolated local mainshocks and associated aftershocks, (3) swarm invigoration, to (4) no significant response. We define "probable remote triggering" as being a widespread seismicity rate increase without an obvious local cause (Fig. 3). We define "possible remote triggering" as being a localized earthquake and aftershocks that may have occurred by chance, or may have been triggered. We define "swarm invigoration" as an already active zone of seismicity that intensifies after surface waves pass through the region from a remote mainshock. To add a systematic way of defining these responses, we quantify their spatial nature by dividing our study regions (Fig. 4) into 0.5° by 0.5° boxes and calculating the mean and variance of the number of subregions that display ±24 h seismicity rate changes in 100 random trials across catalog durations. We then calculate how many subregions display rate increases for each significant regional response to global mainshocks. If this number exceeds a 2σ threshold in the number of 0.5° by 0.5° boxes from random trials and there is no local mainshock, then we identify the response as widespread, and thus probable remote triggering. In other words, we want to find out what the normal daily spatial variability in seismicity rate is, and what constitutes an anomalous region-wide change.

Examples are shown in Figs. 5 and 6; in this case the Basin and Range province catalog is analyzed (see Fig. 4 for location). This catalog

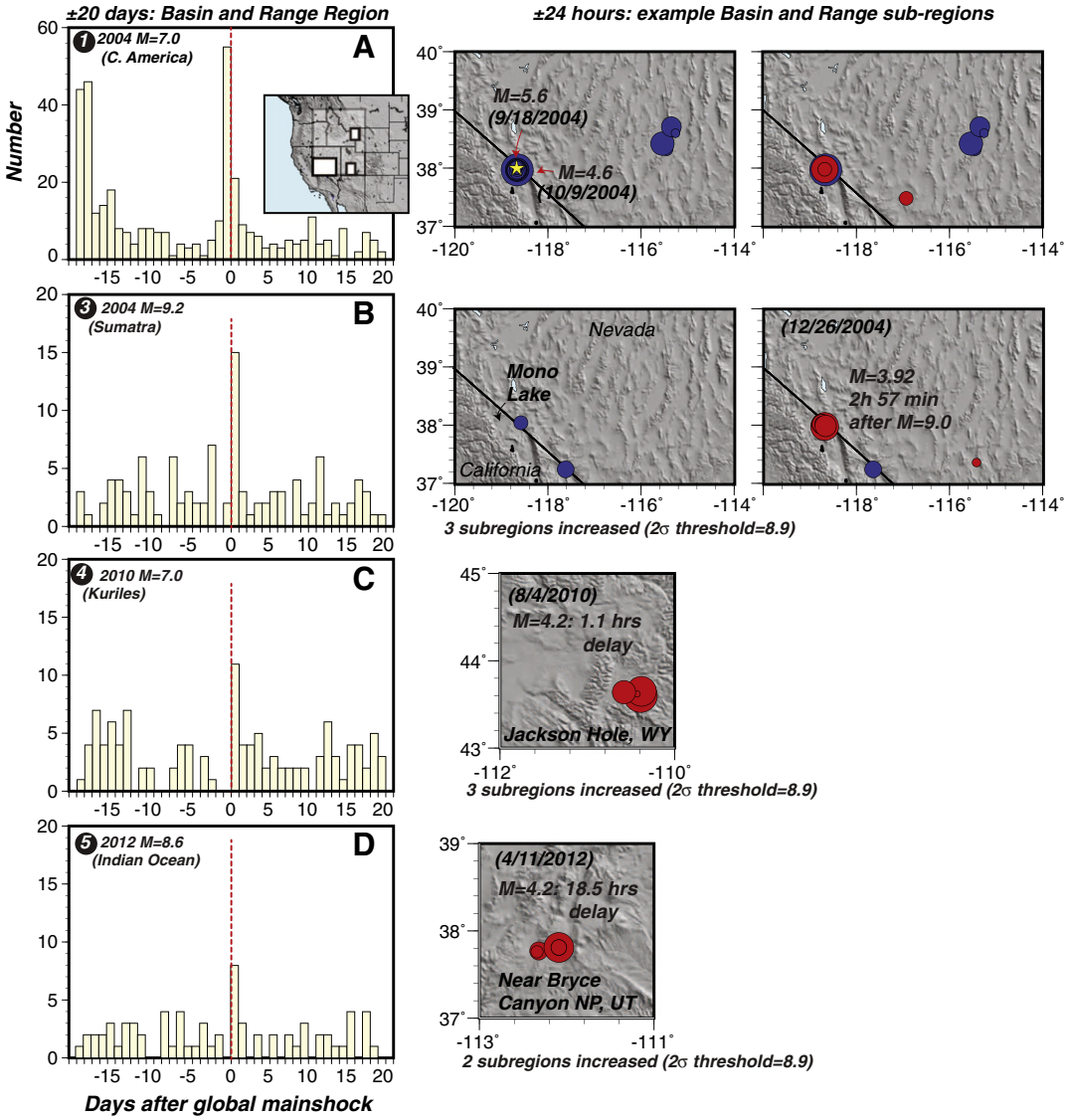

Fig. 6. Detailed analysis of remote earthquake triggering in the Basin and Range province of the western USA. In (A) it is demonstrated that the apparent significant rate decrease is actually just a decaying aftershock sequence. In (B) a $M = 3.9$ event occurs ~3 h after the 2004 $M = 9.2$ Sumatra earthquake. This response is spatially limited as compared with the more regional rate increase associated with the 2002 $M = 7.9$ Denali earthquake shown in Fig. 3. Similarly in (C) and (D) isolated clusters of events near Jackson Hole, Wyoming, and Bryce Canyon, Utah can be tied to remote mainshocks. Their isolation means these events could easily be coincidental, and not examples of remote triggering. Each of these responses are associated with rate changes in 2–3 0.5° by 0.5° subregions, whereas we calculate a 2σ (2 standard deviations) significance threshold of 8.9. The response to the Denali earthquake in the Basin and Range affected 16 subregions. Locations of insets are shown in (A).

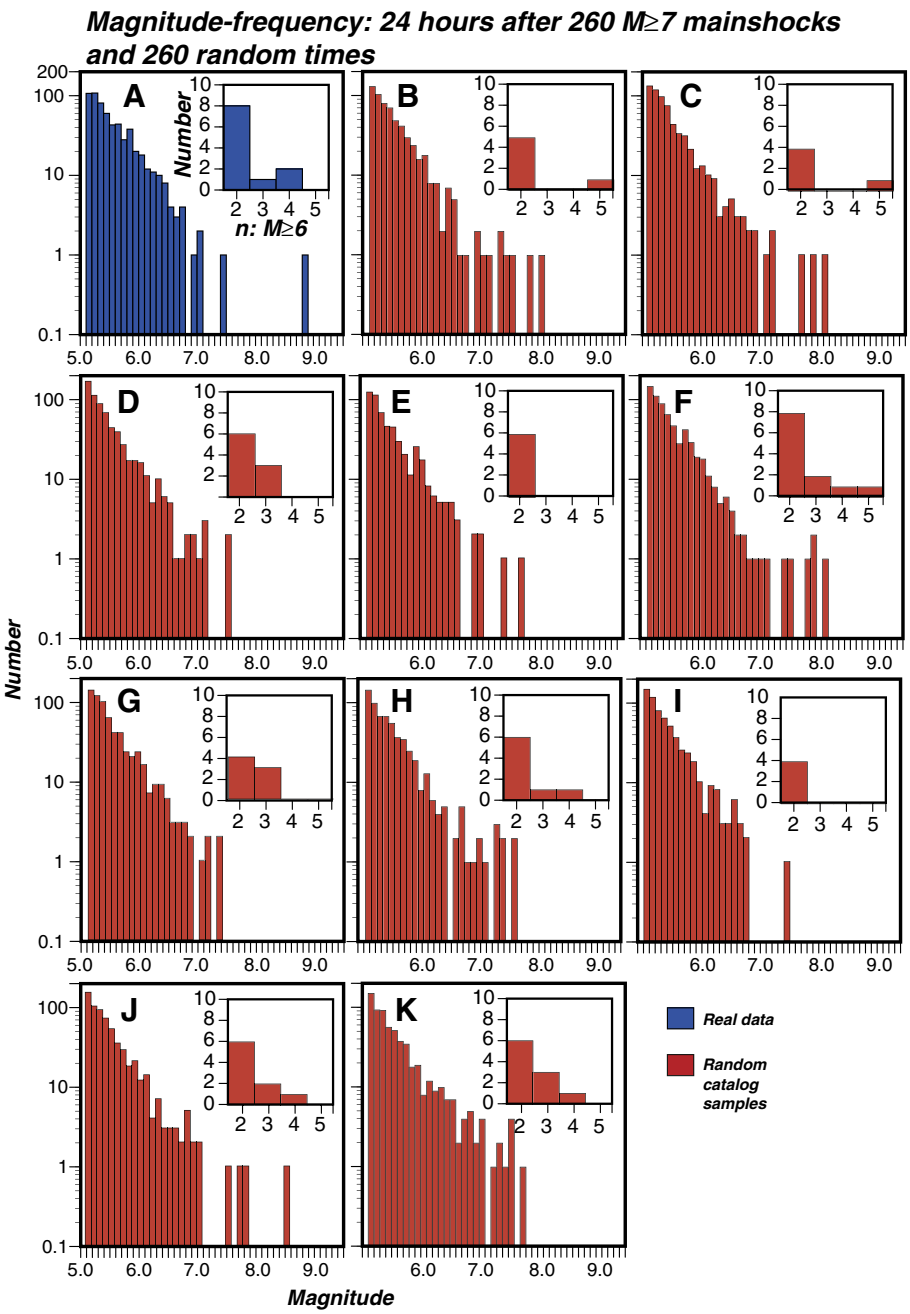

Fig. 7. Comparison of (A) observed and (B–K) randomized incremental magnitude-frequency distributions for 260 24-h periods in the global $M > 5$ earthquake catalog. The inset histograms show how many of 260 random 24-h periods had between 2 and 5 $M \geq 6.0$ earthquakes in them. In other words, how many days out of 260 are there 2 or more $M \geq 6.0$ earthquakes by random chance? The point of this figure is to show that by pure coincidence, at least 4 of 260 24-h periods have 2 to 5 $M \geq 6.0$ earthquakes in them. Except in (A), these periods are not preceded by a $M \geq 7.0$ mainshock.

contains 47,791 $M \geq 2.0$ events. In addition to the very clear rate increase associated with the 2002 $M = 7.9$ Denali earthquake already shown in Fig. 3, three other rate increases at 2σ are observed, associated with the 2004 $M = 9.2$ Sumatra earthquake, a 2010 $M = 7.0$ Kuriles event, and the 2012 $M = 8.6$ Indian Ocean shock.

It is common to see significant earthquake rate reductions associated with 24-h periods after global mainshocks (for example, the event labeled "1" on Fig. 5). In every instance throughout our global analysis, these rate decreases are caused by declining aftershock sequences of local earthquakes. What happens in these cases is that a moderate to large regional earthquake occurs, usually the day before one of the 260 global mainshocks, and we thus measure a strong rate decrease from a decaying aftershock sequence that has nothing to do with the global event. This is illustrated in Fig. 6; the rate decrease labeled "1" in Fig. 5 is associated with a $M = 4.6$ earthquake that happened on the California–Nevada border the day before a $M = 7.0$ Central America mainshock. The $M = 4.6$ event is likely itself an aftershock of $M = 5.6$ earthquake at the same location 21 days previously. The histogram of daily earthquakes in the local area shows that an aftershock sequence of the $M = 4.6$ event was decaying when the Central America mainshock occurred (Fig. 6).

Also demonstrated by Fig. 6 is the variety of remote triggering response that can only be established by looking at regional networks. The widespread seismicity rate increase observed after the 2002 $M = 7.9$ Denali earthquake is associated with 16 unique 0.5° by 0.5° subregions showing a rate increase compared with a mean of 4.4 and

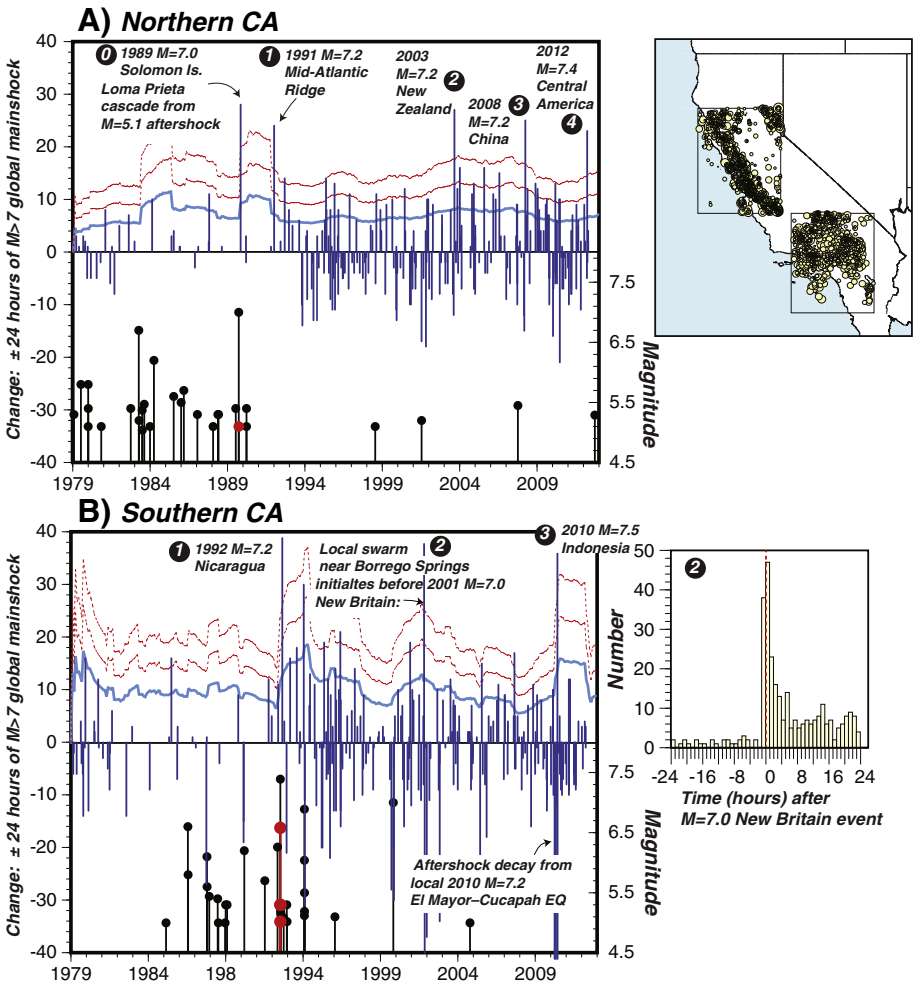

Fig. 8. Daily rate changes in (A) northern and (B) southern California, USA. Blue spikes show changes in the number of earthquakes in the catalog for 24 h periods before and after each of 260 global $M \geq 7.0$ mainshocks. Primary plot features are the same as in Fig. 5. Important events are labeled, numbered, and analyzed in Fig. 9. We identify 4 incidences of significant remote triggering in northern California, and 3 in southern California. The event labled "0" in (A) is a coincidence between a local $M = 5.1$ aftershock (and secondary aftershocks) to the 1989 $M = 7.0$ Loma Prieta earthquake and a $M = 7.0$ Solomon Islands event. One apparently significant rate change in southern California (labeled "2") began before the global mainshock that it is temporally associated with (see hourly histogram at right).

a 2σ threshold of 8.9 (Fig. 3). However, the other rate increases that are temporally associated with global mainshocks identified in Fig. 5 are all small clusters of events that result from an initial, moderate ($M = 3.9$ to $M = 4.6$) earthquake that is followed by smaller local aftershocks (just 2–3 subregions with rate increases). The timing of these initial moderate events falls within ~1 to 18 h after global mainshocks, meaning that they could be examples of delayed dynamic triggering, or they could simply be coincidental occurrences.

In the following section we report results of similar analyses across a wide variety of global regions and tectonic environments to learn more about how faults respond to transient strains imposed by passing surface waves from distant earthquakes.

3. Observations

In the following discussion we will tour and sample the world's earthquake catalogs (Fig. 4). We describe a variety of regional responses to global mainshocks that range from no significant response to widespread regional seismicity rate increases. We focus on areas with notable reactions, but also note those regions that do not appear to be affected (these non-observations are appended in the supplementary data section).

Before describing individual regional responses, it is necessary to keep in mind the distinct possibility of coincidental events; we are describing temporal correlations of earthquakes that occur sometimes on the opposite sides of the earth, often in regions of high seismic activity. We therefore look at sets of 260 24-h periods drawn at random from the global 1979–2012 earthquake catalog to find how many $M \geq 6.0$ earthquakes are expected by chance. The $M \geq 6.0$ threshold is used in these synthetic tests to ensure consistent catalog completion back to its earliest period to enable a fair comparison to the actual catalog, because randomized 24-h periods could have a different temporal distribution than the actual mainshocks. A group of 10 assemblies is shown in Fig. 7. In every case, a minimum of four 24-h periods had at least two $M \geq 6.0$ earthquakes that occurred without any global $M \geq 7.0$ mainshock preceding them. The magnitude frequency relations of the random draws of $M \geq 6.0$ earthquakes are not distinguishable from that of the actual 24-h periods that follow global $M \geq 7.0$ mainshocks, which means that we are not able to rule out random chance in cases where we observe a significant rate change that is described by single local earthquake and its local aftershocks that follow a remote $M \geq 7.0$ mainshock. In other words, any $M \geq 6.0$ global event linked in time with a $M \geq 7.0$ mainshock can always be a coincidence, and that as many as 5 $M \geq 6.0$ events can happen on a given day purely by chance.

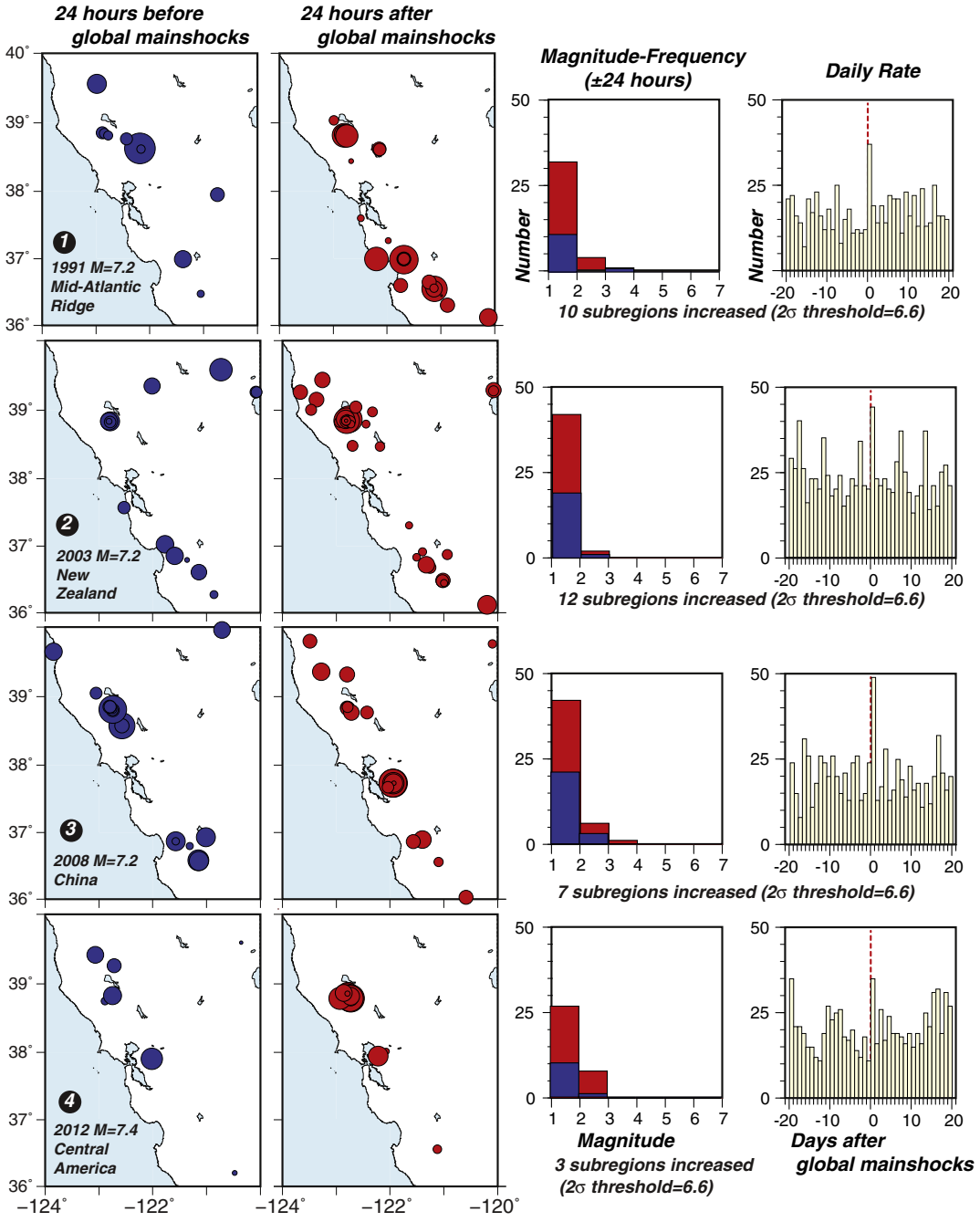

Fig. 9. Detailed analysis of remote earthquake triggering in northern California, USA. Each of the four significant rate increases numbers 1–4 in Fig. 8 are detailed in before–after maps, incremental magnitude–frequency histograms, and ±20 day events-per-day plots. Before information is shaded blue, and after in red. We call these occurrences probable remote triggering because no precipitating local event is evident, and the rate-increase is regional in nature.

3.1. California

We compare two 4° by 4° areas in northern and southern California that are centered over the active San Andreas fault system (Fig. 8). The northern California catalog has 233,570 $M \geq 1.0$ events, and the southern California catalog has 358,927 $M \geq 1.0$ shocks (our use of $M \geq 1.0$ does not imply a completeness threshold of $M = 1.0$, but rather that $M = 1.0$ events are present in the catalog). In northern California we note five cases with significant rate increases. The first (labeled "0" in Fig. 8) is likely a coincidence because it is associated with a cascade of aftershocks to a local $M = 5.1$ earthquake, itself a local aftershock to the 1989 $M = 7.0$ Loma Prieta earthquake. While it is not impossible that the $M = 5.1$ event was triggered by global mainshock, the least astonishing parent mainshock would be the nearby Loma Prieta rupture. A trio of $M = 7.2$ mainshocks from the mid-Atlantic ridge, New Zealand, and China are considered probable dynamic triggering examples in that they represent regionally distributed seismicity rate increases that are not associated with any one local higher magnitude event (Fig. 9). The 2σ threshold for the number of 0.5° by 0.5° subregions showing a rate increase is 6.6, and the responses to these three events indicate effects in 7–12 subregions. None of the four mainshock triggers in northern California overlap with any that may have affected the Basin and Range Province (Figs. 5, 8). This is a common thread throughout our analysis, with virtually no overlap amongst mainshocks, which suggests that conditions have to be ideal for remote dynamic triggering to occur (e.g., Gonzalez-Huizar and Velasco, 2011; Hill, 2008; Parsons et al., 2012).

The southern California catalog shows three significant earthquake rate changes that are associated temporally within 24 h of 260 global mainshocks. The first signal in 1992 comes 65 days after the regional 1992 $M = 7.4$ Landers earthquake, and activation is concentrated in the Landers aftershock zones (Supplementary Figure S1), though the affected area is broad enough to be classified as probable triggering with 16 0.5° by 0.5° subregions having rate increases compared with a 2σ threshold of 8.5. This could therefore be a case of aftershock invigoration induced by remote dynamic stressing, or it could be a process related directly to the Landers earthquake. There is another apparent rate increase in 2001 (Fig. 8), but this is a swarm that actually initiated 2 h before the global mainshock it is associated with (a $M = 7.0$ New Britain event). This appears like a ± 24 h rate increase because the region was very quiet before the swarm such that there are more cumulative events in the post mainshock period. This sort of occurrence demonstrates the importance of careful study of each apparent rate change. The last significant southern California rate change is associated with a 2010 $M = 7.5$ Indonesian mainshock (Fig. 8). This again follows a regional mainshock, the 2010 $M = 7.2$ El Mayor-Cucapah event, and activity is again almost entirely within the aftershock zone of that earthquake, and affects 8 subregions, and is thus considered possible remote triggering. We note that all three cases for remote dynamic triggering in southern California are ambiguous because of their association with prior swarm and/or aftershock sequences

3.2. Greece

We study a large region that encompasses Greece and parts of Turkey (Figs. 10, 11) following the same procedures as applied to California and the Basin and Range province. This catalog spans from 1983 through 2012 and contains 131,016 $M \geq 1.0$ events. It is clear from examining Fig. 10 that the completeness of this catalog is strongly time dependent (the initial portion is mostly $M \geq 3.0$ events). We note seven cases that demonstrate a significant rate increase that can be tied to global mainshocks (Fig. 10). At least four cases in Greece can be classified as probable dynamic triggering because in each instance there is a regionally broad response that is difficult to tie to a local mainshock (Fig. 11), with each case having more than twice as many 0.5° by 0.5° subregions showing rate increases than the 2σ threshold of 13.4.

Other features of note from Greece include a case where a 2008 aftershock sequence from a local $M = 5.1$ in decline is possibly reinvigorated by a $M = 7.4$ mainshock in China, and becomes the site of an $M = 6.1$ event (Fig. 11, event labeled "4"). Additionally, a 2007 $M = 7.1$ mainshock from the New Hebrides region is temporarily associated with a persistent and regional seismicity rate increase the goes on for at least 20 days (Fig. 11, event labeled "3"). Fig. 12 shows a before/after mapping of this rate increase, and its regional and temporal extent. This happened during the period between September 2006 and May 2007 that was identified as a "seismic crisis" by Bourouis and Cornet (2009). We find more cases of possible and probable remote dynamic triggering in Greece than any other region we study, which is consistent with the conclusions of Brodsky et al. (2000) that the Greek region has a low triggering threshold, and is subject to "superswarms". We do not include their 1999 $M = 7.4$ Izmit mainshock example in our analysis because it falls within the 1000 km exclusion zone we apply throughout this review.

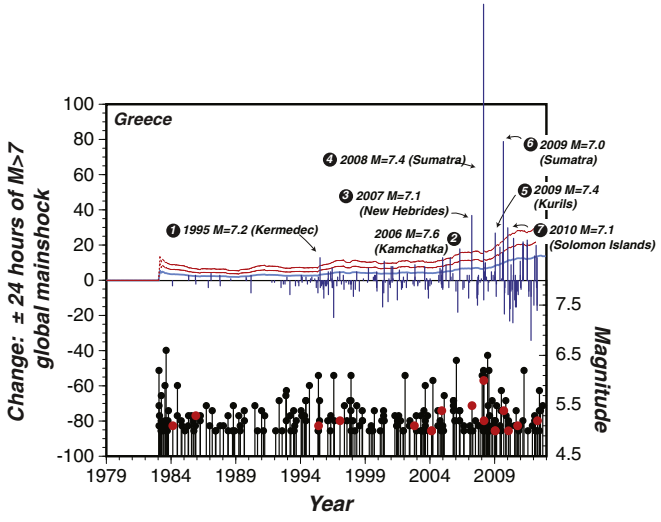

Fig. 10. Daily rate changes in Greece; see Fig. 11 for location. Primary plot features are the same as in Figs. 5, and 8. Seven significant rate increases can be tied to global mainshocks.

3.3. New Zealand

We examine a large catalog (329,044 $M \geq 1.0$ events) that encompasses the islands of New Zealand and note six significant earthquake rate increases that can be associated with global mainshocks (Figs. 13, 14). We interpret four of these rate increases as probable remote triggering based on our defined criteria of regional response without a clear local trigger (events labeled 2–5 on Fig. 14). The response labeled "6" in Fig. 14 falls into our category of possible remote triggering because the rate increase is caused by aftershocks of a $M = 6.7$ local mainshock that occurred 22.9 h after a $M = 7.2$ Aleutian Islands earthquake. Another rate increase we note falls into another category we call "swarm invigoration", where an ongoing swarm appears to be enhanced by the occurrence of a remote mainshock. In this case (event "3" on Fig. 14) an earthquake swarm just south of Rotorua in the Taupo Volcanic Zone was ongoing at the time of the 2008 $M = 8.1$ Antarctic plate earthquake, and then the rate of events doubled in the following 24 h. We note a few other cases of swarm invigoration in other regions.

In all we find 4 probable cases of remote dynamic triggering in New Zealand with the number of 0.5° by 0.5° subregions showing seismicity rate increases exceeding the 2σ threshold of 16.2 (Fig. 14).

3.4. Southeast China

We study a catalog of 6384 $M \geq 3$ events recorded in moderately active southeast China that is likely to be complete at that level (Mignan et al., 2013). This region was chosen for study because it is adjacent to the very active western Pacific subduction zones, and is thus an area that is frequently traversed by high amplitude surface waves from just outside our 1000 km exclusion zone. Despite this characteristic, we note only one possible case of remote triggering that is associated with a California mainshock, the 1989 $M = 7.0$ Loma Prieta earthquake (Fig. 15A). We consider this a case of possible remote triggering because all the activity is isolated within the 1989 Shanxi Datong earthquake swarm (Zhang et al., 1995), that began ~15 h after the global mainshock (Fig. 15B). Thus this could be coincidental or related.

3.5. Chile and Argentina

We sample a catalog in southern South America that contains 19,840 mostly $M \geq 4.0$ events from GSN sources (Fig. 16). We observe two significant rate increases that are not associated with local mainshocks. The first happened in 1994, and is temporally associated with a remote $M = 7.1$ New Zealand mainshock. The seismicity in Chile during the 24 h after this global mainshock is interesting because it begins about 2.9 h after the New Zealand earthquake, and consists of swarm-like M ~ 3.5 to M ~ 4.5 events (and likely many small magnitude events not present in the GSN catalog). Similar to the case described in China above, we classify this as possible dynamic triggering. The second rate increase we observe is associated with the 2010 $M = 8.8$ Maule earthquake and its

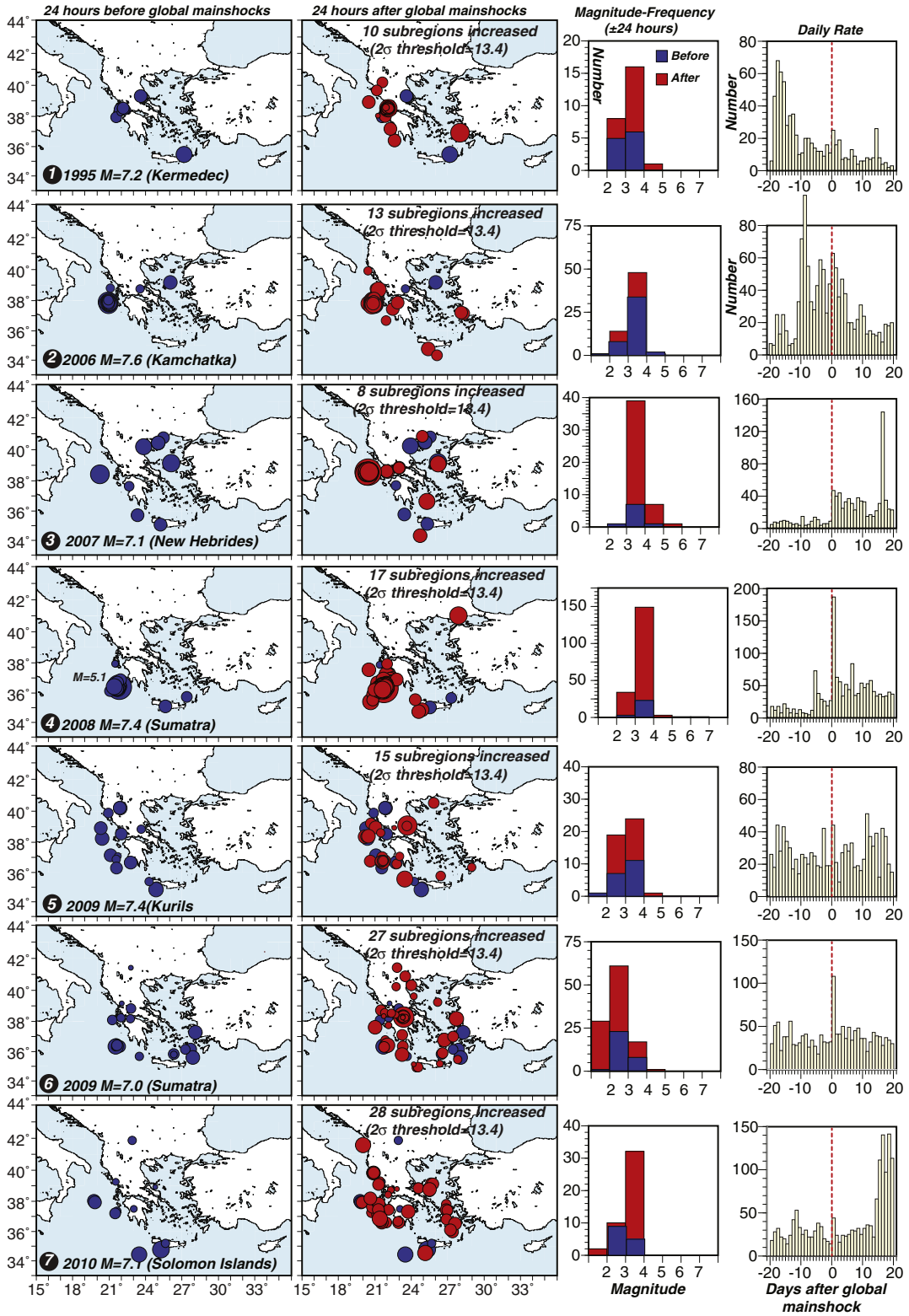

Fig. 11. Mapping of the significant rate changes associated with global mainshocks in Greece as identified and numbered in Fig. 10. Blue shading in the earthquake epicenters and magnitude frequency plots denotes 24-h periods before global mainshocks, and red shading 24 h after. Histograms show ±20 days around global mainshocks. There are four cases (events "4", "5", "6", and "7") of probable dynamic triggering because they affect a wide region, and are not associated with local mainshocks. Event "3" is associated with a long-term rate increase across Greece (see Fig. 12). Event "4" may have reinvigorated an aftershock sequence from a local $M = 5.1$ event that began about 6 h before the $M = 7.4$ Sumatran global mainshock.

aftershocks (Fig. 16A). The Maule shock occurred 10.6 h after a $M = 7.0$ Okinawa, Japan event. There currently is no way to know if this was remote triggering or if this was a coincidence; we thus classify it as possible dynamic triggering.

3.6. Baja California

A relatively small (777 $M \geq 4$ events) catalog from Baja California, Mexico (Fig. 17) has one significant rate increase that is associated

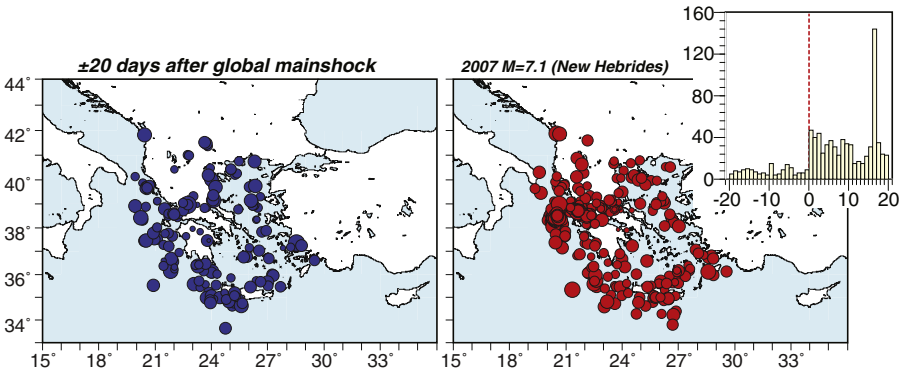

Fig. 12. Mapping of the persistent seismicity rate increase in Greece associated with a 2004 $M = 7.1$ New Hebrides mainshock (see also Fig. 11). In this figure the maps show 20 days of pre- and post-global mainshock events, and illustrate how regional the effects are.

with the 2012 $M = 8.6$ Indian Ocean earthquake (also noted by Gonzalez-Huizar et al., 2012; Pollitz et al., 2012). The largest possibly triggered earthquake that happened within 24 h of the global mainshock is a $M = 7.0$ event that was preceded by a cluster of several smaller earthquakes of $M = 3.7$ to $M = 6.1$. All activity is delayed by almost 20 h, though we do not know if smaller ($M \leq 4$) events began happening before that. It appears that the $M = 7.0$ earthquake may have been triggered locally because $M = 4.7$, $M = 4.9$, and $M = 6.1$ foreshocks happened 3.4 km, 6.1 km, and 19.4 km away respectively, meaning that local static or dynamic stress changes could have triggered the $M = 7.0$ event.

3.7. Australia

A catalog containing 15,754 $M \geq 1.0$ earthquakes covering the entire continent of Australia shows one significant rate increase that can be associated with a global mainshock, a 2001 $M = 7.5$ Indonesia event (Fig. 18). The delayed (14.5 h) response is spatially isolated compared with the mean variability in Australia, and we thus classify this as possible remote triggering. Remote triggering in Australia was noted by Velasco et al. (2008) and Gonzalez-Huizar and Velasco (2011) through high-pass filtering of broadband records; that these events do not emerge in catalog tests suggests that they are of low magnitude.

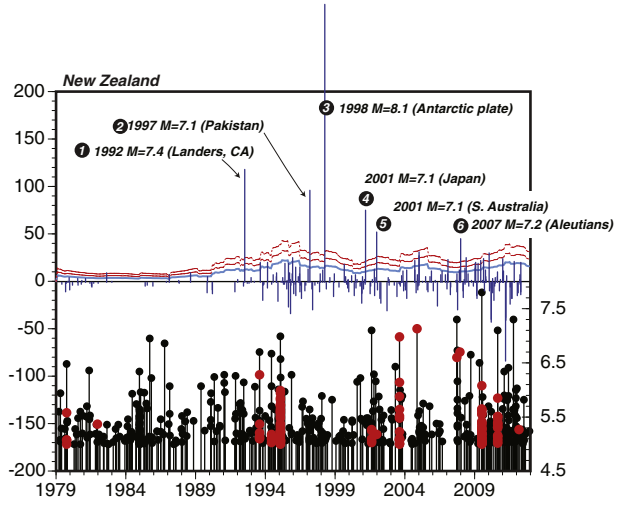

Fig. 13. Daily rate changes in New Zealand; see Fig. 14 for location. Primary plot features are the same as in Figs. 5 and 8. Five significant rate increases can be tied to global mainshocks.

3.8. Volcanic and geothermal regions

It has been pointed out that volcanic and geothermal areas may be especially susceptible to dynamic strains induced by seismic waves (e.g., Cannata et al., 2010; Hill et al., 1993; Hirosi et al., 2011; Manga and Brodsky, 2006; Miyazawa, 2011; Moran et al., 2004; Surve and Mohan, 2012), though triggering is certainly not confined to these settings (e.g., Brodsky et al., 2000; Gomberg et al., 2003). We study three volcanic centers, the Coso geothermal field of southeast California, USA, the Yellowstone Caldera in Wyoming, USA, and the Hawaiian Islands (Fig. 19). All three cases show between 4 and 5 possible episodes of remote dynamic triggering, but none stand out as being significantly more susceptible than other regions that we have examined. The Coso and Yellowstone sites have examples that we classify as probable remote triggering based on our 0.5° by 0.5° subregion criteria, however, these areas are very small (1° by 1°) compared with other catalogs we study, and virtually any seismicity rate increase could affect much of the catalog areas in these cases. The larger (1° by 2°) Hawaiian Islands site shows four cases of possible remote triggering (affecting from one to three 0.5° by 0.5° subregions vs. a 2σ threshold of 4.6).

3.9. Global subduction zones

We have examined catalogs from mixtures of every type of tectonic setting, and while each may have a dominant strain mechanism, all have strong variation. An opportunity exists to isolate mechanisms through an earthquake catalog specific to global subduction zone interfaces; the catalog consists of 3281 $M \geq 5$ events that have been identified as being directly on the interplate contact in global subduction zones by Heuret et al. (2011), and ends in 2007. We find no significant rate increases in the subduction interface catalog that are associated with global mainshocks when we apply the methods that we use on regional catalogs (Fig. 20A). If we extend the analysis to ± 10 day rate changes we find three significant increases, all related to individual large subduction events and their aftershocks (Fig. 20B). Of course the odds of having other large earthquakes occur randomly increases with the longer period we consider, which illustrates the confounding nature of delayed dynamic triggering. As long as the number of possibly triggered large earthquakes is small, it becomes very difficult to establish any causation. The lower magnitude threshold in the subduction zone catalog is $M \sim 5$, similar to the global catalog used by Parsons and Velasco (2011). It is therefore difficult to know if the subduction setting is not conducive to triggering, or if it is a magnitude effect.

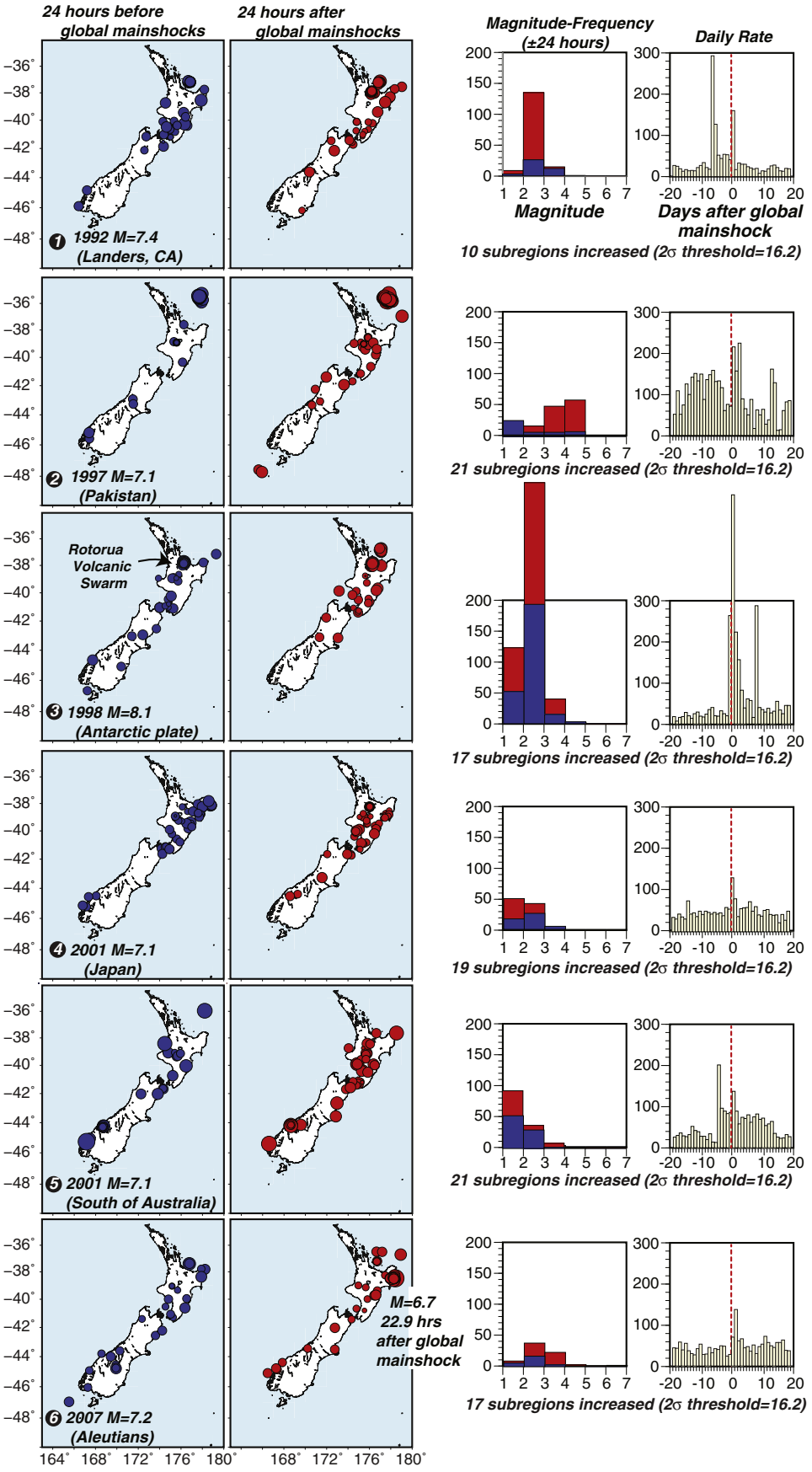

Fig. 14. Mapping of the significant rate changes associated with global mainshocks in New Zealand as identified and numbered in Fig. 13. Blue shading in the earthquake epicenters and magnitude frequency plots denotes 24-h periods before global mainshocks, and red shading 24 h after. Histograms show ±20 days around global mainshocks. We consider cases "2" through "5" as probable dynamic triggering because they appear to affect a wide region, and are not necessarily associated with a single local mainshock. Event "6" is a case of possible remote triggering because the rate increase is entirely the result of aftershocks from a $M = 6.7$ event that occurred ~23 h after a $M = 7.2$ Aleutian Islands mainshock, which could be coincidental.

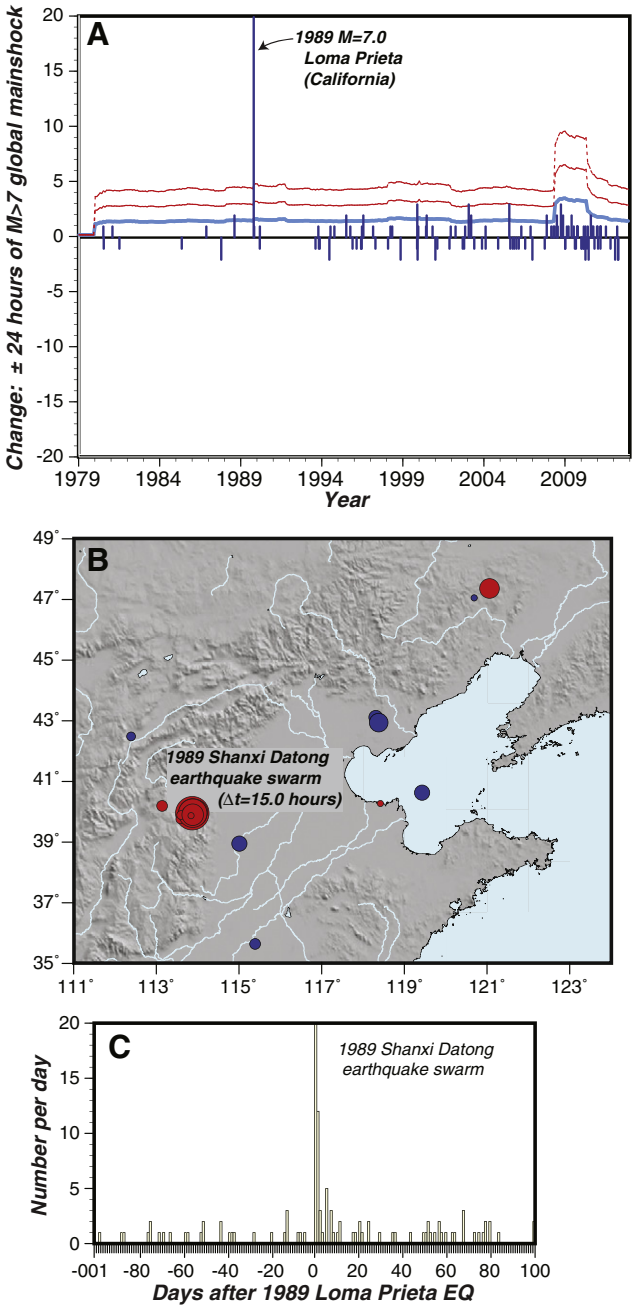

Fig. 15. (A) One global mainshock, the 1989 $M = 7.0$ Loma Prieta earthquake in northern California, is temporally correlated with (B) the onset of the Shanxi Datong earthquake swarm in southeastern China (e.g., Zhang et al., 1995), which began ~15 h later, and occurred in (C) an otherwise seismically quiet period.

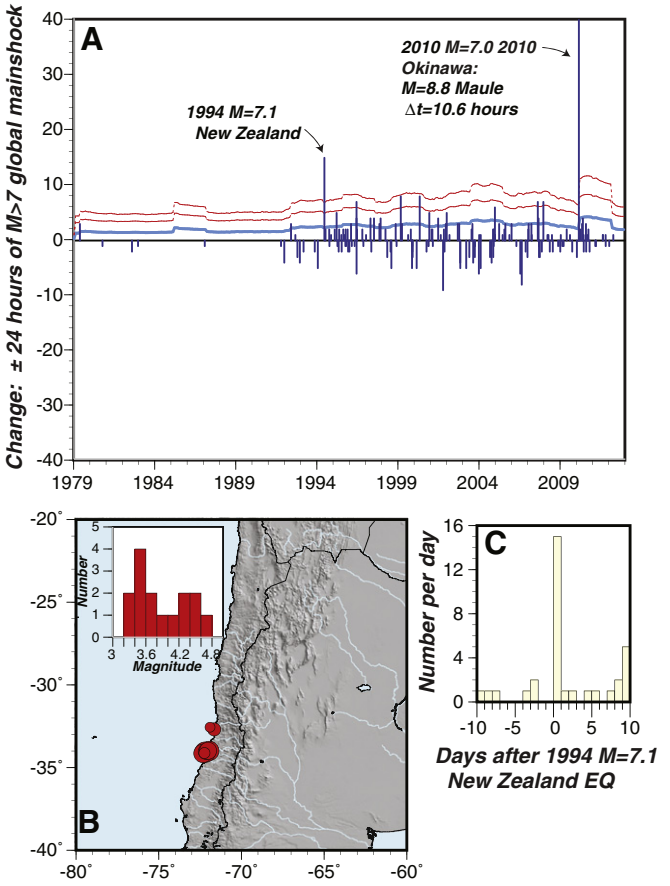

Fig. 16. (A) A 2010 $M = 7.0$ mainshock in Japan can be temporally associated with the $M = 8.8$ Maule, Chile event 10.6 h later, or it could be coincidental. A 1994 $M = 7.1$ New Zealand event, is temporally correlated with (B) a cluster of earthquakes in coastal Chile. The events do not appear to be associated with a local mainshock, as the histogram of magnitudes indicates. The duration (C) of the rate increase is less than 24 h.

3.10. All catalogs

We describe one last test using the regional catalogs that combines them all together. The idea here is that perhaps global mainshocks each cause subtle rate increases everywhere, but when examining any one region they are not significant. We could potentially detect this behavior by stacking all the catalogs together and analyzing them simultaneously. However when do this, we find no rate increases beyond those already found in our region-by-region studies (Fig. 21). This points again to a conclusion that stress, faulting, and surface wave polarization conditions may need to be optimal for remote dynamic triggering to occur (e.g., Gonzalez-Huizar and Velasco, 2011; Hill, 2008; Parsons et al., 2012). We also point out that coincidences do occur; a $M = 7.0$ shock in Japan happened just 3.2 min after a 2007 $M = 7.1$ Vanuatu earthquake, too soon for the fastest seismic waves to have traveled there (Fig. 21).

3.11. Regions with no evidence of dynamic triggering

We focused on describing regions with at least possible remote triggering responses in the sections above. These represent about half of the catalogs studied (12 of 21) (Fig. 22). We briefly comment here on the regions that showed no evidence of remote triggering. These catalogs include some continental interior regions like East Africa, and the New Madrid area of the central United States. Our observations are consistent with the results of Iwata and Nakanishi (2004) and Harrington and Brodsky (2006) in that Japan does not appear very susceptible to remote triggering. A similar high strain rate subduction zone setting in south-central Alaska also does not exhibit any significant rate changes that can be associated with global mainshocks. The very active Sumatra region has had so many local $M \geq 7$ earthquakes that it might be very difficult to find rate increases associated with remote mainshocks because the local seismicity rates are already so high. Similarly, we could not identify significant rate increases along the North Anatolian fault zone of Turkey. A detailed catalog in the Apennines of Italy showed no significant rate increases, nor did a catalog centered on the Philippine Islands.

Single station analyses of Global Seismograph Network (GSN) stations revealed at least twofold rate increases at some stations in every region that we examined (Velasco et al., 2008). That these events are

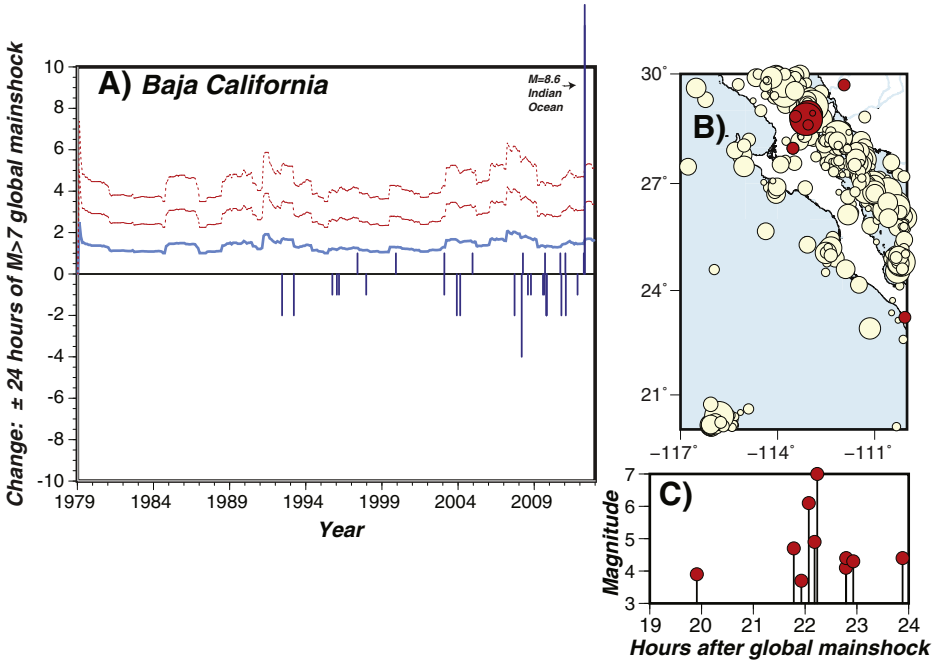

Fig. 17. One global mainshock, the 2012 $M = 8.6$ Indian Ocean earthquake, is temporally correlated with a cluster of earthquakes in (B) the Gulf of California (red events). The primary cluster is shown as a time series vs. magnitude in (C); in this case the largest event ($M = 7.0$) is not the first to occur, but is preceded by smaller shocks. The first event in the series is a $M = 3.9$, almost 20 h after the Indian Ocean mainshock, though we do not know if smaller events began sooner.

not picked up in regional catalogs suggests that they have very low magnitudes, or were masked and/or interfered with during the passage of surface waves.

4. Interpretation of observations

The first important conclusion we draw about remote earthquake triggering is how rare it is. In any one region we see at most 7 cases of possible or probable remote triggering out of 260 candidate mainshocks that are more than 1000 km away. These are cases that can be detected at the threshold magnitudes in our catalogs, which range from $M = 1.0$ to $M = 4.0$. A first quantification of the probability yields at most a ~3% chance of a remote mainshock causing a ~2σ local earthquake rate increase in any of the zones considered in this analysis.

We note four regions where we see at least one case of probable remote triggering, defined here as a widespread seismicity rate increase (affecting a significantly larger number of 0.5° by 0.5° subregions than normal variation) that can be associated with surface waves of a remote earthquake. The four regions are: (1) the Basin and Range Province and (2) Northern California of the western United States, (3) Greece, and (4) New Zealand. These four regions represent a full range of tectonic environments that include strike-slip, extensional, and subduction zones. One feature they all have in common is the presence of volcanic centers. However, when we focus just on magmatic provinces such as Yellowstone Caldera, the Coso Geothermal center, and Hawaii, we do not find them to be especially responsive to passing seismic waves (Fig. 19).

A slight majority (22 of 40) of seismicity rate increases that can be associated with global mainshocks are those we classify as possible remote triggering. These are isolated clusters of earthquakes that typically begin with a moderate magnitude earthquake ($M = 4$ to $M = 6$), and are followed by their aftershocks. It is impossible to know if

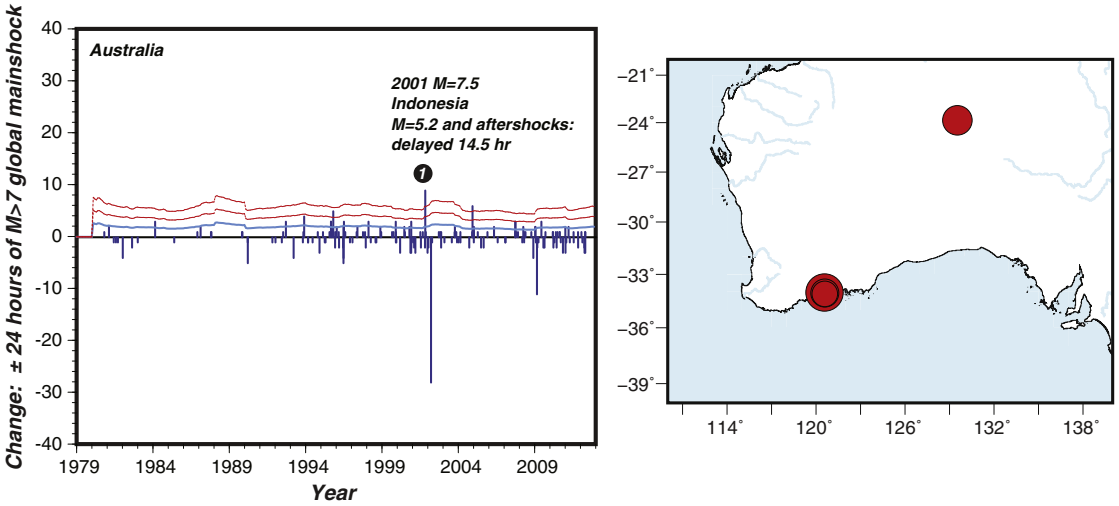

Fig. 18. One global mainshock, a 2001 $M = 7.5$ Indonesia earthquake, is temporally correlated with a $M = 5.2$ local mainshock that was delayed by 14.5 h after surface waves.

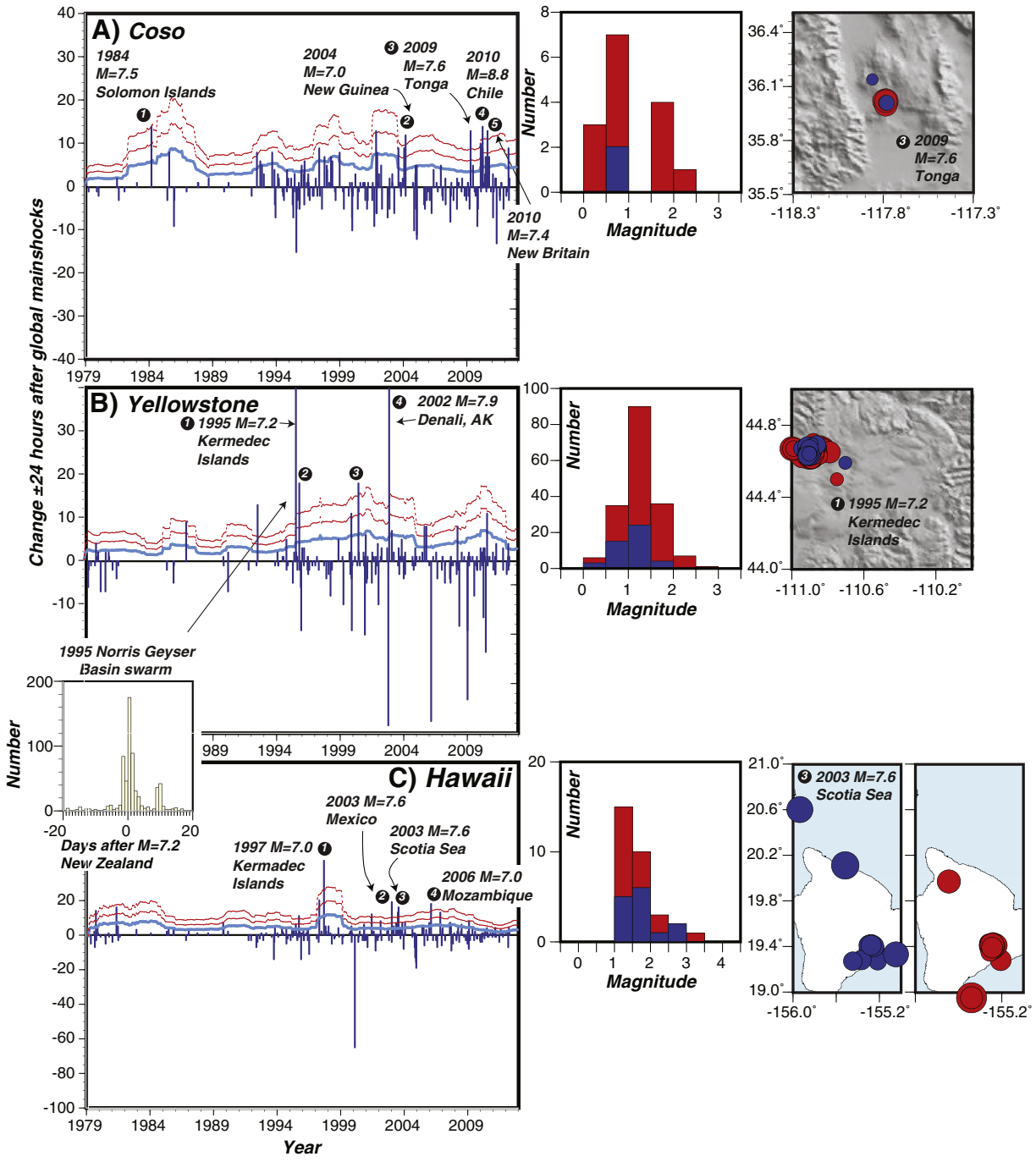

Fig. 19. Three sample volcanic centers are studied, and example maps are shown that typify responses. (A) The Coso volcanic center of southeast California, USA yields five significant rate increase that can be associated with global mainshocks. (B) The Yellowstone caldera region of Wyoming, USA shows four significant rate increases, the first is associated with a 1995 Kermedec Islands mainshock and appears to be a swarm invigoration, affecting the Norris Geyser Basin swarm (see inset histogram). Additionally, responses from a 1995 $M = 8.0$ Mexico ("2"), and 2000 $M = 7.9$ Indonesia ("3") mainshocks are noted along with the already-discussed regional response to the 2002 M=7.9 Denali earthquake ("4") (Fig. 3). In (C) the Hawaiian Islands are shown to have four significant rate increase that can be associated with global mainshocks."

these are precipitated by passing seismic waves, or if they are simply coincidental; tests with the global catalog using random mainshock times show that the expected number of coincidental moderate local events is not surpassed by the observations (Fig. 7).

We show detailed temporal histories of earthquake responses in the four primary regions where we see remote triggering in Figs. 23 and 24. A spectrum of responses is evident that ranges from immediate, swarm-like behavior after seismic waves arrive, to activity that is delayed by many hours. Delayed responses tend to be the local moderate event with aftershocks cases that we call possible remote triggering. There is no consistent observation that delayed responses are preceded by any sort of gradual build-up of seismicity (Figs. 23, 24), with just one example in Baja California (Fig. 17).

4.1. Insights into remote $M \geq 5$ earthquake triggering

One of the key goals of this review is to simultaneously observe a broad magnitude spectrum of remote earthquake triggering by using regional networks that have catalogs complete to the ~$M = 2$ level. We already know that $M > 5$ earthquakes do not occur immediately

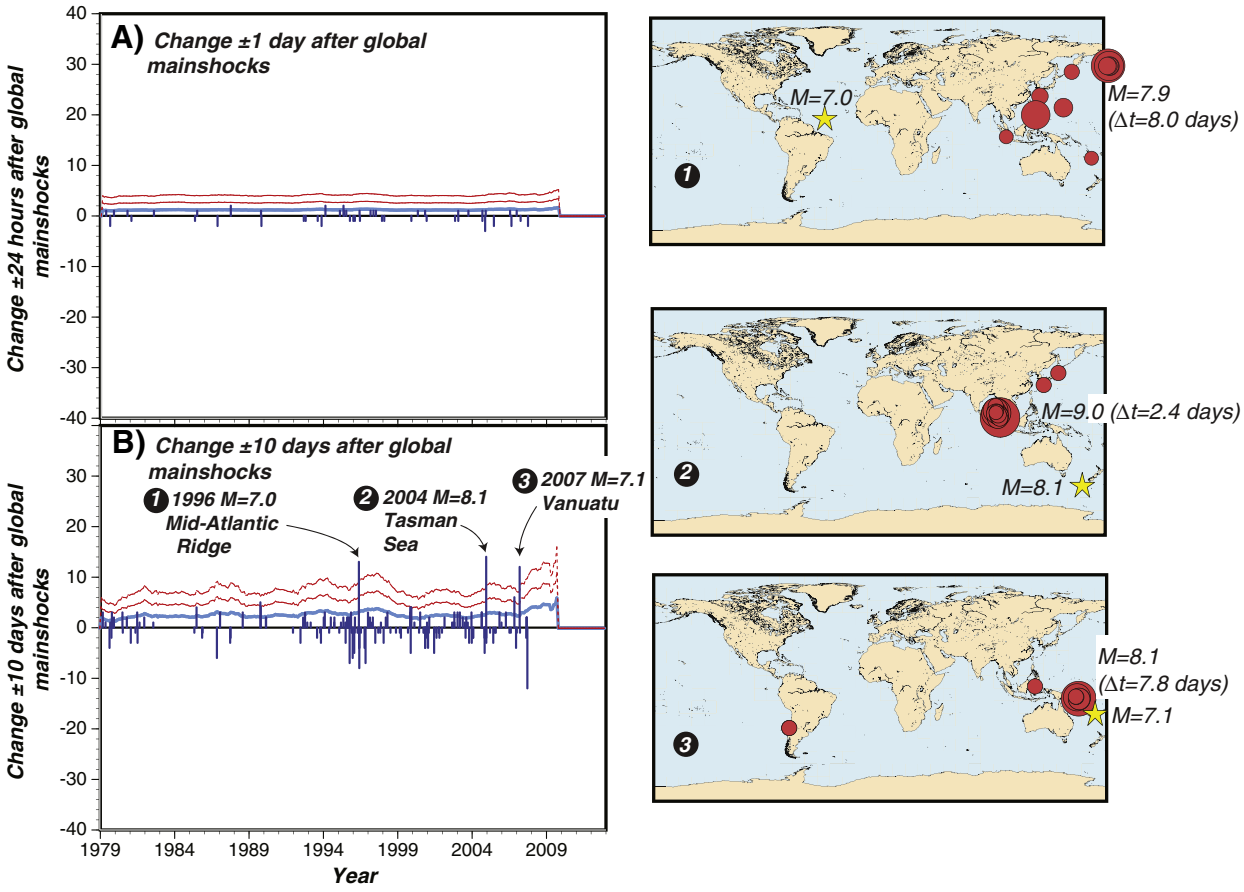

Fig. 20. We study a global subduction interface catalog assembled by Heuret et al. (2011), and (A) note no significant associations between these events and remote global mainshocks after 24 h. However it is possible to associate (B) rate increases in three cases if a 10-day period is examined.

during surface wave arrivals (Fig. 25), but detecting delayed $M > 5$ triggering is difficult because if there is a signal, it cannot be isolated from generally high global activity levels (e.g., Huc and Main, 2003; Parsons and Velasco, 2011). We obviate the problem of possibly missing delayed $M \geq 5$ earthquakes that might be overlooked by stacking global catalogs by using regional $M > 2$ catalogs. We therefore investigate the question of whether remote triggering rates are too low for the comparatively rare $M \geq 5$ events to be expected, and/or whether higher magnitude remotely triggered earthquakes are always delayed.

We can illustrate the potential problem of searching the stacked global catalog for remote $M > 5$ triggering by combining all the regional results where we observed either possible or probable remote triggering into a single magnitude-frequency distribution (Fig. 26). The distribution appears to have a significant deficit of lower ($M < 2.5$), and higher ($M > 4.5$) magnitude events relative to a linear Gutenberg and Richter (1954) ($\log(N) = a\text{-}bM$) relation. The likely cause on the low-magnitude end is variation in detection thresholds of different regional networks. The taper on the high-magnitude end could be caused by small a-values (activity levels) in each regional response such that expected $M > 5$ rates are low. Alternatively, higher magnitude events may be absent for physical reasons. This sort of taper in magnitude–frequency distributions is commonly observed (e.g., Kagan, 1993), and can be simulated with multiple catalogs with different maximum magnitude thresholds (e.g., Geist and Parsons, 2014; Sornette et al., 1991).

We examine individual magnitude–frequency distributions from regional probable and possible remote triggering episodes, and extrapolate them assuming a cumulative Gutenberg–Richter distribution to find the expected 24-h $M \geq 5$ triggered earthquake numbers for each response (Table 1). The expected number of $M \geq 5$ events is extrapolated using a b-value (slope) of 1.0 from event rates at the thresholds given in Table 1. Of the 28 responses we examine, 8 (29%) have high enough activity rates such that at least one $M \geq 5$ earthquake might have been expected. Of those, 3 (11%) are associated with at least one $M \geq 5$ shock. In 5 other instances (18%), no $M \geq 5$ events were observed despite high rates at lower magnitudes. This result implies that in most cases, remote $M \geq 5$ triggering is not observed because the overall triggered rates are very low. When we restrict the analysis to just probable cases, there are only 3 responses where $M \geq 5$ seismicity would be expected during the first 24 h, and of those, one where $M \geq 5$ earthquakes were actually observed (Table 1). Thus one explanation for the absence of remote $M \geq 5$ triggering is that the numbers of remotely triggered earthquakes are too small for high magnitudes to be observed in most cases, and that the delayed higher magnitude events we do observe are primarily coincidental. If however the possible cases that involved possibly delayed higher magnitude triggering are accepted (e.g., Gomberg and Bodin, 1994; Gonzalez-Huizar et al., 2012; Pollitz et al., 2012; Tzanis and Makropoulos, 2002), then more interpretation is necessary.

4.2. Interpretation of possibly delayed $M \geq 5$ earthquake triggering

Remotely triggered $M > 5$ earthquakes are not observed during surface wave passage (Fig. 25), though we do note a persistent minimum delay time of $t \geq 9$ h for possibly triggered $M > 5$ earthquakes (Fig. 27). It is unclear how important the 9 h mark is; the compilation shown in Fig. 27A has the potential to be misleading because there are two $M > 7$ possibly triggered aftershocks that happened ~9–10 h after surface wave arrivals (the 2010 $M = 8.8$ Maule, Chile earthquake and a $M = 7.4$ aftershock), and that are associated with their own numerous $M > 5$ local aftershocks. These subsequent aftershocks give extra weight

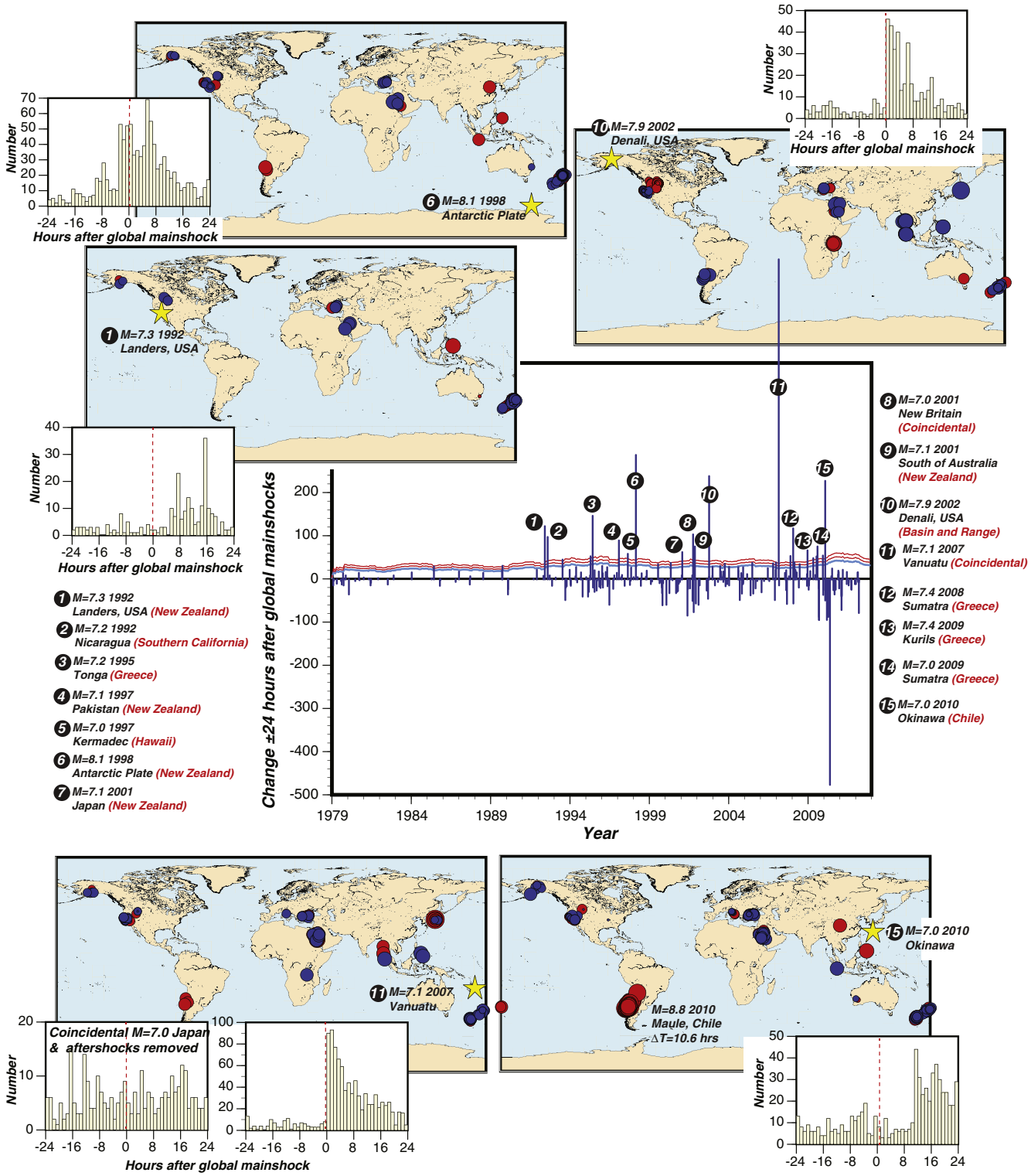

Fig. 21. Analysis of 21 combined catalogs. When catalogs are stacked together, none of the 260 global mainshocks shows any evidence for significant rate changes beyond those already identified as affecting a single region. The exception is the $M = 7.1$ Vanuatu event labeled "11", which is associated with a coincidental $M = 7.0$ shock in Japan that happened only 3 min later, before its seismic waves arrived in Japan.

to the 9-h threshold. We therefore make the same plot in Fig. 27B with all post-Maule aftershocks removed from the catalog. This removes most of the $M > 5$ events and makes the 9-h transition less distinct.

As there is uncertainty whether cases of possible remote triggering are in fact coincidental, we plot only the incidences of probable triggering in Fig. 27C. In this case there is only one $M > 5$ event, a $M = 6.0$ event triggered in Greece ~9.5 h after a 2008 $M = 7.4$ mainshock in Sumatra. This again highlights a repeated result that we find; it is difficult to unequivocally associate $M > 5$ earthquakes with passing seismic waves even if a delay of up to 24 h is allowed. Finally, we plot just the highest magnitude earthquakes from each possible and probable triggering response vs. time in Fig. 27D, but the delay for larger magnitudes is

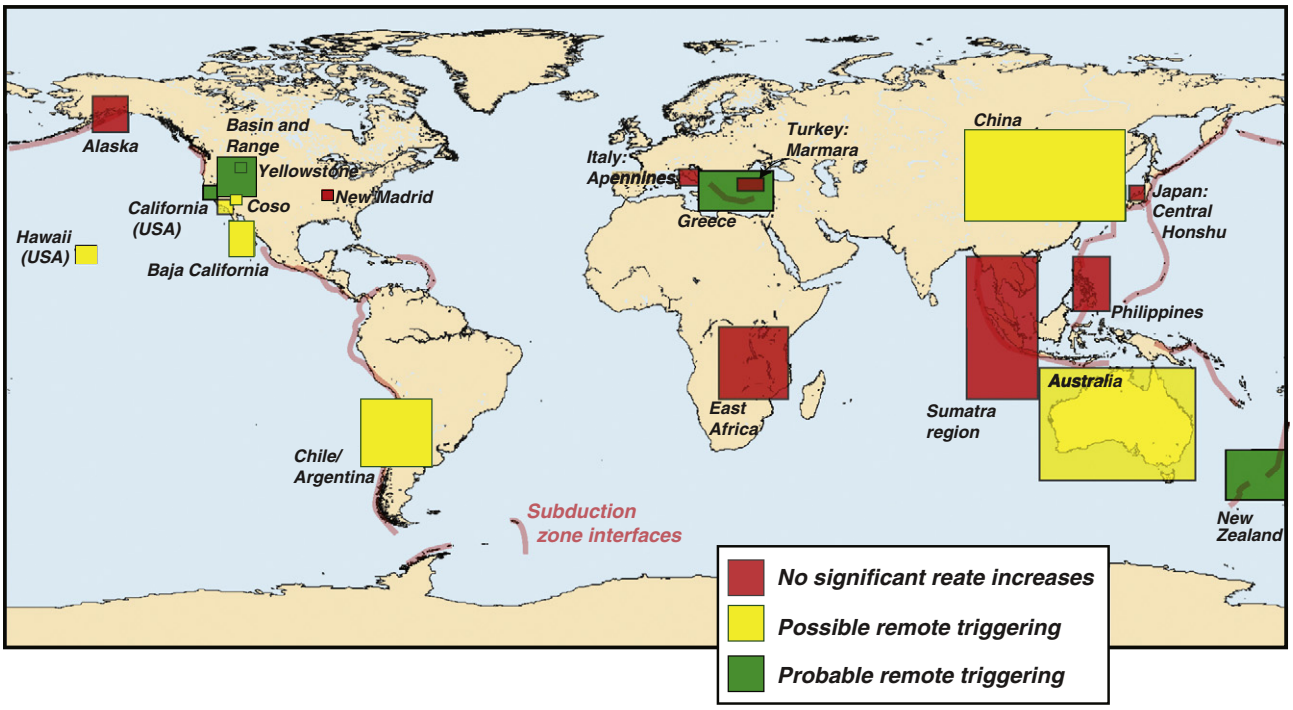

Fig. 22. Mapping of regional catalogs shaded based on our interpretation of remote triggering response. About 50% of the catalogs we studied showed possible remote triggering, and ~20% showed probable remote triggering.

still evident. By contrast, immediate increased rates of lower magnitude earthquakes can be clearly associated with surface wave arrivals (Figs. 23, 24, 27).

We gain some insight into the possibility that the apparent delayed $M > 5$ triggering response is a chance occurrence by conducting the following test. We assemble the magnitude distributions from the possible and probable triggered events plotted in each panel of Fig. 27 (also including those with smaller magnitudes not shown). We assemble the occurrence times of these events in separate distributions. We re-associate magnitudes and times at random across 100 trials, and then track the first occurrences of $M \geq 5.0$ and $M \geq 6.0$ earthquakes. These tallies are shown as histograms in Fig. 28 along with the input distributions. From these histograms we can show the frequency of outcomes when the earliest remotely triggered $M \geq 5.0$ and $M \geq 6.0$ earthquakes could be expected to occur in the absence of any delaying physics. From these tests, we note that it would be unlikely for the >9 h delay to occur given observed magnitude distributions, but possible, with 96% to 100% of the simulations having $M \geq 5.0$ earthquakes happening before 9 h pass. The exception to this is the probable-triggered catalog from Fig. 27C, because it contains only one $M \geq 5.0$ event.

4.3. Delayed dynamic earthquake triggering and tremor in Greece

We identified an intriguing, apparently long-lived (at least 20 days) seismicity rate increase that swept across most of Greece after a 2007 $M = 7.1$ New Hebrides mainshock (Figs. 11, 12). The period between September 2006 and May 2007, encompassing the occurrence of the $M = 7.1$ New Hebrides event, was identified as a "seismic crisis" with swarm characteristics by Bourouis and Cornet (2009). While all these events are temporally correlated, it is of course difficult to know if there is causation. To learn more, we apply a band-pass filter (corner frequencies 2–8 Hz) to regional broadband records to remove surface waves and identify local events. In Fig. 29 we show broadband recordings after the implementation of a low-pass (0.01–0.1 Hz in Fig. 29A, traces 1–3), and a high-pass filter (2–8 Hz in Fig. 29A, traces 4–5) that reveals local events triggered by the global mainshock (Fig. 29B) and triggered tremor (Fig. 29C). Tremor can be seen at frequencies of up to 8 Hz, meaning that the observation is locally sourced and not remnant teleseismic energy (e.g., Peng et al., 2011b). Triggered tremor has been identified in different geotectonic environments worldwide (e.g., Peng et al., 2009; Rubinstein et al., 2009) and can be initiated by the passing of seismic waves from distant sources.

In Fig. 29A we show triggered regional seismicity that corresponds with the S-wave arrival in the high-passed traces of the radial and transverse horizontal components (traces 4 and 5), and triggered tremor with small amplitudes (10^{-5} cm/s) that initiates approximately with the P-wave arrival. We have identified at least 5 more tremor episodes in the first few hours following the mainshock. Shelly et al. (2011) report that triggered tremor may be a possible mechanism for delayed dynamic triggering, which in this case may explain the persistent seismicity rate increase associated with the 2007 $M = 7.1$ New Hebrides mainshock. We note that this is the first identification of triggered tremor in Greece, and that the Corinth Gulf offers a favorable location since the active deformation is related with low-angle normal faulting at seismogenic depths (e.g. Chao et al., 2012) in the back-arc extensional province of the Hellenic subduction zone (Vassilakis et al., 2011). The relationship between the ambient and triggered tremor could provide a physical mechanism to explain the apparent low triggering threshold in central Greece suggested by Brodsky et al. (2000).

4.4. Possible causes of delayed dynamic earthquake triggering

As long as the possibility exists that dynamic triggering of hazardous earthquakes by seismic waves can be delayed, then there is a need to quantify the probability of this, and to understand the physics behind it. In contrast to possible remote triggering observations, the timing of near-source $M > 5$ earthquakes (presumed to be caused by static stress changes) has no apparent magnitude dependence (Fig. 30). At near range, $M > 5$ aftershocks begin immediately, and follow an Omori-law temporal decay that is similar from hourly to yearly time scales. Therefore if we follow the alternative interpretation of our observations, that the lack of immediate $M > 5$ earthquake triggering from remote sources

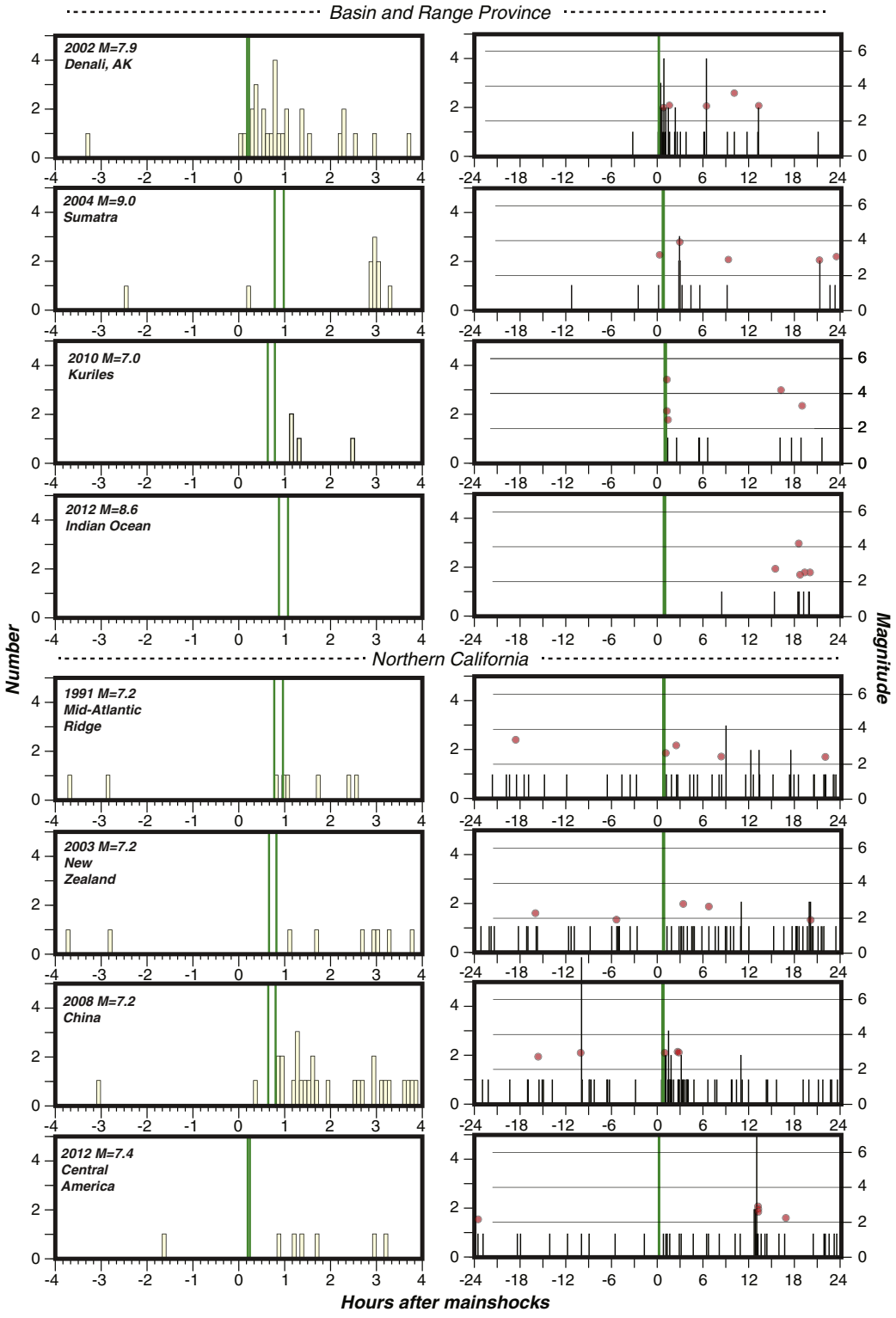

Fig. 23. Temporal details of seismicity rate increases associated with global mainshocks in the Basin and Range Province and in Northern California. The green bands give the time range when surface wave arrivals are expected. Histograms on the left side show ±4 h periods at 10-min intervals, and the right side shows ±24 h periods at hourly intervals.

is not because of low overall activity, and that the delayed events are not coincidental, then possibly different failure mechanisms implied by a static stress increase vs. a cyclical dynamic load might explain magnitude dependent triggering delays. Here we review some physical models for delayed dynamic triggering, and consider the possibility of magnitude dependent delay.

Teleseismic waves are known to affect groundwater levels and pressures (e.g., Roeloffs, 1998). Therefore an increase in pore fluid pressure acting on a fault surface could oppose the component of stress acting normal to the fault surface, reducing its effective friction. Brodsky et al. (2003) proposed a mechanism to explain sustained pore fluid pressure changes through shaking-induced permanent changes in

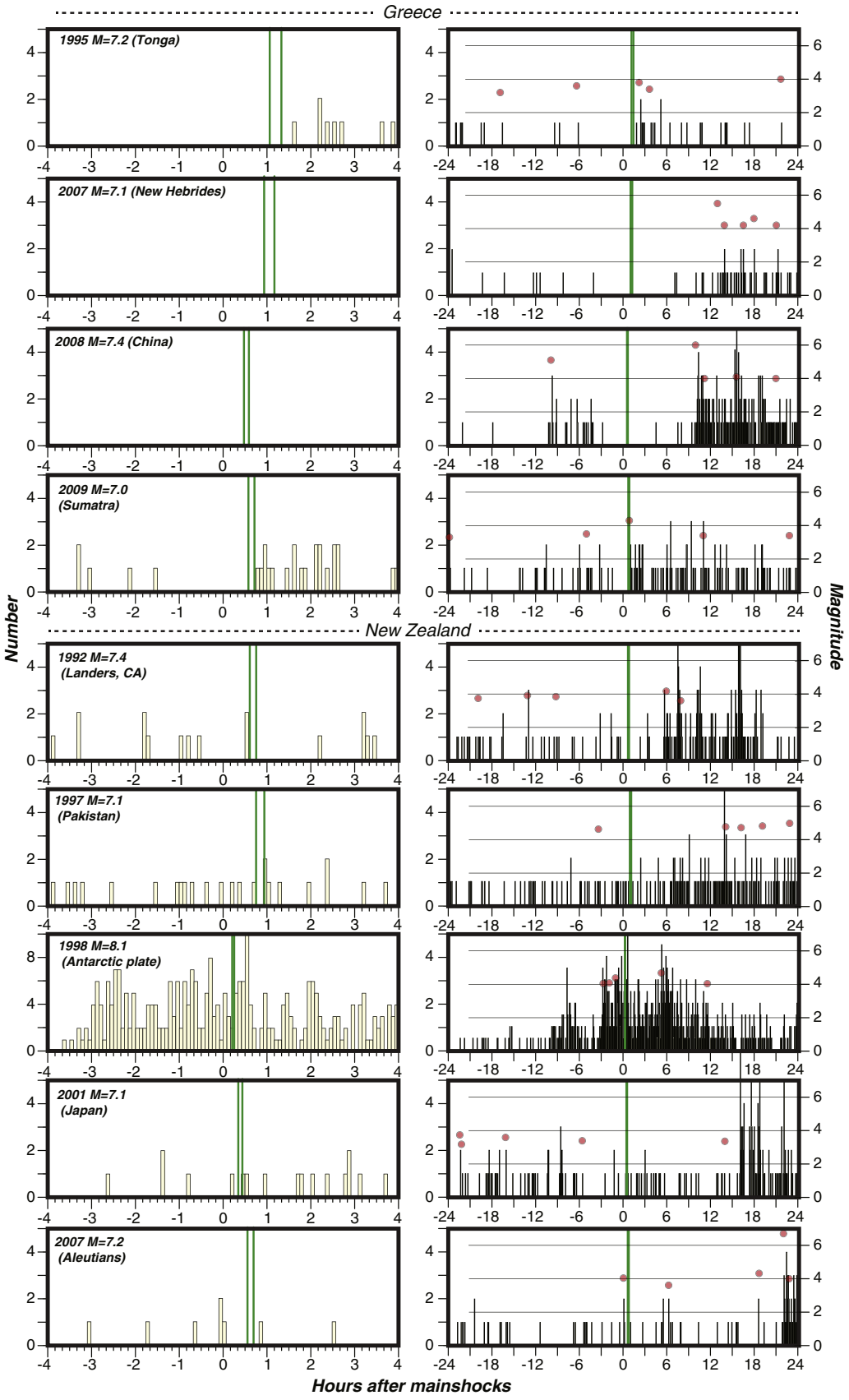

Fig. 24. Same as Fig. 23 except triggering in Greece and New Zealand is shown.

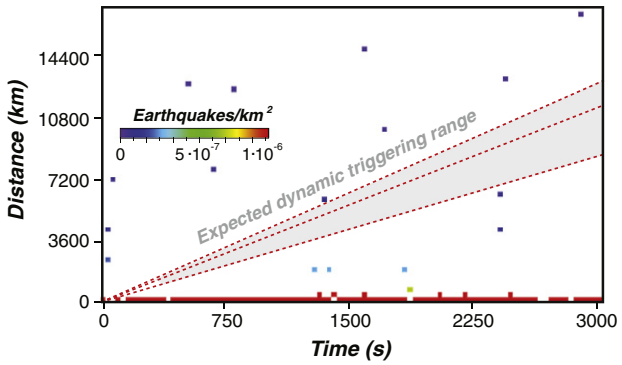

Fig. 25. Global $M > 5$ earthquake density (earthquakes/km^2) during surface wave arrivals from 205 $M \geq 7$ remote mainshocks (after Parsons and Velasco, 2011). Zero $M > 5$ activity is associated with surface wave arrival times (gray shaded area).

fluid flow pathways. Fluid migration in faults can take minutes to hours to respond to imposed normal stress changes (e.g., Lupi et al., 2011), which might explain delayed dynamic earthquake triggering. Work on seismically triggered landslides suggests that full dissipation of elevated pore fluid pressure can take from several years up to decades, allowing significantly delayed failure (e.g., Biscontin and Pestana, 2006; Biscontin et al., 2004; Kokusho and Kojima, 2002). Further work is necessary to extend pore fluid models to explain magnitude dependent delayed triggering if it occurs.

Another delaying mechanism was observed by Peng et al. (2011a), who found correlations between seismicity rate increases and surface wave arrivals. Delays occur because seismicity rate changes are correlated to the first surface wave arrivals, and also to additional phases that circle the globe more than once. The added travel time associated with these additional phases leads to delay relative to mainshock origin times. It is unclear if these later phases would have different ability to trigger higher magnitude events.

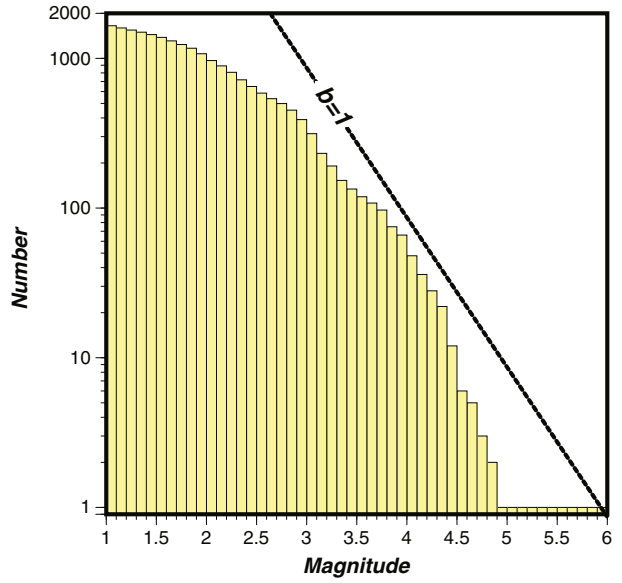

Fig. 26. Magnitude–frequency distribution of all possible and probable triggered events from regional network catalogs shown in Figs. 6, 8–19 and given in Table 1. This plot illustrates how the catalogs are incomplete both on the lower and upper magnitude ranges. The magnitude roll-offs demonstrate the need to examine each regional response individually.

In addition to the case that we present for Greece, there are many observations of dynamically triggered non-volcanic tremor beneath fault zones. Shelly et al. (2011) identify patterns of migrating tremor along the San Andreas fault zone that move more slowly than the seismic phases that triggered them, and that may be tied to creep episodes. Stress changes related to slow slip can then lead to delayed earthquake triggering.

A possible explanation for a characteristic delay time for higher magnitude dynamically triggered aftershocks might come from ideas about fault zone damage and rate and state friction theory (Dieterich, 1979). We consider a hypothesis that, rather than stressing a fault zone to failure, seismic waves instead change the physical properties of a fault zone such as the critical slip distance D_c (e.g., Parsons, 2005). The D_c property is the distance a fault patch must slip before it weakens to the point of earthquake nucleation. Physically this can be thought of as proportional to the displacement required to renew a population of fault contacts (Dieterich, 1979), or as a function of localized shear strain in a fault gouge layer (Marone and Kilgore, 1993). A sudden reduction in the critical slip distance is calculated to result in an advance in earthquake timing that is proportional to that reduction (Fig. 31). Another assumption is necessary to explain magnitude dependent delay, which is that total slip and/or stress drop depend on D_c (e.g., Abercrombie and Rice, 2005; Cocco et al., 2009; Guatteri and Spudich, 2000; Kato, 2012; Mikumo and Yagi, 2003; Okubo and Dieterich, 1984; Tinti et al., 2005, 2009; Uenishi and Rice, 2003), with larger slip implied by larger D_c.

So, if maximum slip in an earthquake is a proxy for magnitude (e.g., Wells and Coppersmith, 1994), we might carry the argument further that a higher magnitude earthquake would have some parts of its rupture area characterized by proportionately larger D_c values as compared with a low magnitude rupture. Thus a small rupture could occur immediately if its D_c values were reduced significantly, whereas a larger rupture might experience delayed triggering (Fig. 31) if D_c is reduced only part of the amount needed to cause unstable slip.

To summarize fault-zone damage concepts, the following incidents would occur: (1) surface waves pass through a fault, (2) shaking either directly affects physical parameters of the fault zone, or fluid pressure changes alter physical properties, (3) the critical slip distances (D_c) that characterize rupture are affected more or less consistently, (4) smaller D_c patches are reduced significantly, leading to immediate failures at lower magnitudes, (5) patches with larger D_c that are associated with greater maximum slip are reduced such that they do not fail immediately, but are still advanced from the change, and (6) these larger slip (hence magnitude) patches fail after a delay. Alternatively, after step (2), a model such as that proposed by Brodsky et al. (2000) could be operating, and since a larger earthquake involves a greater rupture area, it may take time for the fluid migration influence to manifest.

4.5. Delayed higher magnitude dynamic triggering and speculation about earthquake nucleation models

If it is again assumed that higher magnitude dynamically triggered earthquakes require more time to occur than smaller ones, then there are some comments than can be made about different earthquake nucleation models. It further must be assumed that static stress triggering operates differently, by affecting large target fault areas simultaneously and for longer periods than cyclical dynamic stressing.

Earthquakes grow from a seed point, the hypocenter, and spread with time from there. Some stall near the hypocenter, while others grow into great earthquakes (e.g., Iio, 2011 and references contained therein). Conceptual and observational views on the issue of magnitude and nucleation can be broken into three categories. In (1) the cascade model, all earthquakes begin the same way and conditions (i.e., stress, geometry) on a fault surface govern whether the rupture will grow into a large earthquake, or stay small (e.g., Bak and Teng, 1989; Brune, 1979; Dieterich and Richards-Dinger, 2010; Ellsworth and Beroza, 1995; Kato, 2008; Kilb and Gomberg, 1999; Lapusta and Rice, 2003;

Table 1
Expected and observed numbers of $M \geq 5$ earthquakes in the 24-h after surface wave passage from global mainshocks in regions with possible or probable remote triggering observations. 'BRP' is the Basin and Range province of the western U.S., 'NCAL' and 'SCAL' stand for northern and southern California respectively, and 'NZ' is New Zealand. The expected number of $M \geq 5$ earthquakes applies to the first 24 h after surface wave arrivals as extrapolated from the given magnitude levels. Maximum M observed also applies to the initial 24-h period, whereas the observed daily $M \geq 5$ rate is the averaged long-term rate over catalog durations. The factor increased gives expected $M \geq 5$ rate increases during the first 24 h after surface wave arrivals calculated from the expected 24-h $M \geq 5$ numbers. The "•" symbols mark cases of probable remote triggering.

Region	Year	Expected # $M \geq 5$	Max M Observed	Extrapolated from $M=$	Source locn.	Obs. daily $M \geq 5$ rate	Factor incr.
BRP	2002	0.26	3.6	2.1	Denali •	0.0058	45.4
BRP	2004	0.10	3.9	2.8	Sumatra	0.0058	17.9
BRP	2010	0.06	4.8	2.6	Kuriles	0.0058	10.4
BRP	2012	0.06	4.2	2.4	Indian Ocean	0.0058	10.0
NCAL	1991	0.03	3.1	2.3	Mid-Atlantic •	0.0024	14.3
NCAL	2003	0.04	2.8	1.2	New Zealand •	0.0024	14.7
NCAL	2008	0.05	3.0	2.5	China •	0.0024	20.7
NCAL	2012	0.03	2.9	2.0	Central America	0.0024	13.2
SCAL	1992	0.21	3.2	1.7	Nicaragua •	0.0071	29.4
SCAL	2010	0.13	4.9	2.9	New Britain	0.0071	17.7
Greece	1995	0.51	4.0	3.1	Kermedec	0.0183	28.0
Greece	2006	1.57	4.2	3.3	Kamchatka	0.0183	85.7
Greece	2007	1.90	5.5	4.0	New Hebrides	0.0183	103.7
Greece	2008	4.62	6.0	3.1	Sumatra •	0.0183	252.0
Greece	2009	0.76	4.3	2.8	Sumatra •	0.0183	41.7
Greece	2009	0.80	4.1	3.0	Kurils •	0.0183	43.8
Greece	2010	0.97	3.5	3.1	Solomon Islands •	0.0183	52.7
NZ	1992	1.29	4.2	2.6	Landers	0.0523	24.6
NZ	1997	11.07	4.9	3.9	Pakistan •	0.0523	211.6
NZ	1998	2.10	4.7	2.3	Antarctic Plate •	0.0523	40.1
NZ	2001	0.22	3.4	2.0	Japan •	0.0523	4.2
NZ	2001	0.25	3.9	2.4	S. of Australia •	0.0523	4.8
NZ	2007	0.76	6.7	3.2	Aleutians	0.0523	14.6
Chile	1994	2.10	4.7	4.1	New Zealand	0.1034	20.3
China	1989	2.32	5.9	4.4	Loma Prieta	0.0166	140.0
Coso	2009	0.01	2.3	1.7	Tonga	0.0003	35.6
Yellowstone	1995	0.11	2.7	1.3	Kermedec Is.	0.0000	N/A
Hawaii	2003	0.03	3.3	1.4	Scotia Sea	0.0025	12.7

Shibazaki et al., 2011). In (2) the deterministic magnitude model, the seismic nucleation phase of moderate to large earthquakes is different, and may have greater slip amplitude that enables the earthquake to grow through barriers that inhibit weaker nucleation (e.g., Allen et al., 2009; Ellsworth and Beroza, 1995; Olson and Allen, 2005; Umeda, 1990). In (3), the pre-seismic asperity model, high magnitude earthquakes are thought to have a larger pre-seismic nucleation zone that is comparable to its eventual rupture area (e.g., Beeler et al., 2012; Hori and Miyazaki, 2010, 2011; Shibazaki, 2005).

If we accept all the observations portrayed in Fig. 27 as not coincidental, which would thus imply that $M > 5$ remotely triggered earthquakes are delayed, then there are a few features of the nucleation models described above that can be commented on. It would appear that a cascade model would be difficult to reconcile with a minimum delay time of ~9 h, because we routinely see $M \sim 4$ events triggered simultaneously with the passage of surface waves. Our observations (if not coincidental) therefore are more consistent with a deterministic magnitude, or a pre-seismic asperity model. Either of these two models implies a nucleation phase that is distinct at higher magnitudes, and could thus have a delayed nucleation response to transient stressing.

Spatial and temporal modeling of the time series of stresses calculated from broadband recordings of a remote mainshock suggests that a large fault area would not experience uniform stress increase (Parsons et al., 2012). Modeling indicates that stresses that are aligned with fault rake have short durations (up to 4 s), and that a $M > 5$ rupture area could experience imposed stresses favoring and inhibiting slip on different parts of the fault surface simultaneously. Thus if faults follow a pre-seismic asperity model, it might be more difficult for larger magnitude, remote earthquakes to be triggered immediately during the passage of surface waves.

If it is assumed that the observed $M > 5$ earthquakes have actually been triggered, we speculate that a deterministic magnitude nucleation model best fits observations.

5. Mainshock characteristics

Here we examine global mainshocks that are associated with remote triggering (Table 2) to see if they have any common characteristics or systematic features that make them effective triggers. We look generally at mainshock magnitudes, range to triggered events, and focal mechanisms. Additionally, we obtained broadband recordings for some mainshocks in regions where remote triggering was observed (California and Greece). This enables us to also compare mainshock amplitude spectra, peak ground velocity of surface wave phases, propagation directions, and back azimuths of those phases as a function of receiver fault geometry. We compare mainshocks that caused triggering in Greece but not California and vice versa.

5.1. Mainshock magnitude and range

Mainshock magnitude and distance are factors that affect surface wave amplitude at a given site. The distribution of global mainshocks that are associated with remote triggering suggests that surface wave amplitudes are likely not a very important consideration. This is because there is a broad range of mainshock magnitudes and ranges associated with remote triggering that is not significantly different than the complete mainshock distribution (Fig. 32). Further, we commonly observe cases where a moderate magnitude mainshock is associated with remote triggering, whereas a much larger shock from the same region has no effect. The number of independent mainshocks that are associated with triggering is too small to draw any conclusions about a preferred magnitude range (18 probable triggering, 38 probable and possible cases); we compared these groups of mainshock magnitudes against 1000 randomly drawn sets from the 260 $M \geq 7$ mainshock catalog, and find them to be comparable at 95% confidence (Fig. 32).

Triggering at a site therefore is likely a complex combination of factors related to (1) the dynamic stresses caused by the mainshock

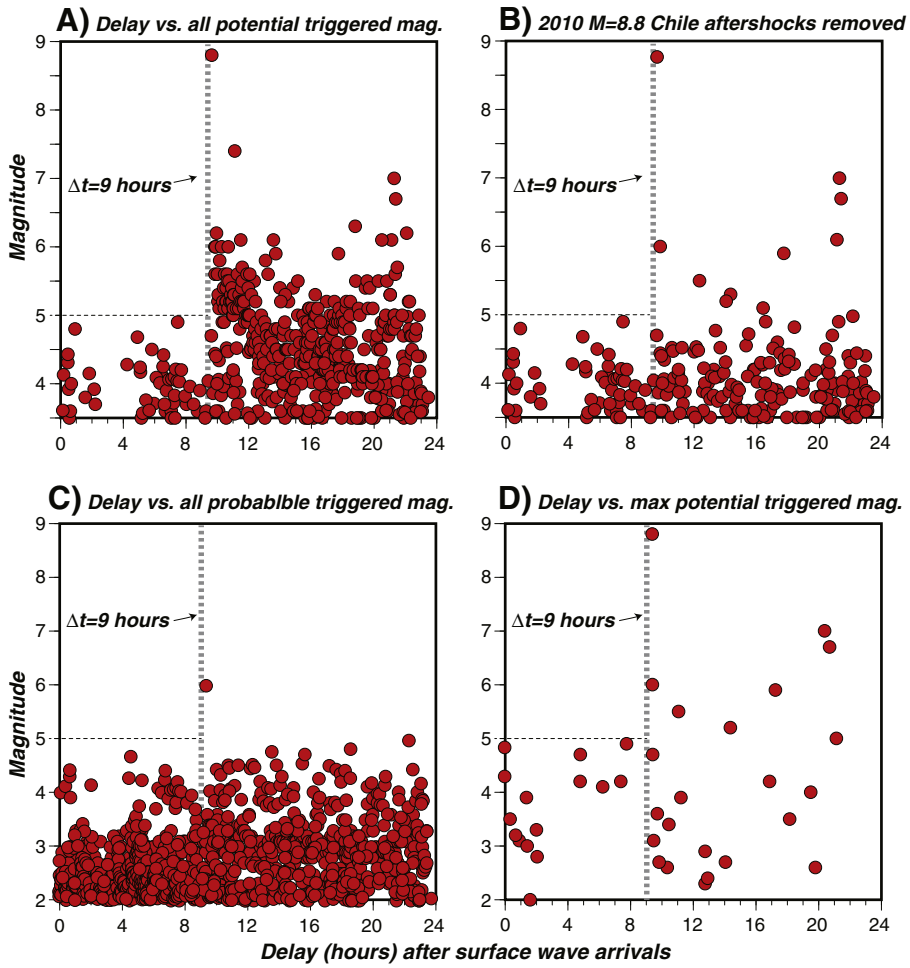

Fig. 27. Delay times vs. magnitudes of (A) all probable and possibly remote triggered earthquakes in this study (Fig. 22), and (B) same as (A) except the local aftershocks from the 2010 $M = 8.8$ Maule earthquake are suppressed. In (C) just the triggered events that are considered probable because they are part of a regionally significant outbreak of seismicity are shown. In (D) delay time vs. maximum magnitude of triggered events in each of the "possible" or "probable" regions is shown. Delays are relative to calculated earliest likely surface wave arrivals based on range values given in Table 2. There appears to be a consistent minimum delay time of ~9 h for possibly triggered $M > 5$ earthquakes.

(wave type, frequency content, peak amplitudes) at specific locations, and (2) the local environment (fault types and geometry, incidence angle, criticality of the region). We need information about the triggered events (focal mechanisms, depth, and origin time) to assess each of the aforementioned components. Previous studies (e.g., Hill and Prejean, in press and references contained therein) have identified conditions favoring dynamic triggering that are specific to different regions and settings worldwide, and have concluded that there is no generalization for why dynamic triggering occurs, but there are many questions remaining to be answered.

5.2. Focal mechanisms

We investigate relationships between mainshock and triggered local focal mechanisms in our test regions of northern California and Greece. We do not see strong evidence for triggered seismicity that is anomalous relative to local tectonics. The spatial distribution of triggered seismicity in California is diffuse (Fig. 9) and focal mechanisms of triggered earthquakes are consistent with regional tectonics, with the majority of them corresponding to strike-slip faulting (Fig. 33). We note an increase in seismicity east of San Francisco Bay (near the junction of Hayward and Calaveras Faults with NNW-SSE trending right-lateral faulting Manaker et al. (2005)) associated with a 2008 $M = 7.2$ China mainshock (Fig. 9). We also observe clustered normal faulting mechanisms associated with a 2012 $M = 7.4$ Mexico mainshock (Fig. 33; in gray) in The Geysers geothermal area, known for extensional tectonics (Oppenheimer, 1986) and high-susceptibility to remote triggering (Stark and Davis, 1996).

The number of available CMT solutions for triggered events in Greece is restricted to one per mainshock. However we do not observe a deviation from the regional faulting style. The focal mechanisms of triggered seismicity following the 2007 $M = 7.1$ New Hebrides, and the 2008 $M = 7.4$ Sumatra mainshocks typify the Cephalonia transform fault, and strike-slip faulting perpendicular to the Hellenic trench system offshore of the southern Peloponnese respectively (Kiratzi and Louvari, 2003) (Fig. 33). The one mechanism from triggered seismicity following the 2009 $M = 7.0$ Sumatra mainshock expresses the extensional tectonics of Central Greece. We conclude that in cases where remote triggering is observed, the rupture style of the triggered seismicity is consistent with the regional faulting style. However, we note that the number of the available next-day CMT solutions from small magnitude triggered events is limited, and the quantification of possible deviations of specific geometry parameters (strike, dip, and rake) between local background and triggered seismicity is limited.

5.3. Comparative peak ground velocity and amplitude spectra

We examine broadband records for probable, possible, and selected cases with no remote triggering in northern California (6 event–station pairs) and Greece (7 event–station pairs), focusing on peak amplitudes

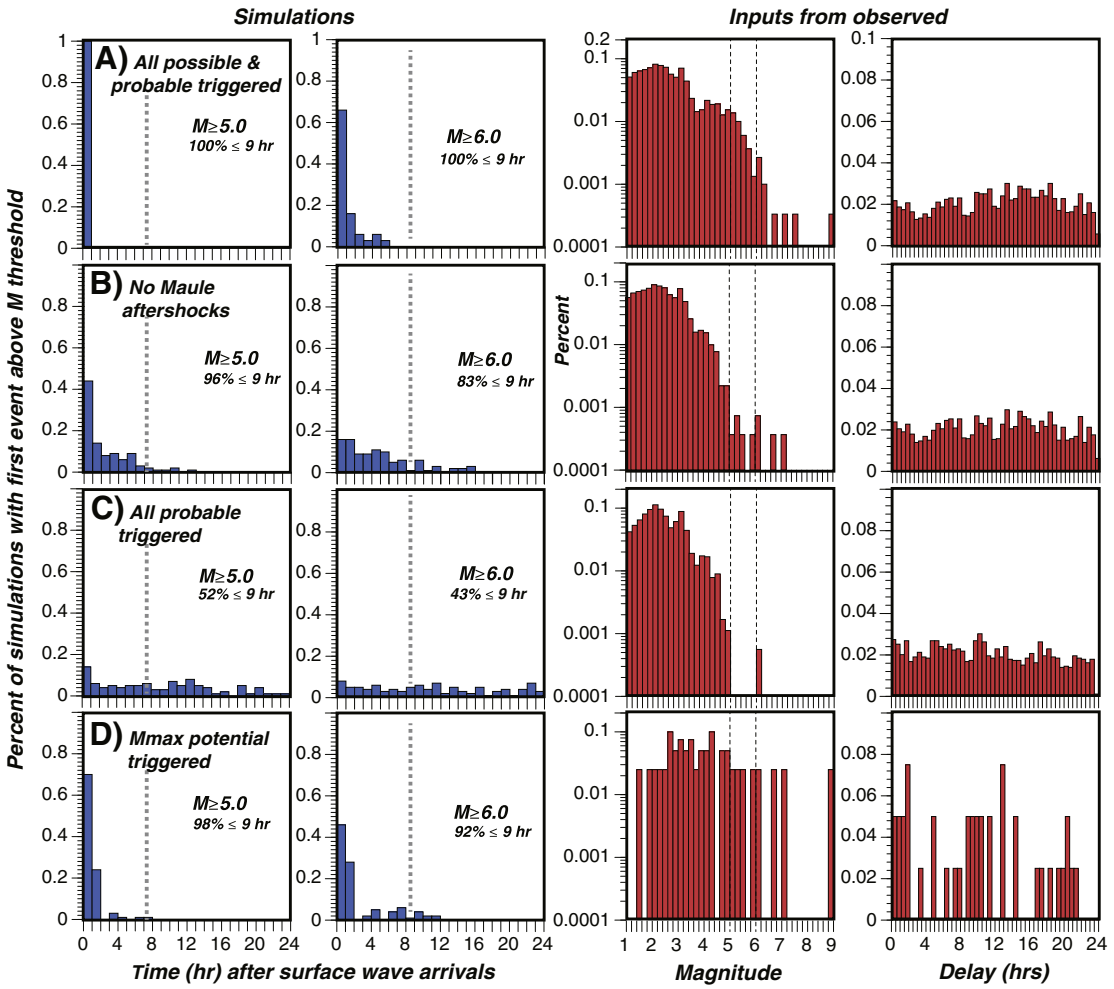

Fig. 28. Simulations of first occurrence of $M \geq 5.0$ and $M \geq 6.0$ earthquakes used to establish significance of observed possibly delayed dynamic triggering of high magnitude events. The observed magnitude frequency distribution of all possible and probable triggered earthquakes is used along with the observed occurrence time after surface wave arrivals distribution, except that the times are randomized vs. magnitude in 100 realizations. Panels (A–D) correspond to the earthquake populations plotted in Fig. 27A–D.

and frequency content between 10 and 100 s periods. We are especially interested in (1) comparing cases where a specific event is related with triggering in California but not in Greece, and vice versa, and (2) whether a regional triggering amplitude threshold exists.

To assess the broadband recording of a mainshock at a given station, we remove instrument responses to estimate the velocity recordings, mean removal, detrending, and apply a Butterworth (4-poles, 2-way) bandpass filter with corner frequencies at 0.01–0.1 Hz. We rotate both horizontal seismograms to obtain the radial and transverse components, and find their peak amplitudes and frequency content by means of Fourier amplitude spectra and the spectrograms for the 3-component recordings. We compare peak ground velocity (PGV) amplitudes recorded in transverse and radial components in northern California and Greece for mainshocks that were associated with probable remote triggering in at least one of the regions (Fig. 34). We do not find evidence supporting a global or regional critical PGV threshold (e.g., Gomberg, 1996). Similarly, Brodsky et al. (2000) reported that the amplitude threshold for triggering in Greece following the 1999 $M = 7.4$ Izmit earthquake was three times lower than that inferred for the Imperial Valley in California after the occurrence of the 1992 $M = 7.4$ Landers earthquake. We do note that the PGV threshold in Greece after the 2009 $M = 7.0$ Sumatra mainshock is the same as that in northern California following the 2012 $M = 7.4$ Mexico earthquake (Fig. 34). The lowest triggering threshold in peak velocity we have identified in this study (2×10^{-5} cm/s) is associated with triggered seismicity in Greece following the $M = 7.1$ New Hebrides mainshock, which is almost two orders of magnitude lower than the average of 3×10^{-3} cm/s, although triggered tremor may have played a role in this. We cannot establish any regional triggering PGV amplitude threshold.

We reach the same conclusion, that a global or regional amplitude threshold cannot be established, when comparing the frequency content of long period surface waves between 10 and 100 s (Fig. 35). For instance, if we consider three 2008 mainshocks ($M = 7.4$, $M = 7.2$ and $M = 7.9$) that were recorded continuously by the northern California Seismic Network, we find that they have comparable Fourier amplitudes, but only the $M = 7.2$ event caused triggered seismicity in California. In Greece, we note that the 2008 $M = 7.2$ and $M = 7.9$ China mainshocks were not associated with remote triggering despite having comparable amplitude spectra to the 2008 $M = 7.4$ Sumatra, 2009 $M = 7.4$ Kuriles, and 2009 $M = 7.1$ Sumatra mainshocks that were. It is noteworthy that the 2007 $M = 7.1$ 2007 New Hebrides mainshock, which triggered seismicity in western and central Greece, had an amplitude spectrum 3 orders of magnitude lower when compared with corresponding spectra from other mainshocks associated with triggering in California and Greece.

5.4. Azimuth

Perhaps a more important factor affecting dynamic stresses acting on a fault plane is the incidence angle and the seismic phase (Gonzalez-Huizar and Velasco, 2011; Hill, 2008, 2012). To assess this in our test

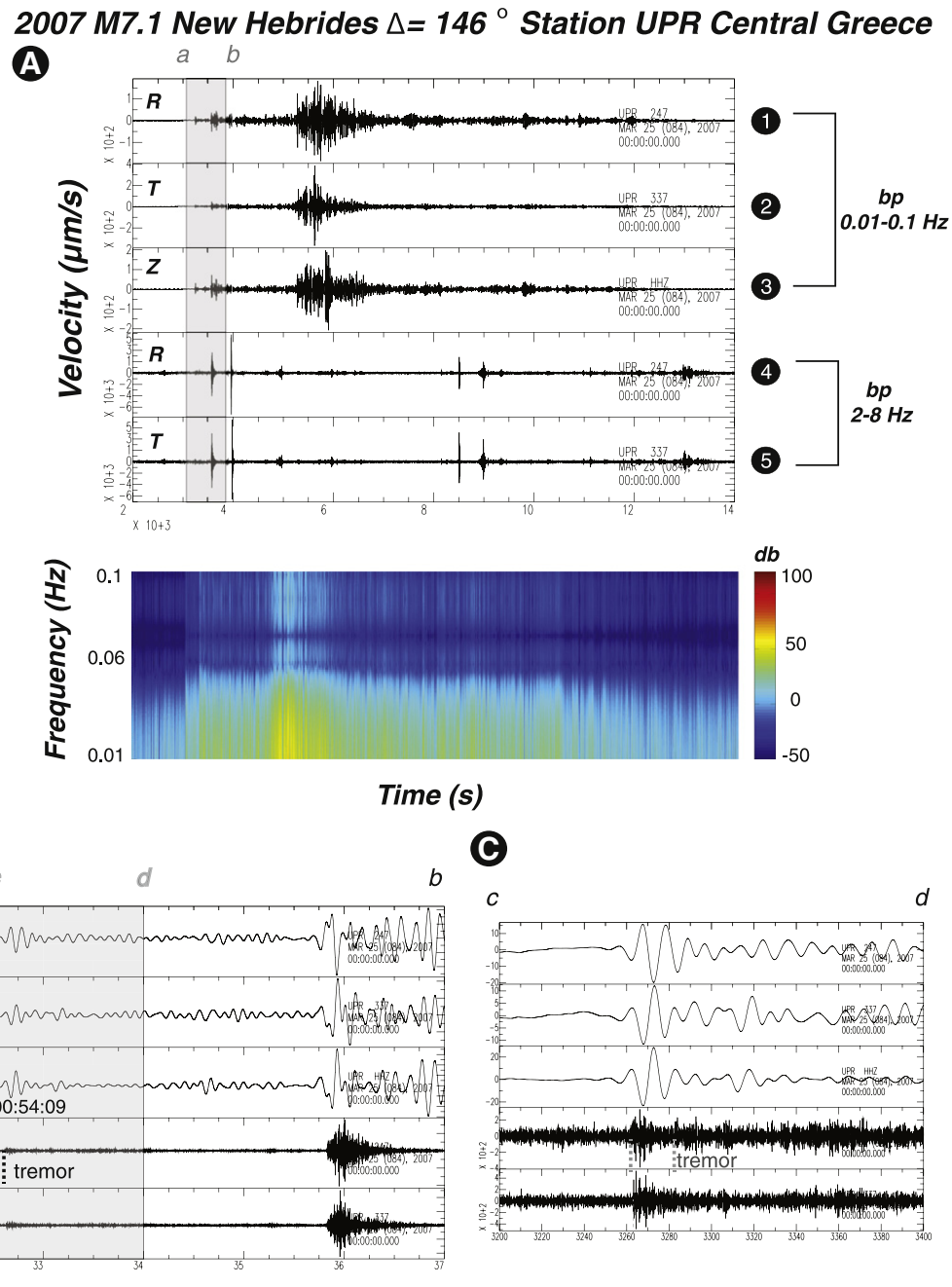

Fig. 29. Waveform analysis for the M7.1 2007 New Hebrides mainshock recorded at the station UPR at Corinth Gulf (central Greece). In (A) we present the low-pass (0.01–0.1 Hz) filtered traces of the radial (trace 1), transverse (trace 2) and vertical component (trace 3), whereas traces 4 and 5 correspond to the high-pass (2–8 Hz) radial and transverse components, respectively. We present the shaded part (a–b section) of (A) panel in detail in panel (B); we observe triggered tremor almost simultaneously with the P-wave arrival and local seismicity bursts with the S-wave arrival. We provide the shaded part (c–d section) of panel (B) in greater detail in panel (C). We are especially interested in triggered tremor in this case, since it may explain the persistent seismicity rate increase nearby the site for ~20 days following the mainshock. The spectrogram of the same recording (radial component) for California revealed extended duration for intermediate periods (10–30 s), however the corresponding spectrogram for the recording at the Greek site presents lower frequency content for the same periods of interest and for a restricted time interval.

regions of northern California and Greece, we adapt a generic San Andreas Fault system representation (vertical strike-slip trending N40°W) and a simplified representation of the extensional central Greece and Corinth Gulf (central Greece) regions (E-W trending normal fault orientation with 30° and 60° dips). We acknowledge that there is resultant uncertainty in our incidence angle calculations because of fault geometry simplifications. In addition to noting the mainshock propagation directions, we calculate the apparent back-azimuths between mainshocks and receivers by estimating the arctangent of the transverse-to-radial amplitude ratio, which gives the Rayleigh-wave incident angle with respect to the theoretical back azimuth of a specific mainshock.

In Fig. 36, we show the propagation directions (solid arrows) for selected mainshocks recorded near the San Andreas fault and in central Greece together with the apparent back azimuths (dashed arrows) calculated from long period surface waves. For northern California, we find that both the 2008 $M = 7.2$ China and the 2012 $M = 7.4$ Mexico mainshocks have near strike-parallel incident angles, which implies a peak triggering potential for Love waves, and a minimal effect from Rayleigh waves (Hill, 2012). We find that both cases of remote triggering in northern California for which we have broadband data have fault parallel incidence angles, though not all events with these angles cause triggering (Fig. 36). Though we did not observe triggered seismicity in

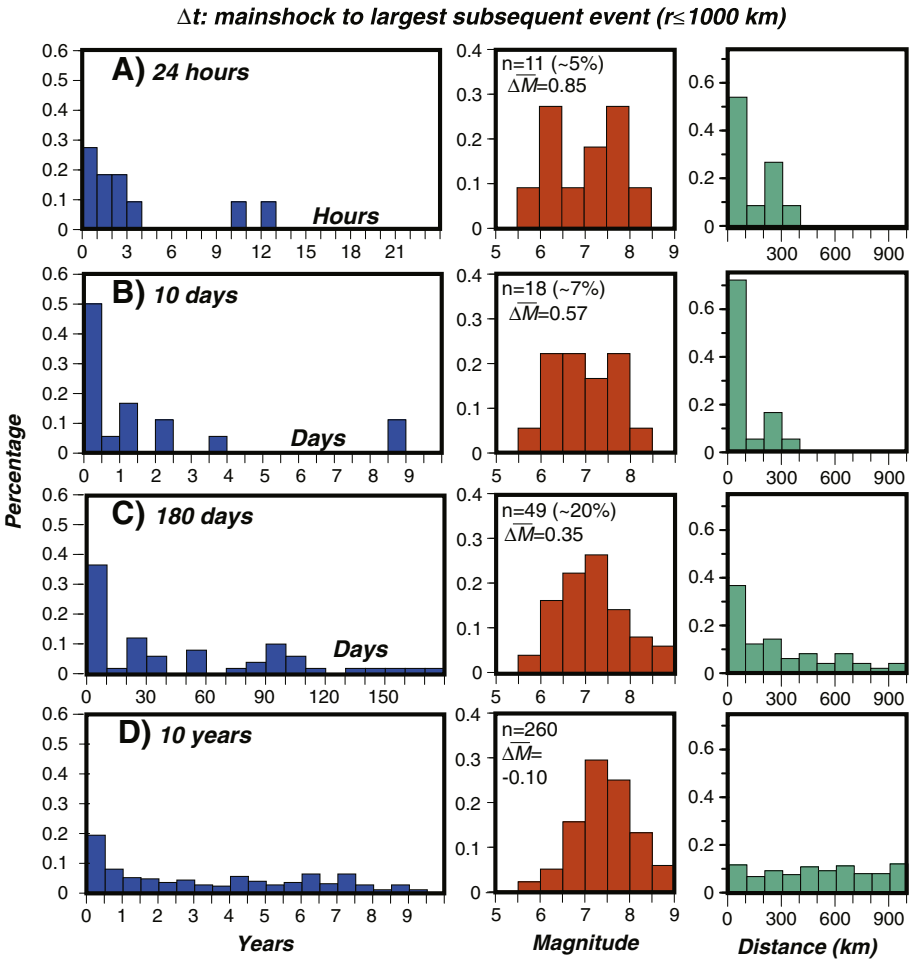

Fig. 30. Delay times vs. magnitudes of probable and possibly near-source triggered earthquakes from a global $M > 5$ catalog. These events follow an Omori law decay in time, and demonstrate no apparent magnitude dependence. Delayed triggering can persist for years.

California following the 2011 $M = 9.0$ Tohoku-Oki earthquake, Hill et al. (2013) report S-wave triggering of tremor beneath the Parkfield section of the San Andreas fault induced by strike-parallel dynamic stresses, and they note that high amplitude tremor bursts with respect to the small Rayleigh-wave perturbing stresses remain to be explained.

For Greece we considered (written communication, David Hill, 2013) the triggering potential for Love and Rayleigh waves on 60° and 30° dipping normal faults with friction coefficient $\mu = 0.4$ at 3 km and 9 km target depths, representing triggered seismicity observed at 0–5 km and 5–15 km depths, with the latter example demonstrated in Fig. 36D. We note that low-angle normal faulting between 6 and 15 km depth characterizes the most active part of the high-extension rate (14–16 mm/yr) Corinth gulf (Bernard et al., 1997 and references therein). For the specific cases of the 2007 $M = 7.1$, 2008 $M = 7.4$, and the 2009 $M = 7.0$ and $M = 7.4$ mainshocks, intermediate incident angles (20°–45°) coincide with peak triggering potential of Love waves ($P_L = 0.5$–0.8) but also with intermediate triggering potential for Rayleigh waves ($P_R \sim 0.5$) as well. It is not clear whether Love or Rayleigh waves are correlated with the triggered seismicity, but in light of the above observation we cannot exclude either phase from playing a critical role in remote earthquake triggering.

5.5. Summary of mainshock characteristics

We find no significant difference between the magnitude and range distributions of global mainshocks associated with remote triggering and those that are not. By comparing waveforms from teleseismic events that are associated with remote triggering in one region, but not in another, we show that there is not any specific mainshock characteristic that correlates with probable earthquake triggering. This indicates that the nature of remote triggering may be more multi-parametric than originally thought. There is no evidence that a global or even a regional amplitude threshold exists, but if it exists it is time dependent, which restricts its usefulness and importance. For two global mainshocks that affected the San Andreas fault, earthquake triggering coincides with high-triggering potential of Love waves. For sites in central Greece we find high-triggering susceptibility associated with a very low amplitude threshold, but it is not clear which surface wave phase is responsible.

6. Conclusions: What have we learned about remote earthquake triggering?

In this review we focused on studying the effects of remote, global $M \geq 7.0$ earthquakes on seismicity in 21 different regions around the world. We did this so that we could more directly witness the character of the effects, and build a library of example responses. We highlight the following advances that we take from this study:

(1) Remote earthquake triggering is rare (as detected on regional networks). We suspect that remote triggering is more common at very low magnitudes (e.g., Velasco et al., 2008). We find that the incidence of possible or probable remote triggering (at the threshold of regional network detection) that affects at least

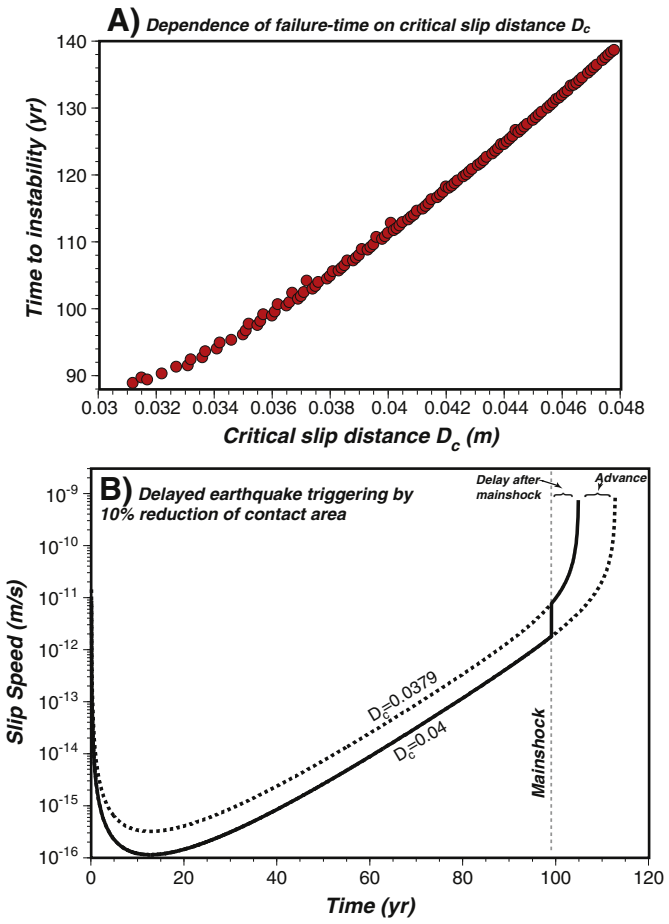

Fig. 31. (A) Illustration of nucleation time as a function of critical slip distance (D_c), and (B) impact of a sudden change in *Dc* on failure time, leading to delayed triggering. Slip velocity was solved numerically by using a 4th-order Runga–Kutta algorithm to solve differential equations from a spring–slider formulation of (Gomberg et al., 1998) of the rate/state formulations (Dieterich, 1979; Ruina, 1983). These figures are reprised from Parsons (2005).

one region among the set of zones considered during the 24-h period after the occurrence of a $M \geq 7.0$ earthquake is 0–3%. Put another way, 97% of the time, global mainshocks have no effect on detectable seismicity in a given region.

(2) We observe remote triggering happening in every tectonic setting, including transform, extensional, convergent, mid-plate, and volcanic environs. We see about as many regions without evidence of significant remote triggering responses as those with. There is no correlation in terms of tectonics, strain rate, or activity levels that we can identify that would predict whether a triggering response is expected.

(3) We observe a wide variety of apparent local responses to seismic waves from distant mainshocks that range from immediate, and regionally distributed seismicity rate increases, to delayed, spatially localized earthquake activity. We commonly see earthquake swarms or existing aftershock sequences apparently becoming invigorated by passing seismic waves.

(4) We do not see any $M > 5$ remotely triggered aftershocks that can be associated with global mainshocks that occur before 9–10 h after surface waves arrive at a region. This could be a consequence of the Gutenberg-Richter magnitude frequency relation such that higher magnitude earthquakes are rare; at least 70% of the triggering responses we observe are not vigorous enough to expect $M \geq 5$ activity during the first 24 h. When we restrict the analysis to probable remote triggering, only 3 responses were active enough to expect $M \geq 5$ earthquakes, and of these, one case had $M \geq 5$ seismicity and two did not. Thus the simplest conclusion about remote $M \geq 5$ triggering is that the numbers of remotely triggered earthquakes are too small, and the responses too subtle for high magnitudes in most cases.
If however one wants to accept that all possible remote triggering is in fact caused by global mainshocks, then the observed ~9-h delay of $M \geq 5$ seismicity must be explained. Simulations using the magnitude frequency distribution of actual possible and probable triggered remote earthquakes show that 96% of the time, $M \geq 5$ events would be expected before the ~9 h threshold if they were distributed randomly in time following surface wave passage. We thus suggest that if these delayed cases are valid examples of remote triggering, then we find it more probable that higher magnitudes are either not directly triggered, or have a longer nucleation process as compared with lower magnitude earthquakes.

(5) A total of 38 different $M \geq 7.0$ global mainshocks are identified as possible, or probable remote triggers. Only 2 of these are seen to affect more than one of our 21 study regions. We can find no identifying features that these mainshocks have in common in terms of magnitude, focal mechanism, distance range to triggered events, recorded amplitude spectra at triggering sites, or observed peak ground velocity at triggering sites. The number of examples that we have is very small, but there may be some trends in terms of the alignment of surface wave phase propagation and receiver faults in specific locations, consistent with the stress modeling concepts of Hill (2008, 2012) and Gonzalez-Huizar and Velasco (2011).

(6) An unusual regional outbreak of seismicity across Greece that persisted at high levels for at least 20 days can be temporally associated with a 2007 $M = 7.1$ New Hebrides mainshock. We also see that this same mainshock excited non-volcanic tremor beneath the Corinth Gulf. These two observations might be coincidental, or there might be a linked physical process that relates shallow seismicity and deep tremor in Greece.

Acknowledgments

We thank Tim Horscroft, Mian Liu, and Hans Thybo for their kind invitation to submit this paper to Tectonophysics. We are grateful to Arnauld Heuret and Derek Keir for sharing the subduction interface catalog and the regional Ethiopian catalog, respectively. We thank the University of Patras (Ass. Prof. Efthimios Sokos) and the Corinth Rift Laboratory for making the continuous waveforms for several mainshocks available. We especially appreciate the efforts to make earthquake catalogs freely available by the Advanced National Seismic System (ANSS), the Japan Meteorological Agency, the World Data Center for Seismology Beijing, Geoscience Australia, GNS Science New Zealand, Istituto Nazionale di Geofisica e Vulcanologia, the Kandili Observatory (Doğan Kalafat), the National Observatory of Athens in Greece, and the Global Seismograph Network (GSN) catalog. We appreciate the review comments by Eric Geist, Hector Gonzalez-Huizar, and an anonymous reader. Figures in this review utilized the GMT mapping software of Wessel and Smith (1991).

Appendix A. Supplementary data

Supplementary data to this article can be found online at http://dx.doi.org/10.1016/j.tecto.2014.01.038.

References

Abercrombie, R.E., Rice, J.R., 2005. Can observations of earthquake scaling constrain slip weakening? Geophys. J. Int. 162, 406–424. http://dx.doi.org/10.1111/j.1365-246X.2005.02579.x.

Allen, R.M., Brown, H., Hellweg, M., Khainovski, O., Lombard, P., Neuhauser, D., 2009. Real-time earthquake detection and hazard assessment by ElarmS across

Table 2
Characteristics of 38 global mainshocks that are associated with remote triggering at $r > 1000$ km. "M max" is the highest magnitude event in the local catalogs that occurred within 24 h of remote mainshocks. "N" is the number of possibly triggered events. "Range" is the distance between global mainshocks and highest magnitude potentially triggered events. "Delay" is the period between earliest possible surface wave arrivals and maximum magnitude possibly triggered events. "N regs." Refers to the number of 0.5° by 0.5° subregions that have rate increases. The symbols "μ" and "+2σ" on the number of 0.5° by 0.5° subregions that have rate increases over 100 randomized times to find the expected variability of each catalog. "Category" refers to our assignment of probable vs. possible remote triggering (see section 2 for details).

Global mainshocks					Remote triggering								
Date	M	Long.	Lat.	Region	Region	M max	N	Range (km)	Delay (hour)	N regs	μ	+2σ	Category
2002.8436	7.9	−147.45	63.51	Denali	Basin and Range	3.6	41	3028	9.83	16	4.4	8.9	Probable
2004.9864	9.2	95.98	3.30	Sumatra	Basin and Range	3.9	16	14,202	2.08	3	4.4	8.9	Possible
2010.5943	7.0	150.76	44.00	Kuriles	Basin and Range	4.8	11	11,142	0.52	3	4.4	8.9	Possible
2012.2777	8.6	93.06	2.33	Indian Ocean	Basin and Range	4.2	8	14,856	17.67	2	4.4	8.9	Possible
1991.9895	7.2	−25.27	−56.03	Mid Atlantic Ridge	North California	3.1	35	13,678	1.59	10	3.1	6.6	Probable
2003.6397	7.2	167.14	−45.10	New Zealand	North California	2.8	27	11,629	2.62	12	3.1	6.6	Probable
2008.2212	7.2	81.47	35.49	China	North California	3.0	25	11,546	1.98	7	3.1	6.6	Probable
2012.2185	7.4	−98.23	16.49	Central America	North California	2.9	23	3427	12.91	3	3.1	6.6	Possible
1992.6721	7.2	−87.34	11.74	Nicaragua	South California	3.2	170	3831	0.81	16	4.3	8.5	Probable
2010.4488	7.5	91.94	7.88	Indonesia	South California	4.9	85	14,525	8.50	8	4.3	8.5	Possible
2012.2777	8.6	93.06	2.33	Indian Ocean	Baja California	7.0	12	15,571	21.23	5	3.4	7.1	Possible
1995.5064	7.2	−177.59	−29.21	Kermedec Islands	Greece	4.0	13	19,132	20.54	10	7.8	13.4	Possible
2006.3041	7.6	167.09	60.95	Kamchatka	Greece	4.2	63	9066	7.83	13	7.8	13.4	Possible
2007.2302	7.1	169.36	−20.62	New Hebrides	Greece	5.5	37	16,844	11.96	8	7.8	13.4	Possible
2008.1403	7.4	95.96	2.77	Sumatra	Greece	6.0	157	8109	9.45	17	7.8	13.4	Probable
2009.0432	7.4	155.15	46.86	Kurils	Greece	4.1	44	9743	6.71	15	7.8	13.4	Probable
2009.6722	7.0	107.30	−7.78	Sumatra	Greece	4.3	79	9939	0.25	27	7.8	13.4	Probable
2010.0108	7.1	157.35	−8.78	Solomon Islands	Greece	3.5	44	14,611	18.94	28	7.8	13.4	Probable
1992.4932	7.3	−116.44	34.20	Landers	New Zealand	4.2	119	10,505	5.31	10	9.9	16.2	Possible
1997.1613	7.1	68.21	29.98	Pakistan	New Zealand	5.0	97	13,534	21.87	21	9.9	16.2	Probable
1998.2305	8.1	149.53	−62.88	Antactic Plate	New Zealand	4.7	293	3280	4.92	17	9.9	16.2	Probable
2001.1515	7.1	126.25	1.27	Japan	New Zealand	3.1	76	6671	9.80	19	9.9	16.2	Probable
2001.9496	7.1	124.69	−42.81	South of Australia	New Zealand	3.9	53	3903	11.39	21	9.9	16.2	Probable
2007.9682	7.2	−179.51	51.36	Aleutians	New Zealand	6.7	46	10,000	21.24	17	9.9	16.2	Possible
1994.4634	7.1	171.66	−42.96	New Zealand	Chile	4.7	15	9287	9.88	4	8.0	13.7	Possible
2010.1585	7.0	128.43	25.93	Okinawa	Chile	8.8	270	17,669	9.62	58	8.0	13.7	Possible
1989.7972	7.0	−121.88	37.04	Loma Prieta	China	5.9	20	9754	17.76	1	5.3	10.0	Possible
1995.5064	7.2	−177.59	−29.21	Kermedec Islands	Yellowstone	2.7	128	10,595	14.61	1	1.0	3.0	Possible
1995.7744	8.0	−104.21	19.06	Mexico	Yellowstone	2.6	18	2878	10.46	3	1.0	3.0	Probable
2000.4282	7.9	102.09	−4.62	Indonesia	Yellowstone	2.0	20	14,431	2.33	2	1.0	3.0	Probable
1984.1063	7.5	160.47	−10.01	Solomon Islands	Coso	1.5	23	9918	20.63	3	1.7	4.0	Probable
2004.1008	7	135.54	−3.62	New Guinea	Coso	1.8	14	11,690	3.97	3	1.7	4.0	Probable
2009.2158	7.6	−174.66	−23.04	Tonga	Coso	2.3	13	8847	13.21	1	1.7	4.0	Possible
2010.1597	8.8	−72.90	−36.12	Maule, Chile	Coso	3.5	22	9253	0.76	1	1.7	4.0	Possible
2010.5467	7.4	150.59	−5.93	New Britain	Coso	2.4	13	10,536	13.47	3	1.7	4.0	Probable
1997.7224	7.0	−177.62	−28.68	Kermedec Islands	Hawaii	3.4	53	3903	10.62	3	1.9	4.6	Possible
2003.0605	7.6	−104.10	18.77	Mexico	Hawaii	2.6	19	5496	20.08	1	1.9	4.6	Possible
2003.5923	7.6	−43.41	−60.53	Scotia Sea	Hawaii	3.3	29	13,140	2.66	2	1.9	4.6	Possible
2006.1478	7.0	33.58	−21.32	Mozambique	Hawaii	2.7	43	18,923	10.83	3	1.9	4.6	Possible
2001.8004	7.5	123.91	−4.10	Indonesia	Australia	5.2	9	3297	14.52	4	7.8	13.4	Possible

California. Geophys. Res. Lett. 36, L00B08. http://dx.doi.org/10.1029/2008GL036766.

Anderson, J.G., 1994. Seismicity in the western Great Basin apparently triggered by the Landers, California, earthquake, 28 June 1992. Bull. Seismol. Soc. Am. 84 (3), 863–891.

Árnadóttir, T., Geirsson, H., Einarsson, P., 2004. Coseismic stress changes and crustal deformation on the Reykjanes Peninsula due to triggered earthquakes on 17 June 2000. J. Geophys. Res. 109, B09307. http://dx.doi.org/10.1029/2004JB003130.

Bak, P., Teng, C., 1989. Earthquakes as self-organized critical phenomenon. J. Geophys. Res. 94, 15,635–15,637.

Beeler, N., Kilgore, B., McGarr, A., Fletcher, J., Evans, J., Baker, S.R., 2012. Observed source parameters for dynamic rupture with non-uniform initial stress and relatively high fracture energy. J. Struct. Geol. 38, 77–89.

Beresnev, I.A., Wen, Kuo-Liang, 1995. Remotely triggered seismicity inferred from Taiwan regional catalog. Geophys. Res. Lett. 22 (23), 3155–3158. http://dx.doi.org/10.1029/95GL03320.

Bernard, P., Briole, P., Meyer, B., Lyon-Caen, H., et al., 1997. The Ms = 6.2, June 15, 1995 Aigion earthquake (Greece): evidence for low angle normal faulting in the Corinth rift. J. Seismol. 1, 131–150.

Biscontin, G., Pestana, J.M., 2006. Factors affecting seismic response of submarine slopes. Nat. Hazards Earth Syst. Sci. 6, 97–107.

Biscontin, G., Pestana, J.M., Nadim, F., 2004. Seismic triggering of submarine slides in soft cohesive soil deposits. Mar. Geol. 203, 341–354.

Bourouis, S., Cornet, F.H., 2009. Microseismic activity and fluid fault interactions: some 530 results from the Corinth Rift Laboratory (CRL), Greece. Geophys. J. Int. 178 (1), 561–580. http://dx.doi.org/10.1111/j.1365-246X.2009.04148.x (531 national).

Brodsky, E.E., Karakostas, V., Kanamori, H., 2000. A new observation of dynamically triggered regional seismicity: earthquakes in Greece following the August, 1999 Izmit, Turkey earthquake. Geophys. Res. Lett. 27, 2741–2744.

Brodsky, E.E., Roeloffs, E., Woodcock, D., Gall, I., Manga, M., 2003. A mechanism for sustained groundwater pressure changes induced by distant earthquakes. J. Geophys. Res. 108 (B8), 2390. http://dx.doi.org/10.1029/2002JB002321.

Brune, J.N., 1979. Implications of earthquake triggering and rupture propagation for earthquake prediction based on premonitory phenomena. J. Geophys. Res. 84, 2195–2198.

Cameron, A.C., Trivedi, P.K., 1998. Regression Analysis of Count Data. Cambridge Press, New York (411 pp.).

Cannata, A., Di Grazia, G., Montalto, P., Aliotta, M., Patanè, D., Boschi, E., 2010. Response of Mount Etna to dynamic stresses from distant earthquakes. J. Geophys. Res. 115, B12304. http://dx.doi.org/10.1029/2010JB007487.

Chao, K., Peng, Z., Wu, C., Tang, C.C., Lin, C.H., 2012. Remote triggering of non-volcanic tremor around Taiwan. Geophys. J. Int. 188, 301–324.

Chelidze, T., Matcharashvili, T., Zhukova, N., 2011. Echo of 2011 great Japan earthquake in Georgia: dynamic triggering of local earthquakes. Bull. Georgian Natl. Acad. Sci. 5 (3), 67–70.

Cocco, M., Tinti, E., Marone, C., Piatanesi, A., 2009. Scaling of slip weakening distance with final slip during dynamic earthquake rupture. Int. Geophys. 94 (C), 163–186.

Daniel, D., Marsan, D., Bouchon, M., 2008. Earthquake triggering in southern Iceland following the June 2000 Ms 6.6 doublet. J. Geophys. Res. 113, B05310. http://dx.doi.org/10.1029/2007JB005107.

Dieterich, J.H., 1979. Modeling of rock friction: 1. Experimental results and constitutive equations. J. Geophys. Res. 84, 2161–2168.

Dieterich, J.H., Richards-Dinger, K.B., 2010. Earthquake recurrence in simulated fault systems. Pure Appl. Geophys. 167, 1087–1104.

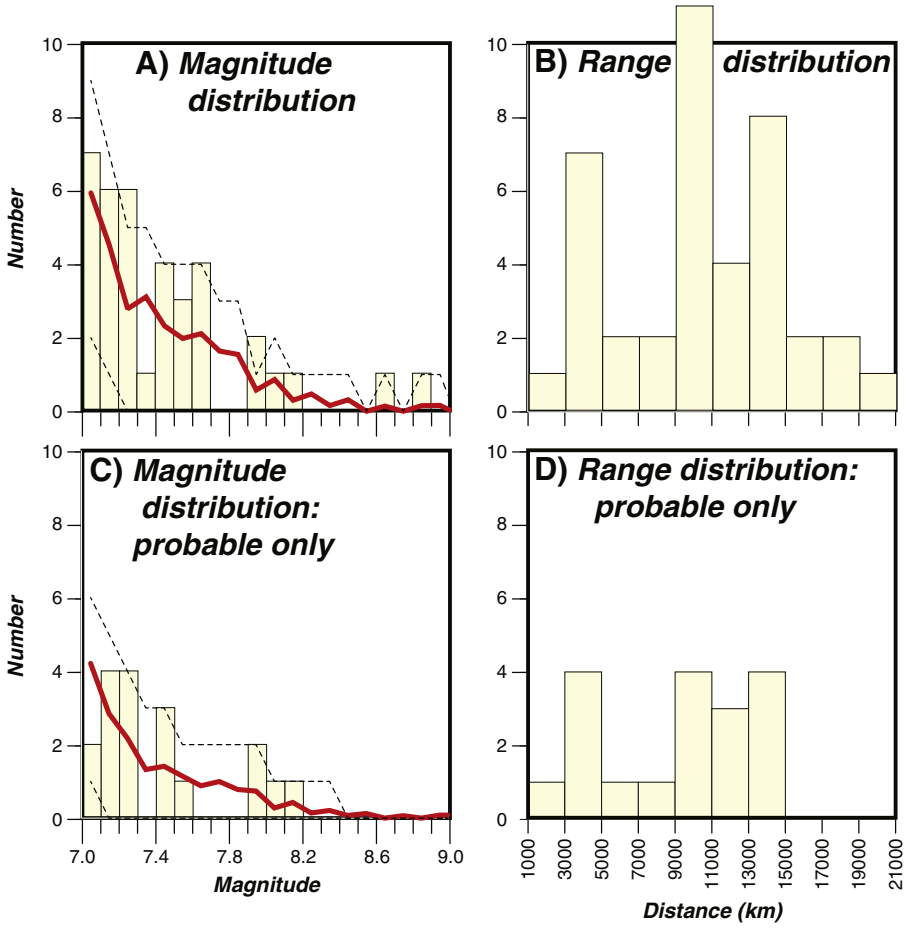

Fig. 32. (A) Magnitude distribution of global mainshocks associated with possible remote triggering, and (B) the range distribution between mainshocks and largest possibly triggered aftershock at $r > 1000$ km. In (C) and (D) the same information is plotted except just for mainshocks that caused probable triggering as identified in Table 2. Red lines show average magnitude–frequency distributions from 1000 randomized draws from the 260 $M \geq 7$ global mainshock catalog. Dashed lines show threshold numbers that 95% of random catalogs have in each magnitude bin.

Doser, D.I., Olsen, K.B., Pollitz, F.F., Stein, R.S., Toda, S., 2009. The 1911 M~6:6 Calaveras earthquake: source parameters and the role of static, viscoelastic, and dynamic coulomb stress changes imparted by the 1906 San Francisco Earthquake. Bull. Seismol. Soc. Am. 99 (3), 1746–1759. http://dx.doi.org/10.1785/0120080305.

Ellsworth, W.L., Beroza, G.C., 1995. Seismic evidence for an earthquake nucleation phase. Science 268, 851–855.

Faenza, L., Marzocchi, W., Boschi, E., 2003. A non-parametric hazard model to characterize the spatio-temporal occurrence of large earthquakes; an application to the Italian catalogue. Geophys. J. Int. 155, 521–531.

Felzer, K.R., Brodsky, E.E., 2006. Decay of aftershock density with distance indicates triggering by dynamic stress. Nature 441 (7094), 735–738. http://dx.doi.org/10.1038/nature04799.

Geist, E.L., Parsons, T., 2014. Undersampling power law size distributions: Effect on the assessment of extreme natural hazards. Natural Hazards 1–31. http://dx.doi.org/10.1007/s11069-013-1024-0.

Glowacka, E., Nava, A.F., Cossio, D.D., Wong, V., Farfan, F., 2002. Fault slip, seismicity, and deformation in the Mexicali Valley, Baja California, Mexico, after the M 7.1 Hector Mine earthquake. Bull. Seismol. Soc. Am. 92, 1290–1299.

Gomberg, J., 1996. Stress/strain changes and triggered seismicity following the M_W7.3 Landers, California, earthquake. J. Geophys. Res. B: Solid Earth 101 (1), 751–764.

Gomberg, J., Bodin, P., 1994. Triggering of the $Ms = 5.4$ Little Skull Mountain, Nevada, earthquake with dynamic strains. Bull. Seismol. Soc. Am. 84 (3), 844–853.

Gomberg, J., Davis, S., 1996. Stress/strain changes and triggered seismicity at The Geysers, California. J. Geophys. Res. B: Solid Earth 101 (1), 733–749.

Gomberg, J., Felzer, K., 2008. A model of earthquake triggering probabilities and application to dynamic deformations constrained by ground motion observations. J. Geophys. Res. B: Solid Earth 113 (10). http://dx.doi.org/10.1029/2007JB005184 (art. no. B10317).

Gomberg, J., Johnson, P., 2005. Dynamic triggering of earthquakes. Nature 437 (7060), 830. http://dx.doi.org/10.1038/437830a.

Gomberg, J., Blanpied, M.L., Beeler, N.M., 1997. Transient triggering of near and distant earthquakes. Bull. Seismol. Soc. Am. 87 (2), 294–309.

Gomberg, J., Beeler, N.M., Blanpied, M.L., Bodin, P., 1998. Earthquake triggering by transient and static deformation. J. Geophys. Res. 103, 24411–24426.

Gomberg, J., Reasenberg, P., Bodin, P., Harris, R., 2001. Earthquake triggering by transient seismic waves following the Landers and Hector Mine, California earthquakes. Nature 411, 462–466.

Gomberg, J., Bodin, P., Reasenberg, P.A., 2003. Observing earthquakes triggered in the near field by dynamic deformations. Bull. Seismol. Soc. Am. 93, 118–138.

Gomberg, J., Bodin, P., Larson, K., Dragert, H., 2004. Earthquake nucleation by transient deformations caused by the M = 7.9 Denali, Alaska, earthquake. Nature 427, 621–624.

Gonzalez-Huizar, H., Velasco, A.A., 2011. Dynamic triggering: stress modeling and a case study. J. Geophys. Res. B: Solid Earth 116, B02304. http://dx.doi.org/10.1029/2009JB007000.

Gonzalez-Huizar, H., Velasco, A.A., Peng, Z., Castro, R.R., 2012. Remote triggered seismicity caused by the 2011, M9.0 Tohoku-Oki, Japan earthquake. Geophys. Res. Lett. 39 (10). http://dx.doi.org/10.1029/2012GL051015 (art. no. L10302).

Guatteri, M., Spudich, P., 2000. What can strong motion data tell us about slip-weakening fault friction laws? Bull. Seismol. Soc. Am. 90, 98–116.

Gutenberg, B., Richter, C.R., 1954. Magnitude and energy of earthquakes. Ann. Geofis. 9, 1–15.

Harrington, R.M., Brodsky, E.E., 2006. The absence of remotely triggered seismicity in Japan. Bull. Seismol. Soc. Am. 96 (3), 871–878. http://dx.doi.org/10.1785/0120050076.

Heuret, A., Lallemand, S., Funiciello, F., Piromallo, C., Faccenna, C., 2011. Physical characteristics of subduction interface type seismogenic zones revisited. Geochem. Geophys. Geosyst. 12, Q01004. http://dx.doi.org/10.1029/2010GC003230.

Hill, D.P., 2008. Dynamic stresses, Coulomb failure, and remote triggering. Bull. Seismol. Soc. Am. 98 (1), 66–92. http://dx.doi.org/10.1785/0120070049.

Hill, D.P., 2012. Dynamic stress, coulomb failure, and remote triggering—corrected. Bull. Seismol. Soc. Am. 102, 2313–2336.

Hill, D.P., Prejean, S., 2014. Dynamic triggering, in: H. Kanamori (ed.) V. 4 Earthquake Seismology, Treatise on Geophysics, 2nd edition (G. Schubert, ed. in chief), Elsevier, Amsterdam. (in press).

Hill, D.P., Reasonberg, P.A., Michael, A., Arabasz, W.J., Beroza, G., Brune, J.N., Brumbaugh, D., Castro, R., Davis, S., dePolo, D., Ellsworth, W.L., Gomberg, J., Harmsen, S., House, L., Jackson, S.M., Johnston, M., Jones, L., Keller, R., Malone, S., Munguia, L., Nava, S., Pechmann, J.C., Sanford, A., Simpson, R.W., Smith, R.S., Stark, M., Stickney, M., Vidal,

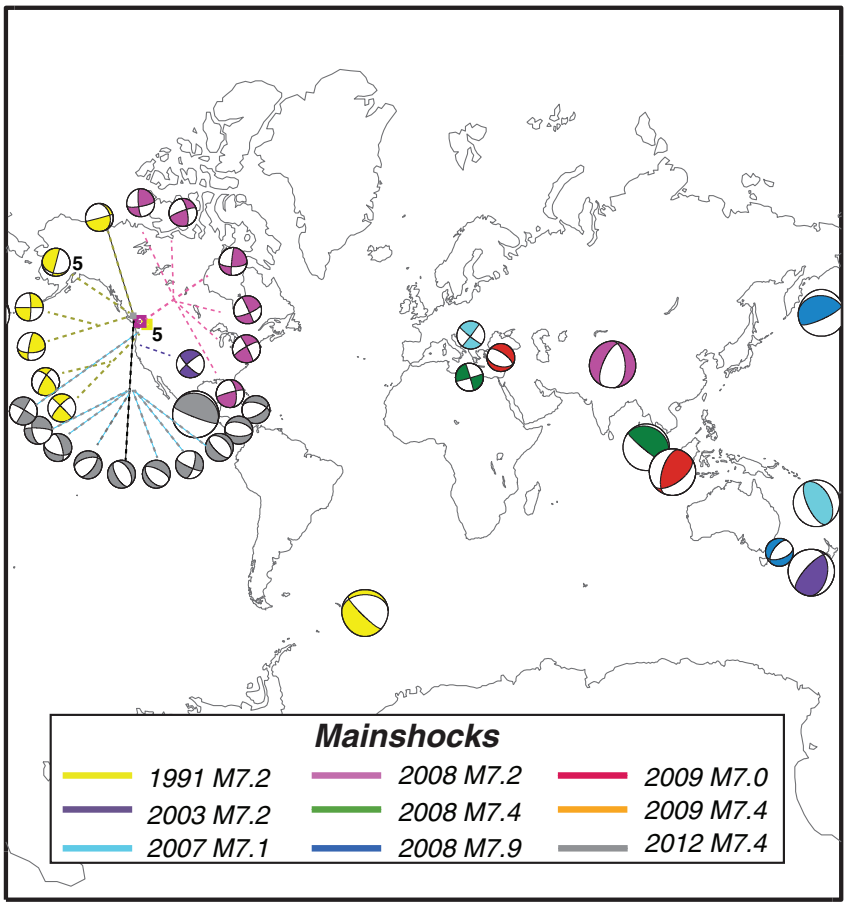

Fig. 33. Focal mechanisms for selected mainshocks (large beach-balls), related with cases of "probable" and "possible" remote triggering listed in Table 2, and potentially triggered events (smaller beach-balls) within the first 24 h following each mainshock. We find that triggered-event focal mechanisms are consistent with regional faulting styles; in northern California, strike-slip faulting dominates with the exception of the $M = 7.4$ 2012 Mexico triggered events, which included normal faulting. However, this is related with seismic activity at The Geysers geothermal area, known for its extensional tectonics.

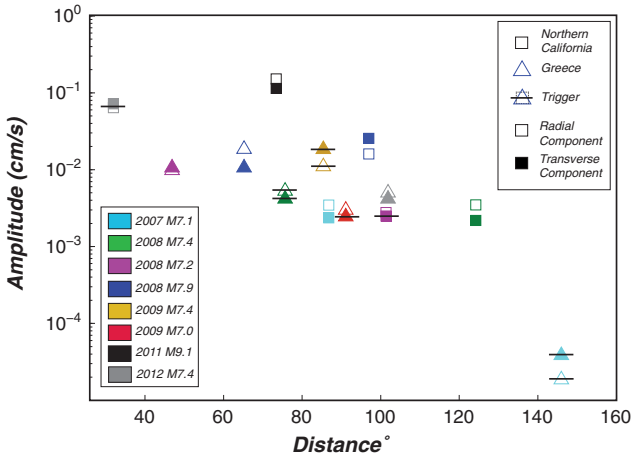

Fig. 34. Plot of measured peak ground velocities (PGV) for the radial (unfilled symbols) and the transverse component (filled symbols) vs. distance for sites in northern California (squares) and Greece (triangles) for mainshocks listed in Table 2. We do not find a consistent global/regional PGV amplitude threshold for remote triggering. For example, the $M = 7.1$ 2007 New Hebrides mainshock had higher amplitude PGV in northern California than in Greece, though it was not associated with dynamic triggering in California. However it caused a significant seismicity rate increase in Central Greece, despite being two orders of magnitude lower amplitude there. The $M = 7.4$ 2008 Sumatra mainshock had comparable amplitudes in both northern California and Greece, but caused remote earthquake triggering only in Greece.

A., Walter, S., Wong, V., Zollweg, J., 1993. Seismicity in the western United States remotely triggered by the M 7.4 Landers, California, earthquake of June 28, 1992. Science 260, 1617–1623.
Hill, D.P., Peng, Z., Shelly, D.R., Aiken, C., 2013. S-wave triggering of tremor beneath the Parkfield, California, section of the San Andreas Fault by the 2011 Tohoku, Japan earthquake: observations and theory. Bull. Seismol. Soc. Am. 103 (2b), 1541–1550.
Hirosi, F., Miyaoka, K., Hayashimoto, N., Yamazaki, T., Nakamura, M., 2011. Outline of the 2011 off the Pacific coast of Tohoku earthquake (Mw 9.0) seismicity: foreshocks, mainshock, aftershocks, and induced activity. Earth, Planets Space 63, 513–518.
Hori, T., Miyazaki, S., 2010. Hierarchical asperity model for multiscale characteristic earthquakes: a numerical study for the off-Kamaishi earthquake sequence in the NE Japan subduction zone. Geophys. Res. Lett. 37, L10304. http://dx.doi.org/10.1029/2010GL042669.
Hori, T., Miyazaki, S., 2011. A possible mechanism of M 9 earthquake generation cycles in the area of repeating M 7~8 earthquakes surrounded by aseismic sliding. Earth, Planets Space 63, 773–777.
Hough, S.E., 2001. Triggered earthquakes and the 1811–1812 New Madrid, central United States, earthquake sequence. Bull. Seismol. Soc. Am. 91, 1547–1581.
Hough, S.E., 2005. Remotely triggered earthquakes following moderate mainshocks (or why California is not falling into the ocean). Seismol. Res. Lett. 76, 58–66.
Hough, S.E., 2007. Remotely triggered earthquakes following moderate main shocks. Spec. Pap. Geol. Soc. Am. 425, 73–86. http://dx.doi.org/10.1130/2007.2425.
Hough, S.E., Kanamori, H., 2002. Source properties of earthquakes near the Salton Sea triggered by the 16 October 1999 Hector Mine, California, earthquake. Bull. Seismol. Soc. Am. 92, 1281–1289.
Huc, M., Main, I.G., 2003. Anomalous stress diffusion in earthquake triggering: correlation length, time dependence, and directionality. J. Geophys. Res. 108 (B7), 2324. http://dx.doi.org/10.1029/2001JB001645.
Husen, S., Wiemer, S., Smith, R.B., 2004. Remotely triggered seismicity in the Yellowstone National Park region by the 2002 M w 7.9 Denali fault earthquake, Alaska. Bull. Seismol. Soc. Am. 94 (6 Suppl. B), S317–S331.

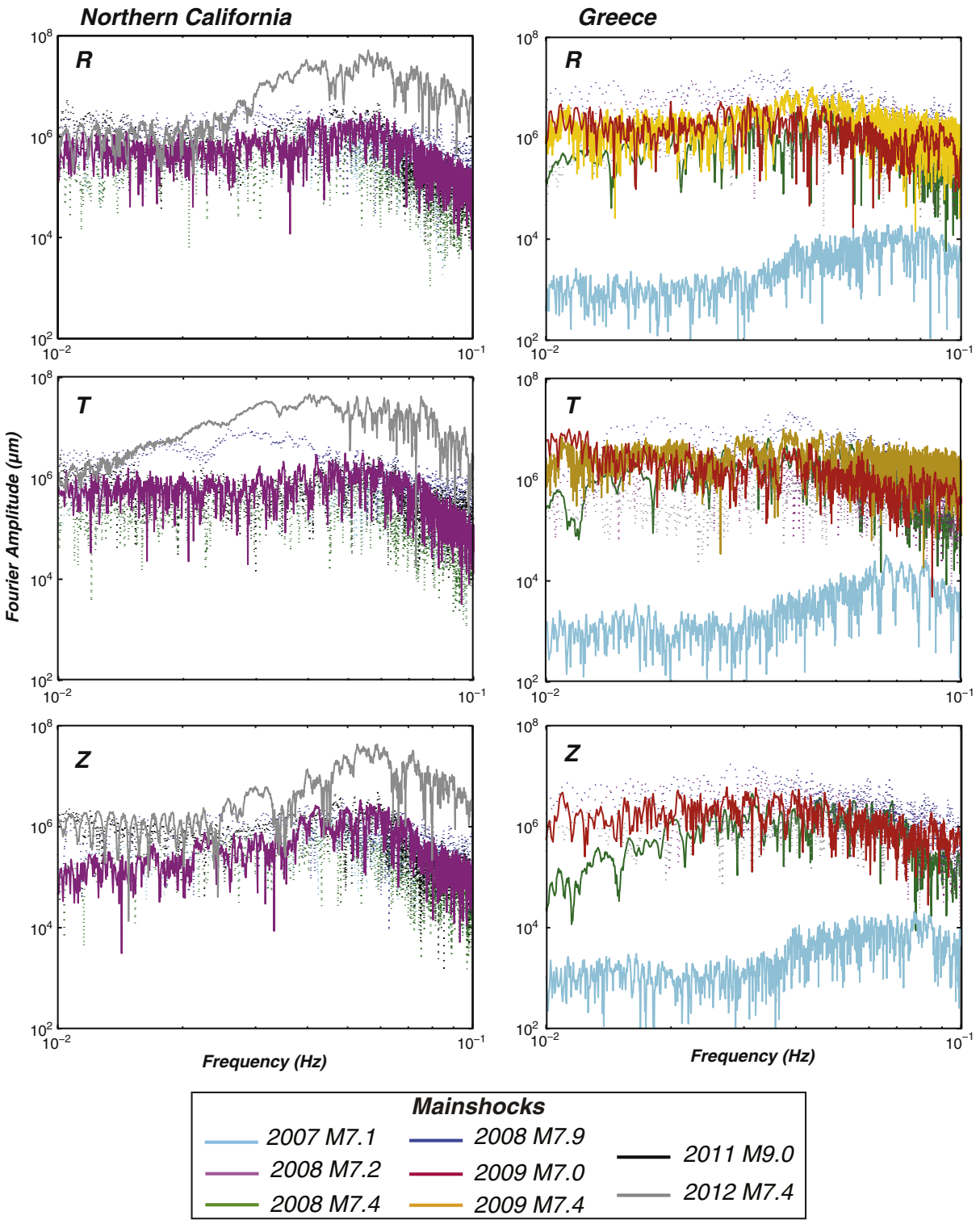

Fig. 35. Plots of smoothed Fourier amplitude spectra for the intermediate and long-period frequency band (0.01–10 Hz) for sites in northern California (left panel) and Greece (right panel) derived from continuous broadband recordings for the mainshocks associated with triggering as listed in Table 2. Symbols *R*, *T*, and *Z* stand for radial, transverse and vertical components, respectively. For northern California, broadband recordings correspond to station KCPB, with the exception of the 2011 $M = 9.0$ Tohoku-Oki event for which we have analyzed the PKD broadband station. For Greek sites we analyzed data from the UPR, SERG and LAKA broadband stations operated by the seismological networks of Patras, Prague and Athens University, respectively. Solid/dashed lines correspond to cases with existing/no evidence of remote triggering, respectively. Northern California sites show triggering susceptibility (i.e., 2008 $M = 7.2$ and 2012 $M = 7.4$ mainshocks), but there are many cases where remote triggering is not evident despite strong shaking. This comparison allows us to confirm our previous conclusion that the frequency content is not related with triggering at a site. For example in California, the $M = 7.4$ 2008 Sumatra event (in dashed green line) exhibited relatively higher frequency content, but did not cause remote triggering, whereas one month later, the 2008 $M = 7.2$ 2008 China event (in solid magenta line) did. Then the 2008 $M = 7.9$ Wenchuan earthquake occurred ~2 months after (in dashed blue), but was not associated with triggering. Note the very low frequency content of the 2007 $M = 7.1$ 2007 New Hebrides mainshock recorded in Greece (solid cyan line) that caused a persistent seismicity rate increase in Greece for ~20 days afterward (Figs. 11, 12).

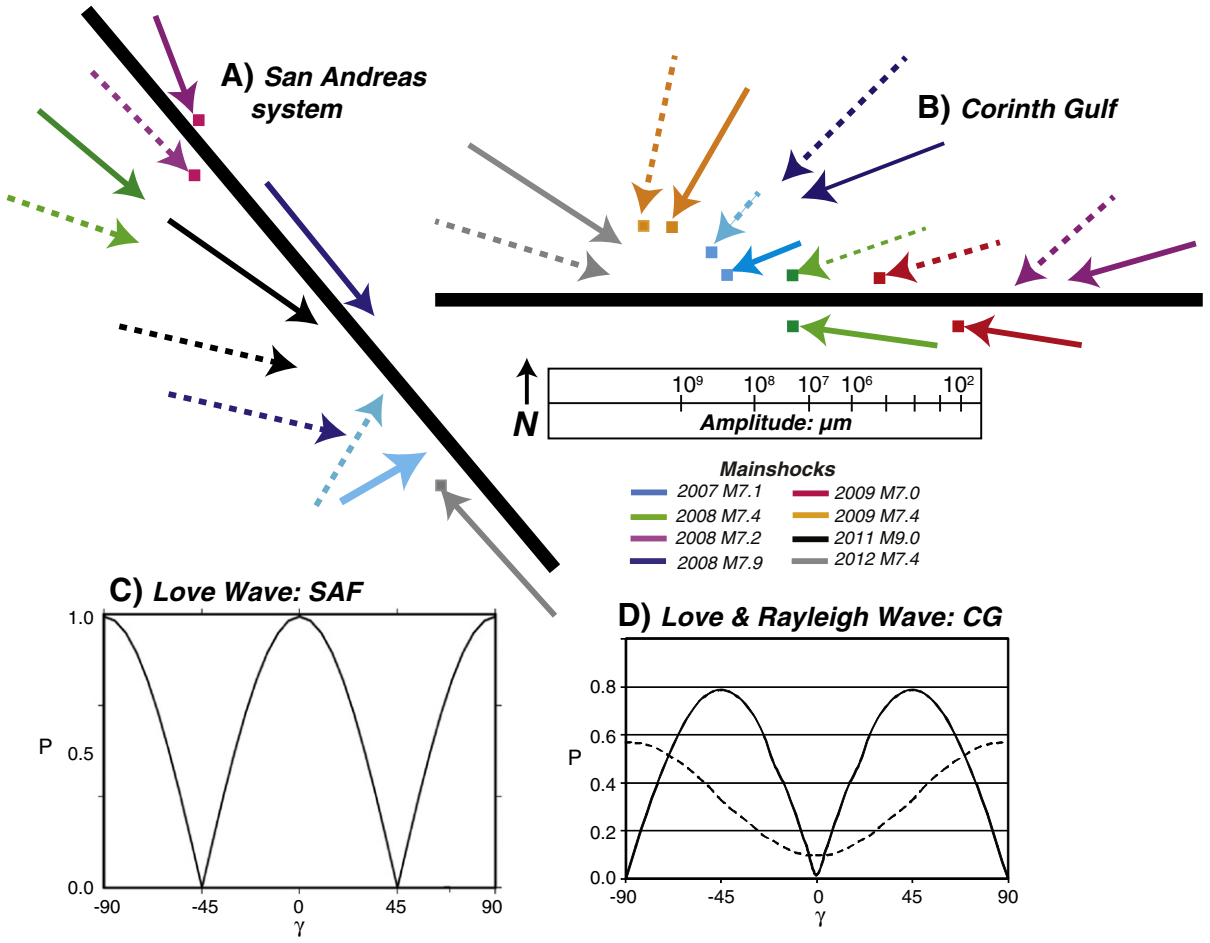

Fig. 36. Plots of propagation direction (solid arrows) and apparent back-azimuth for long-period surface waves (dashed arrows) for cases with associated remote triggering (indicated by the dots) as well as those not associated with remote triggering (no dots). In (A) a vertical frictionless San Andreas fault with generic strike N40°W is shown, and in (B) an E-W trending normal fault, representing the deformation of the Corinth Gulf (in central Greece) is shown. Arrow lengths correspond to the Fourier amplitude spectrum at 20 s period for the transverse and radial components of the specific mainshock, respectively. We also present the Love wave triggering potential (P) as a function of incident angle (γ) taken from Hill (2012, Fig. 9) in (C) for the San Andreas fault (SAF) (target depth 5 km), and the Love and Rayleigh wave triggering potential as a function of incidence angle (written communication, D. Hill, 2013) in (D) for Corinth Gulf (CG) faults (target depth 9 km on a 30° dipping normal fault. The San Andreas fault appears to have high Love-wave triggering potential. For the Corinth Gulf case, most mainshocks related with remote triggering exhibit intermediate incident angle ($20 < \gamma < 45°$), in which case both Love and Rayleigh waves have triggering potential ($P_L \sim 0.5–0.8$, $P_R \sim 0.5–0.3$).

Husker, A.L., Brodsky, E.E., 2004. Seismicity in Idaho and Montana triggered by the Denali fault earthquake: a window into the geologic context for seismic triggering. Bull. Seismol. Soc. Am. 94, S310–S316.

Iio, Y., 2011. Earthquake Nucleation Process. In: Meyers, Robert A. (Ed.), Extreme Environmental Events, Complexity in Forecasting and Early Warning. Springer-Verlag, pp. 320–337 (2011, XXIV, 622 pp.).

Ishimoto, M., Iida, K., 1939. Observations sur les seismes enregistres par le microseimographe construit dernierement (in Japanese with French abstract). Bull. Earthquake Res. Inst. Univ. Tokyo 17, 443–478.

Iwata, T., 2008. Low detection capability of global earthquakes after the occurrence of large earthquakes: investigation of the Harvard CMT catalogue. Geophys. J. Int. 174, 849–856.

Iwata, T., Nakanishi, I., 2004. Hastening of occurrences of earthquakes due to dynamic triggering: the observation at Matsushiro, central Japan. J. Seismol. 8 (2), 165–177. http://dx.doi.org/10.1023/B:JOSE.0000021378.64563.c0.

Jackson, D.D., Kagan, Y.Y., 1999. Testable earthquake forecasts for 1999. Seismol. Res. Lett. 70, 393–403.

Jiang, T., Peng, Z., Wang, W., Chen, Q.-F., 2010. Remotely triggered seismicity in continental China following the 2008 Mw 7.9 Wenchuan earthquake. Bull. Seismol. Soc. Am. 100 (5 B), 2574–2589. http://dx.doi.org/10.1785/0120090286.

Johnston, M.J.S., Prejean, S.G., Hill, D.P., 2004. Triggered deformation and seismic activity under Mammoth Mountain in long Valley Caldera by the 3 November 2002 M w 7.9 Denali fault earthquake. Bull. Seismol. Soc. Am. 94 (6 Suppl. B), S360–S369.

Jousset, P., Rohmer, J., 2012. Evidence for remotely triggered microearthquakes during salt cavern collapse. Geophys. J. Int. 191, 207–233.

Kagan, Y.Y., 1993. Statistics of characteristic earthquakes. Bull. Seismol. Soc. Am. 83, 7–24.

Kagan, Y.Y., 2003. Accuracy of modern global earthquake catalogs. Phys. Earth Planet. Inter. 135, 173–209.

Kato, N., 2008. Numerical simulation of recurrence of asperity rupture in the Sanriku region, northeastern Japan. J. Geophys. Res. 113, B06302. http://dx.doi.org/10.1029/2007JB005515.

Kato, N., 2012. Dependence of earthquake stress drop on critical slip-weakening distance. J. Geophys. Res. 117, B01301. http://dx.doi.org/10.1029/2011JB008359.

Kilb, D., Gomberg, J., 1999. The initial subevent of the 1994 Northridge, California, earthquake: is earthquake size predictable? J. Seismol. 3, 409–420.

Kilb, D., Gomberg, J., Bodin, P., 2000. Triggering of earthquake aftershocks by dynamic stresses. Nature 408, 570–574.

Kiratzi, A., Louvari, E., 2003. Focal mechanisms of shallow earthquakes in the Aegean Sea and the surrounding lands determined by waveform modeling: a new database. J. Geodyn. 36 (1–2), 251–274. http://dx.doi.org/10.1016/s0264-3707(03)00050-4.

Kokusho, T., Kojima, T., 2002. Mechanism for postliquefaction water film generation in layered sand. J. Geotech. Geoenviron. Eng. 128, 129–137.

Lapusta, N., Rice, J.R., 2003. Nucleation and early seismic propagation of small and large events in a crustal earthquake model. J. Geophys. Res. 108 (B4), 2205. http://dx.doi.org/10.1029/2001JB000793.

Lei, X., Xie, C., Fu, B., 2011. Remotely triggered seismicity in Yunnan, southwestern China, following the 2004 M w9.3 Sumatra earthquake. J. Geophys. Res. B: Solid Earth 116 (8). http://dx.doi.org/10.1029/2011JB008245 (art. no. B08303).

Lin, C.-H., 2012. Remote triggering of the M w 6.9 Hokkaido earthquake as a result of the M w 6.6 Indonesian earthquake on September 11, 2008. Terr. Atmos. Ocean. Sci. 23 (3), 283–290. http://dx.doi.org/10.3319/TAO.2012.01.12.01(T).

Lupi, M., Geiger, S., Graham, C.M., 2011. Numerical simulations of seismicity-induced fluid flow in the Tjörnes Fracture Zone, Iceland. J. Geophys. Res. 116, B07101. http://dx.doi.org/10.1029/2010JB007732.

Manaker, D.M., Michael, A.J., Burgmann, R., 2005. Subsurface structure and kinematics of the Calaveras–Hayward Fault stepover from three-dimensional Vp and seismicity, San Francisco Bay Region, California. Bull. Seismol. Soc. Am. 95 (2), 446–470.

Manga, M., Brodsky, E., 2006. Seismic triggering of eruptions in the far field: volcanoes and geysers. Annu. Rev. Earth Planet. Sci. 34 (2006), 263–291.

Marone, C., Kilgore, B., 1993. Scaling of the critical slip distance for seismic faulting with shear strain in fault zones. Nature 362, 618–621.

Meltzner, A.J., Wald, D.J., 2003. Aftershocks and triggered events of the great 1906 California earthquake. Bull. Seismol. Soc. Am. 93, 2160–2186.
Mignan, A.C., Jiang, J.D., Zechar, S., Wiemer, Z.Wu., Huang, Z., 2013. Completeness of the mainland China earthquake catalog and implications for the setup of the China earthquake forecast testing center. Bull. Seismol. Soc. Am. 103, 845–859. http://dx.doi.org/10.1785/0120120052.
Mikumo, T., Yagi, Y., 2003. Slip-weakening distance in dynamic rupture of in-slab normal-faulting earthquakes. Geophys. J. Int. 155, 443–455. http://dx.doi.org/10.1046/j.1365-246X.2003.02047.x.
Miyazawa, M., 2011. Propagation of an earthquake triggering front from the 2011 Tohoku-Oki earthquake. Geophys. Res. Lett. 38 (23). http://dx.doi.org/10.1029/2011GL049795 (art. no. L23307).
Miyazawa, M., Mori, J., 2006. Evidence suggestion fluid flow beneath Japan due to periodic seismic triggering from the 2004 Sumatra–Andaman earthquake. Geophys. Res. Lett. 33, L05303-L. http://dx.doi.org/10.1029/2005GL025087.
Mohamad, R., Darkal, A.N., Seber, D., Sandvol, E., Gomez, F., Barazangi, M., 2000. Remote earthquake triggering along the dead sea fault in Syria following the 1995 Gulf of Aqaba earthquake (M s = 7.3). Seismol. Res. Lett. 71 (1), 47–52.
Moran, S.C., Power, J.A., Stihler, S.D., Sánchez, J.J., Caplan-Auerbach, J., 2004. Earthquake triggering at Alaskan volcanoes following the 3 November 2002 Denali fault earthquake. Bull. Seismol. Soc. Am. 94 (6 Suppl. B), S300–S309.
Okubo, P.G., Dieterich, J.H., 1984. Effect of physical fault properties on friction instabilities produced on simulated faults. J. Geophys. Res. 89, 5817–5827.
Olson, E.L., Allen, R.M., 2005. The deterministic nature of earthquake rupture. Nature 438, 212–215. http://dx.doi.org/10.1038/nature04214.
Oppenheimer, D.H., 1986. Extensional tectonics at The Geysers Geothermal Area, California. J. Geophys. Res. 91 (B11), 11463–11476. http://dx.doi.org/10.1029/JB091iB11p11463.
Pankow, K.L., Arabasz, W.J., Pechmann, J.C., Nava, S.J., 2004. Triggered seismicity in Utah from the 3 November 2002 Denali Fault earthquake. Bull. Seismol. Soc. Am. 94, 332–347.
Papadopoulos, G.A., 1998. An unusual earthquake time cluster in the Greek mainland during May–June 1995. J. Geodyn. 26 (2–4), 261–269.
Parsons, T., 2002. Global Omori law decay of triggered earthquakes: large aftershocks outside the classical aftershock zone. J. Geophys. Res. 107, 2199. http://dx.doi.org/10.1029/2001JB000646.
Parsons, T., 2005. A hypothesis for delayed dynamic earthquake triggering. Geophys. Res. Lett. 32. http://dx.doi.org/10.1029/2004GL021811.
Parsons, T., Velasco, A.A., 2011. Absence of remotely triggered large earthquakes beyond the main shock region. Nat. Geosci. 4, 312–316. http://dx.doi.org/10.1038/ngeo1110.
Parsons, T., Kaven, J.O., Velasco, A.A., Gonzalez-Huizar, H., 2012. Unraveling the apparent magnitude threshold of remote earthquake triggering using full wave-field surface wave simulation. Geochem. Geophys. Geosyst. G3, 13. http://dx.doi.org/10.1029/2012GC004164.
Peng, Z., Vidale, J.E., Wech, A.G., Nadeau, R.M., Creager, K.C., 2009. Remote triggering of tremor along the San Andreas fault in central California. J. Geophys. Res. 114. http://dx.doi.org/10.1029/2008JB006049 (18 pp.).
Peng, Z., Wang, W., Chen, Q.-F., Jiang, T., 2010. Remotely triggered seismicity in north China following the 2008 M w 7.9 Wenchuan earthquake. Earth, Planets Space 62 (11), 893–898. http://dx.doi.org/10.5047/eps.2009.03.006.
Peng, Z., Long, L.T., Zhao, P., 2011b. The relevance of high-frequency analysis artifacts to remote triggering. Seismol. Res. Lett. 82, 654–660. http://dx.doi.org/10.1785/gssrl.82.5.654.
Peng, Z., Wu, C., Aiken, C., 2011a. Delayed triggering of microearthquakes by multiple surface waves circling the Earth. Geophys. Res. Lett. 38, L04306. http://dx.doi.org/10.1029/2010GL046373.
Peng, Y., Zhou, S., Zhuang, J., Shi, J., 2012. An approach to detect the abnormal seismicity increase in Southwestern China triggered co-seismically by 2004 Sumatra M w 9.2 earthquake. Geophys. J. Int. 189 (3), 1734–1740. http://dx.doi.org/10.1111/j.1365-246X.2012.05456.x.
Pollitz, F.F., Stein, R.S., Sevilgen, V., Bürgmann, R., 2012. The 11 April 2012 east Indian Ocean earthquake triggered large aftershocks worldwide. Nature 490 (7419), 250–253.
Prejean, S., Hill, D.P., Brodsky, E.E., Hough, S.E., Johnston, M.J.S., Malone, S.D., Oppenheimer, D.H., Pitt, A.M., Richards-Dinger, K.B., 2004. Remotely triggered seismicity on the United States west coast following the Mw 7.9 Denali Fault earthquake. Bull. Seismol. Soc. Am. 94, S348–S359.
Roeloffs, E., 1998. Persistent water level changes in a well near Parkfield, California, due to local and distant earthquakes. J. Geophys. Res. 103, 869–889.
Rubinstein, J.L., Gomberg, J., Vidale, J.E., Wech, A.G., Kao, H., Creager, K.C., Rogers, G., 2009. Seismic wave triggering of nonvolcanic tremor, episodic tremor and slip, and earthquakes on Vancouver Island. J. Geophys. Res. 114, B00A01. http://dx.doi.org/10.1029/2008JB005875 (22 pp.).
Ruina, A., 1983. Slip instability and state variable friction laws. J. Geophys. Res. 88, 10,359–10,370.
Savage, H.M., Marone, C., 2008. Potential for earthquake triggering from transient deformations. J. Geophys. Res. B: Solid Earth 113 (5). http://dx.doi.org/10.1029/2007JB005277 (art. no. B0530210).
Shanker, D., Singh, B., Singh, V.P., 2000. Earthquake time cluster in North-East India during February to April 1988. Acta Geod. Geophys. Hung. 35 (2), 195–204.
Shelly, D.R., Peng, Z., Hill, D.P., Aiken, C., 2011. Triggered creep as a possible mechanism for delayed dynamic triggering of tremor and earthquakes. Nat. Geosci. 4, 384–388. http://dx.doi.org/10.1038/NGEO1141.
Shibazaki, B., 2005. Nucleation process with dilatant hardening on a fluid-infiltrated strike-slip fault model using a rate- and state-dependent friction law. J. Geophys. Res. 110, B11308. http://dx.doi.org/10.1029/2005JB003741.
Shibazaki, B., Matsuzawa, T., Tsutsumi, A., Ujiie, K., Hasegawa, A., Ito, Y., 2011. 3D modeling of the cycle of a great Tohoku-oki earthquake, considering frictional behavior at low to high slip velocities. Geophys. Res. Lett. 38, L21305. http://dx.doi.org/10.1029/2011GL049308.
Singh, S.K., Anderson, J.G., Rodríguez, M., 1998. Triggered seismicity in the Valley of Mexico from major Mexican earthquakes. Geofis. Int. 37 (1), 3–15.
Sornette, D., Vanneste, C., Sornette, A., 1991. Dispersion of b-values in Gutenberg–Richter Law as a consequence of a proposed fractal nature of continental faulting. Geophys. Res. Lett. 18, 897–900.
Spudich, P., Steck, L.K., Hellweg, M., Fletcher, J.B., Baker, L.M., 1995. Transient stresses at Parkfield, California, produced by the M 7.4 Landers earthquake of June 28, 1992: observations form the UPSAR dense seismograph array. J. Geophys. Res. 100 (B1), 675–690.
Stark, M.A., Davis, S.D., 1996. Remotely triggered microearthquakes at The Geysers geothermal field, California. Geophys. Res. Lett. 23, 945–948.
Steeples, D.W., Sreeples, D.D., 1996. Far-field aftershocks of the 1906 earthquake. Bull. Seismol. Soc. Am. 86, 921–924.
Sturtevant, B., Kanamori, H., Brodsky, E.E., 1996. Seismic triggering by rectified diffusion in geothermal systems. J. Geophys. Res. 101, 25269–25282.
Surve, G., Mohan, G., 2012. Possible evidence of remotely triggered and delayed seismicity due to the 2001 Bhuj earthquake (Mw = 7.6) in western India. Nat. Hazards 64 (1), 299–310. http://dx.doi.org/10.1007/s11069-012-0237-y.
Taira, T., Silver, P.G., Niu, F., Nadeau, R.M., 2009. Remote triggering of fault-strength changes on the San Andreas fault at Parkfield. Nature 461 (7264), 636–639. http://dx.doi.org/10.1038/nature08395.
Tape, C., West, M., Silwal, V., Ruppert, N., 2013. Earthquake nucleation and triggering on an optimally oriented fault. Earth Planet. Sci. Lett. 363, 231–241. http://dx.doi.org/10.1016/j.epsl.2012.11.060.
Tibi, R., Wiens, D.A., Inoue, H., 2003. Remote triggering of deep earthquakes in the 2002 Tonga sequences. Nature 424 (6951), 921–925. http://dx.doi.org/10.1038/nature01903.
Tinti, E., Fukuyama, E., Piatanesi, A., Cocco, M., 2005. A kinematic source-time function compatible with earthquake dynamics. Bull. Seismol. Soc. Am. 95, 1211–1223.
Tinti, E., Cocco, M., Fukuyama, E., Piatanesi, A., 2009. Dependence of slip weakening distance (Dc) on final slip during dynamic rupture of earthquakes. Geophys. J. Int. 177, 1205–1220. http://dx.doi.org/10.1111/j.1365-246X.2009.04143.x.
Tzanis, A., Makropoulos, K., 2002. Did the 7/9/1999 M5.9 Athens earthquake come with a warning? Nat. Hazards 27 (1–2), 85–103. http://dx.doi.org/10.1023/A:1019957228371.
Uenishi, K., Rice, J.R., 2003. Universal nucleation length for slip-weakening rupture instability under non-uniform fault loading. J. Geophys. Res. 108 (B1). http://dx.doi.org/10.1029/2001JB001681.
Ukawa, M., Fujita, E., Kumagai, T., 2002. Remote triggering of microearthquakes at the Iwo-Jima volcano. J. Geogr. 111, 277–286.
Umeda, Y., 1990. High-amplitude seismic waves radiated from the bright spot of an earthquake. Tectonophysics 175, 81–92.
Van Der Elst, N.J., Brodsky, E.E., 2010. Connecting near-field and far-field earthquake triggering to dynamic strain. J. Geophys. Res. B: Solid Earth 115 (7). http://dx.doi.org/10.1029/2009JB006681 (art. no. B07311).
Vassilakis, E., Royden, L., Papanikolaou, D., 2011. Kinematic links between subduction along the Hellenic trench and extension in the Gulf of Corinth, Greece: a multidisciplinary analysis. Earth Planet. Sci. Lett. 303 (1–2), 108–120. http://dx.doi.org/10.1016/642 j.epsl.2010.12.054.
Velasco, A.A., Hernandez, S., Parsons, T., Pankow, K., 2008. The ubiquitous nature of dynamic triggering. Nat. Geosci. 1, 375–379. http://dx.doi.org/10.1038/ngeo204.
Vere-Jones, D., 1970. Stochastic models for earthquake occurrence (with discussion). J. R. Stat. Soc. B32, 1–62.
Vincenty, T., 1975. Direct and inverse solutions of geodesics on the ellipsoid with application of nested equations. Surv. Rev. XXII (176), 88–93.
Wells, D.L., Coppersmith, K.J., 1994. New empirical relationships among magnitude, rupture length, rupture width, rupture area, and surface displacement. Bull. Seismol. Soc. Am. 84, 974–1002.
Wen, K.-L., Beresnev, I.A., Cheng, S.-N., 1996. Moderate-magnitude seismicity remotely triggered in the Taiwan region by large earthquakes around the Philippine Sea plate. Bull. Seismol. Soc. Am. 86 (3), 843–847.
Wessel, P., Smith, W.H.F., 1991. Free software helps map and display data. EOS Trans. AGU 72, 441.
West, M., Sanchez, J.J., McNutt, S.R., 2005. Periodically triggered seismicity at Mount Wrangell, Alaska, after the Sumatra earthquake. Science 308, 1144–1146.
Wu, J., Peng, Z., Wang, W., Chen, Q., 2011. Dynamic triggering of shallow earthquakes near Beijing, China. Geophys. J. Int. 185, 1321–1334.
Yukutake, Y., Honda, R., Harada, M., Aketagawa, T., Ito, H., Yoshida, A., 2011. Remotely triggered seismicity in the Hakone volcano following the 2011 off the Pacific coats of Tohoku earthquake. Earth, Planets Space 63, 737–740. http://dx.doi.org/10.5047/eps.2011.05.004.
Zhang, Z., Tian, H., Liu, X., Liu, G., 1995. Mechanical features of Shanxi Datong earthquake swarm sequence and their numerical simulation by using finite element method. Acta Seismol. Sin. 8, 13–23.
Zhao, P., Peng, Z., Sabra, K.G., 2010. Detecting remotely triggered temporal changes around the Parkfield section of the San Andreas fault. Earthquake Sci. 23 (5), 497–509. http://dx.doi.org/10.1007/s11589-010-0748-0.